Structural and Functional Characterization of the mammalian Target of Rapamycin Complex 2

Inauguraldissertation

zur

Erlangung der Würde eines Doktors der Philosophie

vorgelegt der

Philosophisch-Naturwissenschaftlichen Fakultät

der Universität Basel

von

Francesca Mangia

2022

Genehmigt von der Philosophisch-Naturwissenschaftlichen Fakultät
auf Antrag von

Prof. Dr. Maier, Timm
Prof. Dr. Handschin, Christoph
Prof. Dr. Olga Mayans

Basel, 23.06.2020

Prof. Dr. Martin Spiess
Dekan

I Abstract

Proteins are the fundamental units of life. They take part in any process within the cells and their regulation is essential to adapt to different environmental and intracellular conditions. Cells integrate a large variety of inputs and in turn need to rapidly respond and generate outputs to control key mechanisms such as metabolism, growth and proliferation. Multisubunit protein complexes have evolved to sense and integrate these stimuli. The atypical protein kinase mTOR (mammalian target of rapamycin) is the master regulator of cell growth and proliferation. The association with other proteins enables mTOR to sense intracellular inputs, integrate these signals and respond by phosphorylation of downstream proteins that control cell physiology. Dysregulated mTOR signaling is linked to cancer, and to metabolic and neurodegenerative diseases. mTOR functions in two structurally and functionally distinct signaling complexes, mTORC1 and mTORC2.

This thesis provides high-quality structural information on human mTORC2, containing the protein subunits mTOR, mLST8, Rictor and SIN1 determined by cryo-electron microscopy at 3.2 Å resolution.

The work resolves the enigmatic structure and interplay of the core mTORC2 subunits Rictor and SIN1. Contrary to previous hypotheses, it is the Rictor C-terminal domain that blocks the rapamycin binding site and causes rapamycin insensitivity of mTORC2. We demonstrate how intrinsically disordered parts of SIN1 integrate into Rictor and wrap around mLST8 to position mTORC2 substrates.

We rationalize modes of mTORC2 regulation via control of complex stability and visualize novel ligand binding sites for nucleotides in Rictor and for inositol hexakisphosphate in mTOR. In summary, the results presented in this thesis provide a completely new framework to analyze mTORC2 regulation and its function. These studies open the route for further analyzing interactions with signaling proteins and membranes and pave the way for the development of specific mTORC2 inhibitors.

II Table of Contents

III List of Figures

IV Abbreviations

4EBP1	Eukaryotic translation initiation factor 4E-binding protein
ACC	Acetyl-CoA carboxylase
ACLY	ATP-citrate lyase
AGC	Protein kinase A, protein kinase G and protein kinase C
AKT	RAC-alpha serine/threonine-protein kinase
AMP	AMP-activated protein kinase
AMPK	5' adenosine monophosphate-activated protein kinase
ARM	Armadillo
ATF4	Activating Transcription Factor 4
ATM	Ataxia telangiectasia mutated
ATP	Adenosine triphosphate
ATR	Ataxia telangiectasia and Rad3-related protein
BAT	Brown adipose tissue
CAD	Carbamoyl-phosphate synthetase 2, aspartate transcarbamylase,
cAMP	3',5'-cyclic adenosine monophosphate
CASTOR	Cellular arginine sensor of mTORC1
ChREBPb	Carbohydrate-responsive element–binding protein
Co-IP	Co-immunoprecipitation
CRIK	Citron Rho-interacting kinase
CRIM	Conserved region in the middle
Cryo-EM	Cryo-electron microscopy
DDIT4	DNA-damage-inducible transcript 4
DEPTOR	DEP domain-containing mTOR interacting protein
DMPK	Myotonin protein kinase
DNA-PKcs	DNA-dependent protein kinase catalytic subunit
DSBs	Double stranded breaks
DSSO	Disuccinimidyl sulfoxide
eIF4E	Eukaryotic translation initiation factor 4E
EnaC	Epithelial Na^+ channel
ER	Endoplasmic reticulum
ERK1/2	Extracellular-signal-regulated kinase ½

FAS	Fatty acid synthase
FAT	FRAP, ATM and TRRAP
FATC	FAT C-terminal
FKBP12	FK506-binding protein of 12 kDa
FLCN	Folliculin
FNIP1	Folliculin-interacting protein 1
FNIP2	Folliculin-interacting protein 2
FoxO1	Forkhead box protein O1
FoxO3a	Forkhead box protein O3a
FRAP	FKBP12-rapamycin associated protein
FRB	FKBP12-rapamycin binding domain
GAP	GTPase-activating protein
GATOR	GAP activity toward Rags
GTP	Guanosine-5'-triphosphate
GDP	Guanosine-5'-diphosphate
GEF	Guanosine nucleotide exchange factor
GLUT1	Glucose transporter 1
GLUT4	Glucose transporter 4
GPCRs	G protein-coupled receptors
GRK	G protein-coupled receptor kinase
GSK3	Glycogen synthase kinase 3
GTPase	Guanosine triphosphate
HAT	Histone acetyltransferase
HDAC	Class IIa histone deacetylases
HEAT	Huntingtin, elongation factor 3, protein phosphatase 2A and yeast kinase Tor1
HER2	Human epidermal growth factor receptor 2
HM	Hydrophobic motif
IGF1	Insulin-like growth factor 1
InsP6	Inositol hexakiphosphate
IP	Immunoprecipitation
kDa	Kilo dalton
KO	Knockout
LATS	Large tumor suppressor

MAF1	Repressor of RNA polymerase III transcription MAF1 homolog
MAST	Microtubule-associated Ser/Thr kinase
MDa	Mega dalton
mLST8	mammalian lethal with sec-13 protein 8
MRCK	Myotonic dystrophy kinase-related CDC42-binding kinase
MSK	Mitogen- and stress-activated protein kinase
MTHFD2	Mitochondrial tetrahydrofolate cycle enzyme methylene-tetrahydrofolate dehydrogenase 2
mTORC1/2	mammalian target of rapamycin complex ½
NDR	Nuclear DBF2-related kinase
NHE1	Na^+/H^+ exchanger 1
NHE3	Na^+/H^+ exchanger 3
NHEJ	Nonhomologous end joining
NMD	Nonsense-mediated mRNA decay
PA	Phosphatidic acid
PDK1	Phosphoinositide-dependent kinase 1
PH	Pleckstrin homology
PHLPP	PH domain and Leucine rich repeat Protein Phosphatases
PI3K	Phosphoinositide 3-kinase
PIK	Phosphoinositide kinase
PIP2	Phosphatidylinositol-4,5-bisphosphate
PIP3	Phosphatidylinositol 3,4,5-trisphosphate
PKA	cyclic AMP-dependent protein kinase
PKC	Protein kinase C
PKG	cGMP-dependent protein kinase
PKS	Polyketide synthase
PLC	Phospholipase C
PLD	Phospholipase D
PLK	Polo-like kinase
PP2A	Protein phosphatase 2
PPARγ	Peroxisome proliferator-activated receptor-γ
PPIase	Peptidylprolyl isomerase
PR	Phosphorylation region
PRAS40	Proline-rich Akt substrate of 40 kDa

PRD	PIKK regulatory domain
PRK	Protein kinase C related kinase
PTEN	Phosphatase and TENsin homolog deleted on chromosome 10
PTM	Post transnational modification
Rac1	Ras-related C3 botulinum toxin substrate 1
Raptor	Regulatory-associated protein of mTOR
RBD	Ras binding domain
REDD1	Protein regulated in development and DNA damage response 1
RhoGDI2	Rho guanine nucleotide dissociation inhibitor 2
Rictor	Rapamycin-insensitive companion of mTOR
RMSD	Root-mean-square deviation
ROMK	Renal outer medullary K^+ channel
ROS	Reactive oxygen species
RSK	Ribosomal S6 kinase
RSKL	Sugen kinase 494 (SGK494) and RSK-like
RTKs	Receptor tyrosine kinases
S6K	S6 kinase
SAGA	Spt-Ada-Gcn5 acetyltransferase complex
SCD1	Stearoyl-CoA desaturase
Ser	Serine
SGK	Serum- and glucocorticoide-induced protein kinase
SIN1	mammalian stress-activated map kinase-interacting protein 1
SMG1	Suppressor with Morphological effect on Genitalia family member
SREBP	Sterol regulatory element-binding protein
TBC1D7	TBC1 domain family member 7
TFE3	Transcription factor E3
TFEB	Transcription factor EB
Thr	Threonine
TIF-1A	Transcription initiation factor 1A
TOR	Target of rapamycin
TOS	TOR signaling
TPRs	Tetratricopeptide repeats
TRRAP	Transformation/transcription domain-associated protein
TSC1	Tuberous sclerosis 1 protein

TSC2	Tuberous sclerosis 2 protein
Tyr	Tyrosine
UBF	Upstream binding factor
ULK1	UNC-51-like kinase 1
WAT	White adipose tissue
WT	Wild-type
XL-MS	Cross-linking Mass Spectrometry
αKG	α-ketoglutarate

1 Introduction

1.1 Phosphorylation is a mechanism to control protein function

Proteins are the functional units of all known life. Their functions are required for catalysis, signaling, structural stability and transport of materials across and within cells. A large variety of proteins exist to cope with these diverse tasks. It is of central importance to all organisms to tightly regulate the protein functions and to adapt the proteins to rapidly changing environments. The activity of proteins is regulated on multiple levels. Long term regulation is carried out by biosynthesis of new proteins and degradation of redundant proteins. Short term regulation is achieved by small molecules binding to target proteins and causing their activation or inhibition, by signaling cascades and by post translational modifications (PTM). Phosphorylation is one of the most studied PTMs and it is involved in a variety of cellular functions like differentiation, apoptosis and cell growth[1]. The phosphorylation process is catalyzed by protein kinases and it involves the adenosine triphosphate (ATP)-dependent transfer of a phosphoryl group onto a specific amino acid in the target protein. In mammalian cells, threonine, serine and tyrosine are the most commonly phosphorylated amino acids with a phosphorylated fraction of around 84%, 15% and <1%, respectively[2]. Protein kinases work in balance with protein phosphatases, which remove the phosphoryl group from a phosphorylated protein substrate in a molecular switch mechanism. Phosphorylation controls a protein's function by changing its conformation or modulating the interaction with another protein[3]. Therefore, by mediating changes in protein conformation and protein interactions, phosphorylation can regulate enzymatic activity, subcellular localization or stimulating signaling by other PTMs[4]. Multiple kinases phosphorylate both overlapping and different sets of substrates, even on multiple sites within the same protein, forming a vast network of metabolic control points[5]. Thus, for a cell which needs to rapidly respond to intracellular and extracellular cues, reversible protein phosphorylation serves as a fast molecular switch to modulate its targets either directly or indirectly.

1.2 mTOR – master regulator of cell growth and proliferation

1.2.1 Discovery of rapamycin and its target mTOR

In 1964, a group of scientists sailed to Easter Island in the Pacific ocean to study the health of the local population. They isolated a macrolide produced by the bacterium *Streptomyces hygroscopicus* from a soil sample. The natural product was found to inhibit growth and proliferation of *Candida albicans*, *Microsporum gypseum* and *Trichophyton granulosum*[6]. In homage to the location of its discovery, the compound was named after the Polynesian name for Easter Island, Rapa Nui, and called rapamycin(Figure 1.1)[6]. Rapamycin is produced from the precursor shikimic acid by a modular polyketide synthase (PKS), which is organized in three multimodular cassettes: RAPS1, RAPS2, RAPS3[7]. The molecule is formed by incorporation of pipecolate, methylation and oxidation.

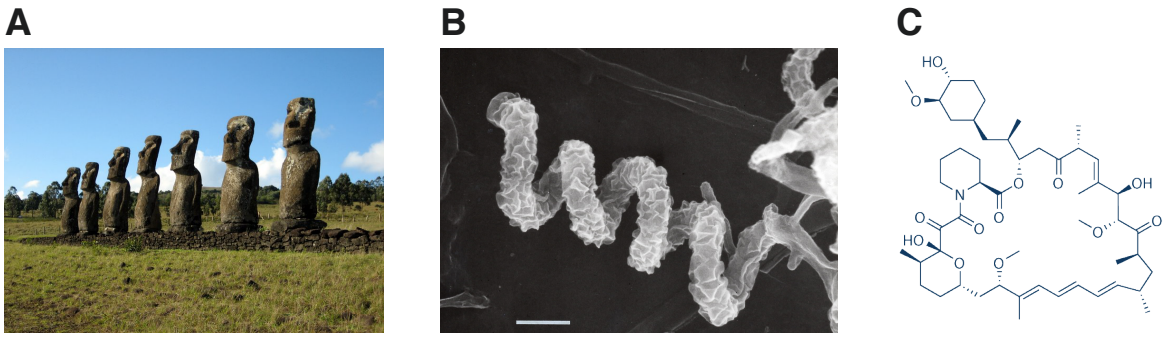

Figure 1.1 Rapamycin is a macrolide produced by *Streptomyces hygroscopicus*.
A Ahu Akivi, Rapa Nui, showing the large stone statues, the moai, for which Easter Island is famous. Image source: http://www.ianandwendy.com/OtherTrips/SouthPacific/Easter-Island/index.htm. Multi-license with GFDL and Creative Commons CC-BY-SA-2.5 and older versions (2.0 and 1.0). **B** Scanning electron microscopy micrograph of *Streptomyces hygroscopicus*. The spores adopt a cylindrical form. The scale bar indicates 1 mm. Image source: "Digital Atlas of Actinomycetes" (http://atlas.actino.jp/), by Y. Takashi & Y. Iwai **C** Chemical structure of rapamycin.

Subsequent studies on the macrolide rapamycin showed its antiproliferative and immunosuppressive effects in mammals[8]. In 1991, the group of M. N. Hall identified two rapamycin target genes in a genetic screen in budding yeast, TOR1 and TOR2. They demonstrated that rapamycin requires the FK506-binding protein of 12 kDA (FKBP12), a peptidylprolyl isomerase, to inhibit TOR[9]. In 1994, human ortholog mammalian TOR (mTOR) was identified in three independent studies[10-12]. These groundbreaking studies from the early

1990s showed that (m)TOR is essential for cell growth and proliferation. This opened up a new field of mTOR biology and it became apparent that mTOR is linked to a vast number of metabolic processes (see sections 1.2.5 and 1.2.7).

1.2.2 mTOR belongs to the PIKK kinase family

mTOR is a member of the phosphatidylinositol-3 kinase related kinase (PIKK) family, which was identified by sequence analysis in 1995[13]. While the members of this newly identified family were classified as closely related to the phosphatidylinositol class of lipid kinases, they form a distinct family of protein kinases[13]. Besides mTOR, the PIKK family comprises five additional members: Ataxia telangiectasia mutated (ATM), Ataxia telangiectasia and Rad3-related protein (ATR), DNA-dependent protein kinase catalytic subunit (DNA-PKcs), Suppressor with Morphological effect on Genitalia family member (SMG1) and Transformation/transcription domain-associated protein (TRRAP). PIKKs are very large proteins whose size varies between 2549 and 4128 amino acids.

PIKKs share a common domain architecture with a carboxy-terminal kinase domain and helical repeats of varying length at the amino-terminus. The kinase domain contains the PIKK regulatory domain (PRD) and the FAT C-terminal (FATC) motif. The kinase is encapsulated by α-solenoidal tetratricopeptide repeats (TPRs), which form a conserved region termed the Frap (FKBP12-rapamycin associated protein, obsolete name for mTOR), ATM, and TRRAP (FAT) domain [14]. The FAT domain and the kinase form a single structural unit, which is commonly referred to as FATKIN. The remainder of PIKKs consists of long arrays of α-solenoidal Huntingtin, elongation factor 3, protein phosphatase 2A and yeast kinase Tor1 (HEAT) repeats[15]. The HEAT repeats vary both in length and in their structural arrangement and serve as a platform for interaction partners.[16] (Figure 1.2).

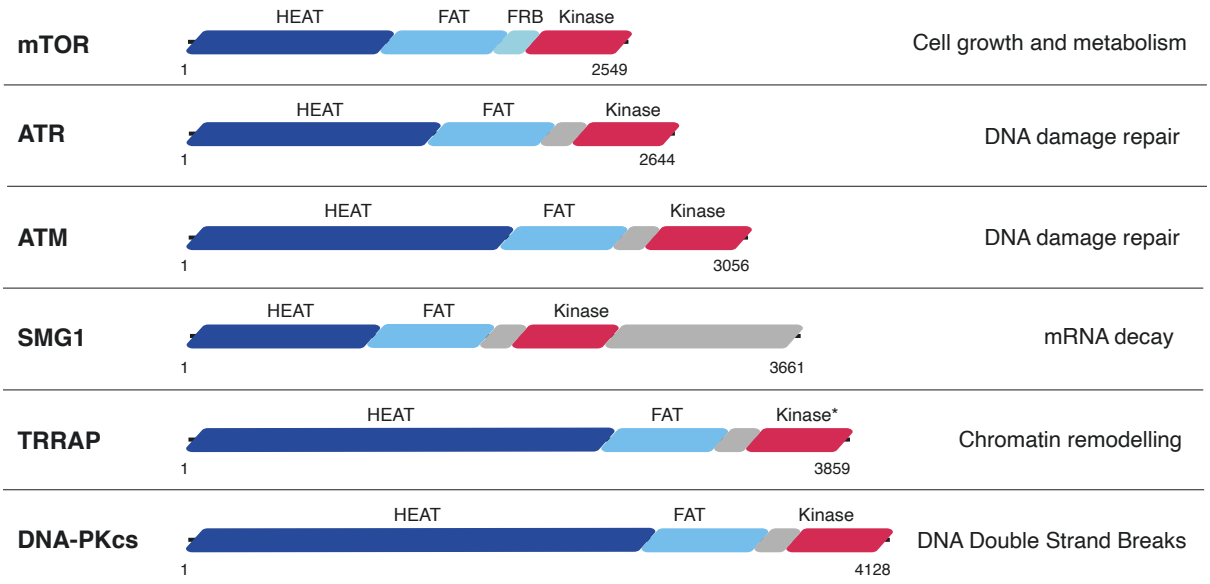

Figure 1.2 Domain organization of the PIKK family members.
PIKKs protein share a conserved domain organization. Domain boundaries and residues numbers are indicated for each protein and below the corresponding scheme. On the left are indicated the cellular processes regulated by each PIKK. Figure adapted from Imseng, S[17].

PIKKs are involved in the regulation of a wide range of eukaryotic processes such as growth regulation and DNA repair[16]. In particular, ATM and ATR and DNA-PKcs control the DNA damage response signaling[18].

ATM and **ATR** are activated by double stranded breaks (DSBs) in DNA. In addition, ATR is also activated in response to DNA replication stress[19]. In turn, ATM and ATR phosphorylate a large array of substrates to execute damage repair functions[20].

DNA-PKcs is the largest member of the PIKK family (469 kDa) and, together with the Ku70/80 heterodimer[21], is a central component of the nonhomologous end joining (NHEJ) DNA double-strand breaks repairing mechanism[22]. DNA-PK activation has been suggested to occur upon large conformational changes, opening up the active site when Ku70/80:dsDNA binds to the N-terminus and to the circular cradle region[23,24].

TRRAP is the only member of the PIKK family lacking all catalytic residues. It is a common component of many histone acetyltransferase (HAT) complexes and plays a role in transcription and DNA repair by recruiting HAT complexes to chromatin[16]. TRRAP is a monomeric component of two large macromolecular assemblies, the Spt-Ada-Gcn5 acetyltransferase complex (SAGA) and the nucleosome acetyltransferase of H4 complex (called NuA4 in yeast and TIP60 in mammals)[25].

SMG1 primarily controls nonsense-mediated mRNA decay (NMD): mRNAs with premature stop codons or inappropriately spliced mRNAs[26]. The key event in NMD is SMG1-mediated phosphorylation of the RNA helicase UPF1[27-29], allowing the recruitment of downstream effectors, which results in degradation of premature mRNA[26]. SMG1 forms a complex with two cofactors, SMG8 and SMG9[30]. Recently, high-resolution structural information of this complex was determined by cryo-Electron Microscopy (cryo-EM) by two groups independently[30,31].

1.2.3 mTOR exerts its functions in two distinct multiprotein complexes

mTOR exists as two structurally and functionally distinct complexes: mTOR complex 1 and 2 (mTORC1 and mTORC2) (Figure 1.3). The dimeric core of both complexes is formed by mTOR and mammalian lethal with SEC13 protein 8 (mLST8), also termed GβL[32]. Deletion of mLST8 does not affect mTORC1-mediated substrate phosphorylation[33] but impairs mTORC2 integrity[34,35]. mTORC1 contains the defining 149 kDa subunit regulatory-associated protein of mTOR (Raptor)[32,36,37]. Raptor recruits mTORC1 substrates by binding a short recognition site, termed TOR signaling motifs (TOS), which is present in several canonical mTOR substrates[38,39]. Moreover, Raptor is required for subcellular localization of mTORC1. Proline-rich Akt substrate of 40 kDa (PRAS40) interacts through its TOS motif with Raptor and negatively regulates mTORC1 by preventing substrate association[40-42]. mTORC2 is defined by the specific subunits rapamycin-insensitive companion of mTOR (Rictor)[43,44], stress-activated map kinase-interacting protein 1 (SIN1)[45,46] and it associates with the facultative subunit protein observed with Rictor-1/2 (Protor-1/2)[47,48]. DEP domain-containing mTOR interacting protein (DEPTOR) is a negative regulator of both complexes and is the only known protein inhibitor interacting with both mTORC1 and mTORC2 [49].

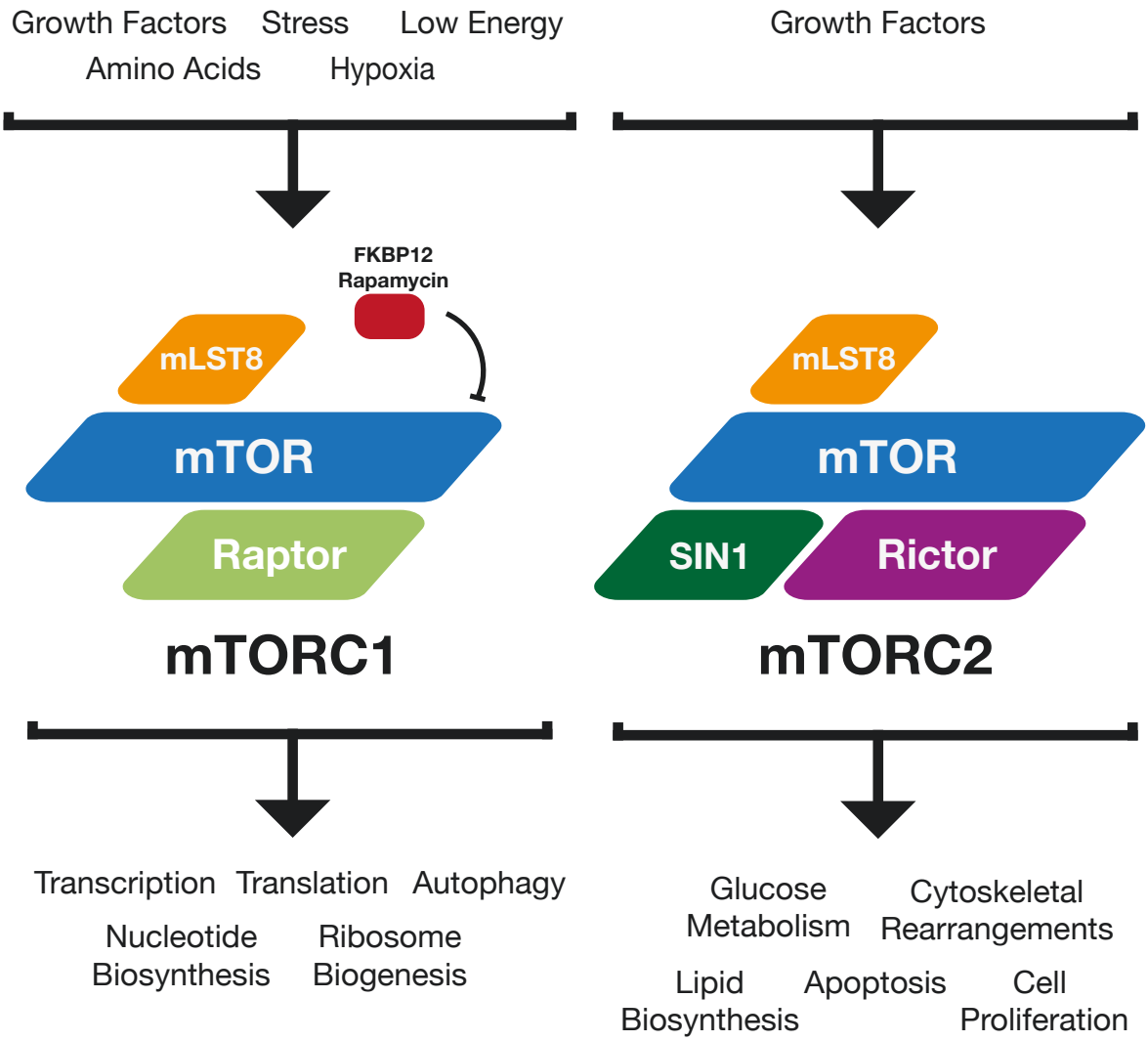

Figure 1.3 mTOR complex 1 and 2 assembly factors and signaling
The mTOR complexes regulate cell growth and metabolism by integrating environmental inputs such as growth factors and amino acids. mTORC1 is composed of three core components: mTOR, Raptor and mLST8 and it is sensitive to rapamycin. mTORC2 contains mTOR, mLST8, Rictor and SIN1 and is insensitive to acute rapamycin treatment.

mTORC1 is acutely inhibited by the macrolide rapamycin [50-52], whereas mTORC2 is not inhibited by rapamycin but chronic rapamycin treatment impairs mTORC2 formation[53]. While mTORC1 regulates cell growth and metabolism upon response to growth factors and amino acids[54], mTORC2 is activated by insulin and phosphoinositide 3-kinase (PI3K) signalling[55,56] and, in turn, controls cell survival, proliferation and lipid biosynthesis[57-59].

1.2.4 Upstream regulators of mTORC1

mTORC1 integrates upstream signals including amino acids and growth factor levels, energy and stress to trigger its activation (Figure 1.4). Activation of mTORC1 occurs when the presence of amino acids stimulate mTORC1 translocation from the cytosol to the lysosome, where it encounters the small G protein Ras homolog enriched in brain (Rheb), and growth factors activate lysosomal Rheb, enabling it to activate mTORC1 in turn[54].

Growth factors

Insulin or insulin-like growth factor 1 (IGF1) stimulates mTORC1 activity via the phosphatidylinositol-4,5-bisphosphate 3-kinase (PI3K) pathway[60]. Upon binding of growth factors to the receptor tyrosine kinases (RTKs), RAC-alpha serine/threonine-protein kinase (AKT), ribosomal protein S6 kinase alpha-1 (RSK1) as well as extracellular-signal-regulated kinase 1/2 (ERK1/2) are activated, resulting in inhibitory phosphorylation of the tuberous sclerosis complex (TSC)[54]. The TSC complex consists of TSC1, TSC2, and TBC1D7, and has GAP activity toward Rheb, inducing the switch from active Rheb-GTP state to inactive Rheb-GDP bound state.[61,62]. GTP-bound Rheb binds to mTORC1 at an allosteric site remote from the kinase domain and renders the latter into a catalytically competent configuration[42]. Independently of TSC and Rheb, growth factors can also modulate mTORC1 activity through PRAS40, a negative regulator of mTORC1[41]. PRAS40 acts by associating with Raptor, mTOR and mLST8 and blocking the substrates-recruitment sites on mTORC1[40-42].

Amino acids

Amino acids are a major input signal for mTORC1 signaling. In particular, leucine and arginine are essential for mTORC1 activity in mammalian cells[63]. Amino acid signaling is transmitted to mTORC1 by the heterodimeric complex of two Rag GTPases, RagA or RagB and RagC or RagD[64]. The RagA/B-RagC/D complex localizes to the lysosome by binding the pentameric Ragulator complex. The Ragulator includes the subunits p18, p14, MP1, C7orf59 and HBXIP, also termed LAMTOR1-LAMTOR5[65-67] and is anchored to the lysosomal lipid bilayer via myristoylation and palmotoylation of the p18 subunit[65,67,68]. Under amino acid-replete conditions, RagA/B is bound to GTP and RagC/D is bound to GDP (RagA/B-GTP:RagC/D-GDP), whereas the nucleotide binding status of the Rags is inversed under amino acid starvation (RagA/B-GDP and RagC/D-GTP) [64,69]. The RagA/B-GTP:RagC/D-GDP form binds Raptor, leading to recruitment of mTORC1 to the lysosome for subsequent activation by Rheb[54]. Recent structural analyses of RagA-GTP:RagC-GDP in complex with mTORC1[70] or

with Raptor-Ragulator[71] revealed the binding site of RagA-GTP on Raptor. The signaling cascade from amino acid sensing to the nucleotide binding state of the Rags is tightly regulated by a series of upstream factors with GAP or GTP exchange factor activity, among which an important one is the trimeric GAP activity toward Rags (GATOR1) complex[72]. At low amino acids levels, GATOR1 hydrolyzes the GTP bound to RagA/B, resulting in inability of the Rags to bind mTORC1[73,74]. GATOR1, in turn, is regulated by other upstream factors, including the complex KICSTOR consisting of the subunits KPTN, ITFG2, C12orf66 and SZT2, which acts by tethering GATOR1 to the lysosome[75,76]. GATOR1 interacts also with the negative regulator GATOR2 but the molecular mechanisms of this interaction still need to be elucidated. GATOR2 is considered to be involved in leucine and arginine sensing[77]. In the absence of leucine, the leucine sensor Sestrin-2 binds and inhibits GATOR2, preventing the inhibition of GATOR1 and therefore recruitment of mTORC1 to the lysosomal surface[78]. During leucine stimulation, amino acids bind Sestrin-2, which dissociates from GATOR1 and ultimately leads to RagA/B being GTP-loaded and able to bind mTORC1[77,78]. GATOR2 is also involved in arginine sensing via interaction with cellular arginine sensor for mTORC1 1 (CASTOR)[79]. In a similar mechanism as Sestrin-2, CASTOR1 inhibits GATOR2 in the absence of arginine. When the latter is present, CASTOR1 binds to it and dissociates from GATOR2[79,80]. An additional arginine sensing mechanism is provided by SLC38A9, a lysosomal transmembrane protein which regulates mTORC1 signaling through the Ragulator-Rags complex[81]. A further sensing pathway for amino acids known to date is the folliculin-mediated pathway (FLCN) with its binding partners folliculin-interacting protein 1 and 2 (FNIP1 and FNIP2) complex, identified as the GAP for RagC/D and thus positively regulating mTORC1[82,83] and the glutamine sensing pathway involving the glutaminolysis product α-ketoglutarate[84].

Energy and oxygen availability, and other cellular stresses

Under scarce availability of energy and oxygen, several cellular processes act to suppress mTORC1 signaling. The primary supply of energy for the cell is adenosine triphosphate (ATP) and its levels are sensed by the AMP-activated protein kinase (AMPK) complex[60]. AMPK phosphorylates TSC2 at Thr1227 and Ser1345 and therefore leads to TSC2 activation and subsequent mTORC1 inhibition[85]. Moreover, AMPK inhibits mTORC1 by phosphorylation of Raptor at Ser722 and Ser792[86]. Interestingly, cyclic AMP-dependent protein kinase (PKA) phosphorylates Raptor on Ser791, but not Ser792, and it has been reported to inhibit[87] or activate mTORC1[88].

An additional inhibitory input of mTORC1 is oxidative stress. Reactive oxygen species (ROS) upregulate DNA-damage-inducible transcript 4 (DDIT4) protein, also known as protein regulated in development and DNA damage response 1 (REDD1) that activates TSC[89,90].
Other cellular stresses, such as DNA damage, act as negative regulators of mTORC1. The tumor suppressor p53, activated in response to DNA damage, induces upregulation of AMPK β subunit, PTEN and TSC2, which all together contribute to inhibiting mTORC1 activity[91].

1.2.5 Downstream effectors of mTORC1

The two mTOR complexes integrate the availability of nutrients, energy and presence of growth factors and, in turn, respond by adjusting anabolic and catabolic processes. mTORC1 phosphorylates substrates that increase the production of proteins, lipids, nucleotides and ATP and substrates that inhibit autophagy (Figure 1.4).

Protein synthesis

Protein synthesis is the most energy-consuming process in a growing cell[92]. mTORC1 tightly regulates this process by phosphorylating eukaryotic initiation factor 4E-binding proteins (4E-BPs) to promote cap-dependent translation[93,94] and p70 S6 kinase 1 (S6K1)[95]. mTORC1 phosphorylates S6K1 at Thr389, leading to a subsequent phosphorylation at Thr229 by phosphoinositide-dependent kinase 1 (PDK1) and full activation of S6K to induce translation initiation and elongation[95,96]. S6K1 and mTORC1 directly upregulate the activity of the RNA polymerase I and RNA polymerase III through phosphorylation of the regulatory factors upstream binding factor (UBF)[97], transcription initiation factor 1A (TIF-1A) [98] and MAF1[99]. S6K phosphorylates diverse substrates, including insulin receptor substrate 1 (IRS1). This phosphorylation inhibits IRS1 and, thus, activates a negative feedback loop acting on PI3K and mTORC2[100].

Lipid and nucleotide biosynthesis

Cells need lipids to form new membranes during cell growth. mTORC1 modulates lipid metabolism via the transcription factors sterol regulatory element binding protein 1/2 (SREBP1/2) and peroxisome proliferator-activated receptor-γ (PPARγ). SREBP1/2 can be activated by S6K1 in a mechanism that remains unclear[101] or via Lipin-1[102]. Activated mTORC1 phosphorylates Lipin-1, preventing its translocation to the nucleus and therefore allowing expression of SREBP1/2[102]. PPARγ is modulated simultaneously by the mTORC1 and PI3K/AKT pathways to regulate nutrient availability and insulin signals[103].

mTORC1 facilitates DNA replication and rRNA synthesis in proliferating cells. It induces purine synthesis via the tetrahydrofolate cycle through activation of the transcription factor Activating Transcription Factor 4 (ATF4) and its downstream target, mitochondrial tetrahydrofolate cycle enzyme methylene-tetrahydrofolate dehydrogenase 2 (MTHFD2)[104]. mTORC1 also promotes pyrimidine synthesis by phosphorylating and activating carbamoyl-phosphate synthetase 2, aspartate transcarbamylase, and dihydroorotase (CAD) via S6K[105,106].

Autophagy

To balance sources of energy at critical times in development and in response to nutrient stress, cells respond with a self-degradative mechanism called autophagy. Autophagy is crucial when the availability of nutrients is scarce. mTORC1 suppresses autophagy by inhibitory phosphorylation of the autophagy-inducing kinase unc-51-like autophagy-activating kinase 1 (ULK1)[107]. mTORC1 also suppresses autophagy by phosphorylating and thus inhibiting the transcription factor EB (TFEB). Together with the related transcription factor E3 (TFE3), TFEB is involved in the activation of genes for lysosomal biogenesis[108-110].

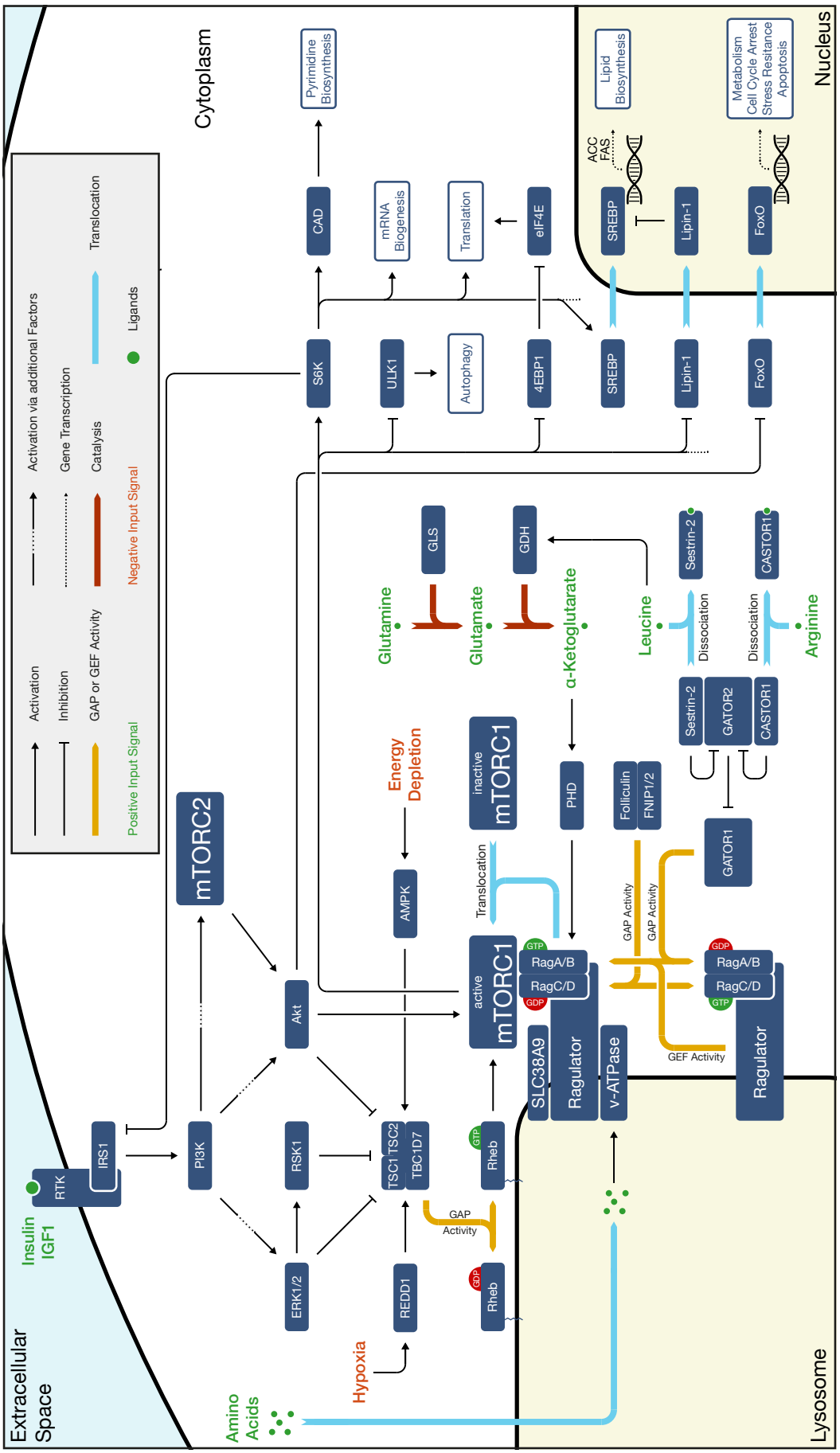
Extracellular Space
Cytoplasm
Nucleus
Lysosome
Activation
Inhibition
GAP or GEF Activity
Positive Input Signal
Activation via additional Factors
Gene Transcription
Catalysis
Negative Input Signal
Translocation
Ligands
Insulin
IGF1
RTK
IRS1
PI3K
Akt
mTORC2
ERK1/2
RSK1
TSC1 TSC2
TBC1D7
REDD1
Hypoxia
Amino Acids
Rheb
GTP
GDP
GAP Activity
AMPK
Energy Depletion
inactive mTORC1
active mTORC1
Translocation
RagA/B
RagC/D
Ragulator
SLC38A9
v-ATPase
GAP Activity
GEF Activity
PHD
α-Ketoglutarate
Glutamine
Glutamate
GLS
GDH
Leucine
Arginine
Sestrin-2
CASTOR1
GATOR2
GATOR1
Dissociation
Folliculin
FNIP1/2
S6K
ULK1
Autophagy
4EBP1
eIF-4E
CAD
mRNA Biogenesis
Translation
Pyrimidine Biosynthesis
SREBP
Lipin-1
FoxO
ACC
FAS
Lipid Biosynthesis
Metabolism
Cell Cycle Arrest
Stress Resitance
Apoptosis

Figure 1.4 mTORC1 signaling pathway
mTOR responds to environmental cues such as amino acids, which localize mTORC1 to the lysosomal surface through the Rags-Ragulator complex. Here, mTORC1 is activated by Rheb, which is activated by growth factor stimulation via PI3K signaling. mTORC1 also responds to cellular energy status and oxygen levels. mTORC1 has effects on a multitude of metabolic processes through phosphorylation of its substrates. Figure adapted from Imseng, S. PhD Thesis[17].

1.2.6 Upstream regulators of mTORC2

Since its discovery, rapamycin has been a potent tool to elucidate the mTORC1-signaling network. Due to the mTORC2 insensitivity to short-term rapamycin treatment, research on mTORC2 signaling is more challenging and its regulators are therefore less well characterized than those of mTORC1. The activation of mTORC2 is mainly dependent on insulin/PI3K signaling (Figure 1.5).

Growth factors and Insulin

The regulation of mTORC2 activity has been largely explored through receptor signaling by growth factors such as insulin and IGF and through its connection with AKT signaling. Binding of growth factors to RTKs leads to activation of PI3K, which phosphorylates the plasma membrane phospholipid phosphatidylinositol-4,5-bisphosphate (PIP2) to generate phosphatidylinositol 3,4,5-trisphosphate (PIP3)[56,111]. PIP3 acts as a second messenger and interacts with the pleckstrin homology (PH) domains of AKT and phosphoinositide-dependent kinase 1 (PDK1). PIP3 binding results in their translocation from the cytosol to the plasma membrane[112]. In a similar fashion, PIP3 was reported to interact with the PH domain of mTORC2's unique component, SIN1[45]. However, alternative recruitment mechanisms have been proposed: one, in which upon growth factor stimulation, a pool of mTORC2 is recruited to the plasma membrane through the SIN1 PH domain, which is present only in SIN1.1 and SIN1.2 isoforms[45]. A second mechanism suggests that SIN1.1 does not translocate to the plasma membrane in response to insulin stimulation, proposing a model in which a pool of mTORC2 is stably present at the plasma membrane [113]. Furthermore, in agreement with mTORC2-mediated-PIP3 stimulation [111], Yue *et al.*, report that deletion of the Phosphatase and TENsin homolog deleted on chromosome 10 (PTEN), which converts PIP3 to PIP2, increases mTORC2 activity in muscle stem cells[114]. Accumulation of PIP3 in the cell and subsequent recruitment of AKT and PDK1 to the plasma membrane is stimulated also through G protein-coupled receptors (GPCRs) that activate phospholipase C (PLC)[115]. In summary, growth factor stimulation act via PI3K and PIP3 to induce translocation of AKT and

PDK1 and mTORC2 to the plasma membrane. There, PDK1 and mTORC2 phosphorylate AKT for full activation [116].

Ribosome

A yeast-genetic screen reveals that the ribosome is required for TORC2 signaling and studies in mammalian cells suggest that insulin-stimulated PI3K signaling promotes mTORC2-ribosome association, and stimulates AKT phosphorylation by mTORC2. [56]. This is in line with a study from Oh *et al*., that shows colocalization of actively translating ribosomes with mTORC2 and interaction of the latter with the large ribosomal subunit protein rpL23a [117]. mTORC2 mediates phosphorylation of the nascent polypeptide at the turn motif (TM) site, Thr450, of Akt1, to determine proper conformation of the AKT nascent chain[117].
mTORC2 associates with membranes such as those of[118], endosomes[113], the endoplasmic reticulum (ER)[119] and the Golgi apparatus[120,121], suggesting that mTORC2 might associate specifically with membrane-bound ribosomes.

Small GTPases

The upstream regulation which modulates mTORC1 signaling has been extensively studied and recent progresses have been made in elucidating the mTORC1 binding and the activation mechanism by the small GTPase Rheb[42]. Several small GTPases have been suggested to be mTORC2 activators but the individual mechanisms are unknown. In several model systems, including *Dictyostelium discoideum*, the small GTPase Rap1 binds mTORC2 and positively regulates cell migration[122], while Rac1 binding to mTORC2 induces cell growth[123]. Moreover, AKT phosphorylation by mTORC2 was suggested to be stimulated by the GDP-bound small G protein Rho GTPase, which assembles in a complex with Ras–GTP and mTORC2[124]. A recent study in human cells suggests the small GTPase Ras to be the mTORC2 activator[125]. An integrated approach of proteomics and CRISPR genetics identified wild-type (WT) and mutated Ras as proximal to mTORC2[125]. Oncogenic Ras directly binds to the mTORC2 components mTOR and SIN1 and stimulates mTORC2 kinase activity at the plasma membrane[125]. These findings reinforce mTORC2 activation by small GTPases, but the exact mechanisms await structural characterization.

Lipids

Lipid species, in particular phosphatidic acids (PAs), are linked to both mTORC1 and mTORC2 regulation[126].

Phosphatidic acid is not only a building block for the synthesis of other lipids, but also a second messenger for several signaling proteins, including protein kinases and phosphatases[127]. PA binds to the FRB domain of mTOR[128,129]. A recent study suggests that PA induces translocation of mTORC1 to the lysosome and its activation through the phospholipase D (PLD)-PA pathway in the absence of amino acids, Rag GTPases, growth factors or Rheb[130]. Less is known about the role of PA upstream of mTORC2. Exogenous fatty acids via the *de novo* synthesis of PA activate mTORC2 in various cancer cell lines[126]. By contrast, PA was also shown to disrupt the mTORC2 complex assembly in primary hepatocytes[131]. These discordant findings need to be elucidated to explore if PA can have different effects on mTORC2 in different cell lines and subcellular localizations.

Energy availability

Monitoring the energy level in a cell is an essential function. The major source of energy is ATP, whose levels are sensed by the protein kinase AMPK. As discussed in chapter 1.2.4, AMPK negatively regulates mTORC1 at low ATP levels[60]. Decreasing glutamine catabolites[132] and AMPK activation[133] increase mTORC2 activation. Activated AMPK directly phosphorylates mTOR and Rictor, leading to stimulated AKT phosphorylation and increased cell survival[133].

1.2.7 Downstream effectors of mTORC2

mTORC2 is activated by insulin and phosphoinositide 3-kinase (PI3K) signaling and acts on cell proliferation, cytoskeletal organization and lipid biosynthesis by phosphorylating members of the protein kinase A, protein kinase G and protein kinase C (AGC) kinase family[58,134,135] (Figure 1.5).

Cell proliferation

mTORC2 promotes cell proliferation mainly by activating the substrate AKT, which in turn acts on a large set of substrates including transcription factors, proteins and lipid kinases, as well as ubiquitin ligases[116]. The first AKT substrate to be reported was the Ser/Thr protein kinase glycogen synthase kinase 3 (GSK3)[136]. AKT exerts an inhibitory phosphorylation on GSK3, which no longer phosphorylates and inhibits its downstream targets involved in control of cell survival or proliferation[137]. mTORC2-mediated activation of AKT drives cell survival and proliferation through inhibitory phosphorylation of the transcription factor Forkhead-box (FOXO1/3a) under growth-promoting conditions[138]. Activation of PI3K-AKT

signaling leads to translocation of FoxO proteins from the nucleus and inhibition of their transcriptional activity[138,139].

Cytoskeletal Rearrangements

mTORC2 regulates actin filament and cytoskeleton reorganization through phosphorylation of the protein kinase Cα (PKCα)[43,44]. More recent studies show that mTORC2 also phosphorylates several other members of the PKC family, including PKCδ[140], PKC[141], as well as PKCγ and PKCε[142], all of which are involved in cytoskeletal remodeling and cell migration. PKC acts through Rho GTPases and is the main effector of mTORC2-mediated migration[143]. Studies in mammals also report regulation by cAMP production as a means of mTORC2 modulation of neutrophil chemotaxis[144]. mTORC2 acts on the small Rho GTPases Rac1 and Cdc42 to regulate actin assembly and organization in neutrophils[144]. Knockdown of mTOR, Rictor or mLST8 showed defects in actin reorganization and decreased Rac1 activation upon serum restimulation[43,44]. An early study suggests that Rac1 associates with mTOR in both mTORC1 and mTORC2, [123] but the mechanism through which cytoskeleton reorganization is mediated remains to be elucidated. In contrast, another study in a HER2-amplified breast cancer has shown how active Rac1 was required for Rictor-dependent invasion and motility, and rescue of invasion and motility in Rictor depleted cells, suggesting that Rictor interacts with Rac1[145]. Moreover, mTORC2 suppresses the endogenous inhibitor of Rac1, Rho guanine nucleotide dissociation inhibitor 2 (RhoGDI2) through phosphorylation of PKC[145,146]. mTORC2 and RhoA can further regulate chemotaxis in neutrophils by regulation of F-actin polarization and myosin II phosphorylation, independent of actin cytoskeletal reorganization[147]. A study from Sato *et al.*, suggests that mTORC2 regulates focal adhesions and cell migration by direct phosphorylation of the actin cross-linking protein Filamin A at Ser2152[148]. Filamin A is a large protein that crosslinks actin filaments and is involved in anchoring membrane proteins to the actin cytoskeleton[149]. mTORC2 phosphorylation of Filamin A at Ser2152 can accelerate cell mobility in wound-healing assays[148].

Glucose Metabolism

Recent studies have linked mTORC2 to glucose metabolism and homeostasis. mTORC2 signaling regulates several aspects of glucose metabolism, including glucose uptake, glycolysis, gluconeogenesis, and oxidative phosphorylation[150]. In response to growth factors, mTORC2 activates glucose metabolism through two main factors, AKT and c-Myc. Rictor knockouts in the liver, adipose tissue, and muscle induce deficiency in glucose uptake. The

individual studies, however, conclude different mechanisms[151-153]. In liver-specific Rictor knockout mice, glucose uptake is decreased due to reduced glucokinase and SREBP1c activity[154]. This leads to constitutive gluconeogenesis, impaired glycolysis and lipogenesis[154]. In the adipose tissue, regulation of glucose uptake by mTORC2 is exerted via two different effectors in the brown (BAT) and white adipose tissue (WAT)[151,153]. In BAT, mTORC2 acts via Akt1 S473 phosphorylation which in turn activates the hexokinase, but does not directly affect glucose transporter 1 (GLUT1) and GLUT4 translocation[151]. In WAT, mTORC2 regulates glucose uptake in an AKT-independent manner via Carbohydrate-responsive element–binding protein (ChREBPβ) expression[153]. mTORC2 is also involved in glucose metabolism by regulating glycolysis in an AKT dependent and independent manner[155]. In glioblastoma, mTORC2 phosphorylates and thereby inactivates Class IIa histone deacetylases (HDAC), causing an increase of FoxO1 and FoxO3 acetylation. This in turn promotes upregulation of c-Myc and thus expression of glycolytic genes through suppression of miR-34-c[156]. Overall, mTORC2 promotes glucose metabolism through different cell- and tissue-specific mechanisms.

Lipid Metabolism

mTORC2 stimulates lipogenesis and inhibits lipolysis[157]. mTORC2 promotes lipogenesis via AKT-dependent and -independent mechanisms. mTORC2 phosphorylation of AKT induces activation of the transcription factors SREBP and hREBP, which in turn regulate expression of lipogenic genes, such as ATP-citrate lyase (ACLY), acetyl-CoA carboxylase (ACC), fatty acid synthase (FAS), and stearoyl-CoA desaturase (SCD1)[55]. Moreover, Akt1 prevents SREBP1 degradation in cancer cells[158]. In PTEN- and TSC1- deficient mice, mTORC2 was shown to promote liver cancer, at least in part by activating SREBP1[58]. A study in HER2-positive and PI3K-mutant breast cancer cells revealed mTORC2-AKT dependent phosphorylation and activation of ACLY and promotion of cell growth[159]. A recent study reinforces the role of mTORC2 in *de novo* lipogenesis and show that mTORC2-Akt signaling acts on ACLY during brown adipocyte differentiation[160]. mTORC2-AKT dependent ACLY phosphorylation induces acetyl-CoA synthesis and *de novo* lipogenesis in a signaling pathway downstream of glucose uptake and glycolysis[160].

Ion Transport

Electrolyte homeostasis is a tightly regulated process in mammals. The central player of Na^+/K^+ regulation is the epithelial Na^+ channel (ENaC), which drives K^+ transport across the

apical membrane and Na^+ reabsorption[161]. This process involves aldosterone, which stimulates transcription of Sgk1[162] and in part depends on mTORC2[163,164]. mTORC2 signaling has been linked to Na^+/K^+ homeostasis, mainly via phosphorylation and activation of Sgk1[165]. Several *in vitro* and *in vivo* studies using cell systems and genetically modified mice have revealed that mTORC2 acts through Sgk1 to regulate a wide variety of transporters. These include Na^+/K^+ -ATPase, the carrier Na^+/H^+ exchangers (NHE1) and (NHE3) and several ion channels, such as ENaC and the renal outer medullary K^+ channel (ROMK)[166]. In the connecting tubule and in the collecting duct, insulin and IGF increase Na^+ reabsorption through activation of mTORC2-Sgk1, which inhibits degradation of ENaC by phosphorylating the ubiquitin ligase Neural Precursor Cell Expressed Developmentally Downregulated Gene 4-2 (NEDD4-2)[166]. Sgk1 is further involved in the upregulation of ROMK, a potassium channel for renal tubular K^+ secretion[167]. At high K^+ conditions, mTORC2 is upregulated and increases the activity and abundance of ROMK via phosphorylation of Sgk1 and PKCα. However, the underlying mechanism leading to upregulation of mTORC2 expression remains unclear.

Apoptosis

Apoptosis is a cellular mechanism that involves cell changes and cell death. It plays a pivotal role in the pathogenesis of several disease. mTORC2 negatively regulates apoptosis through various effectors and in different tissues. The best studied link between mTORC2 and apoptosis is through inhibition of the transcription factor FoxO3a[168]. Another mechanism of mTORC2-driven apoptosis involves increased c-Myc phosphorylation and expression, which inhibits expression of the transcription factor E2F1 and causes enhanced apoptosis[169].

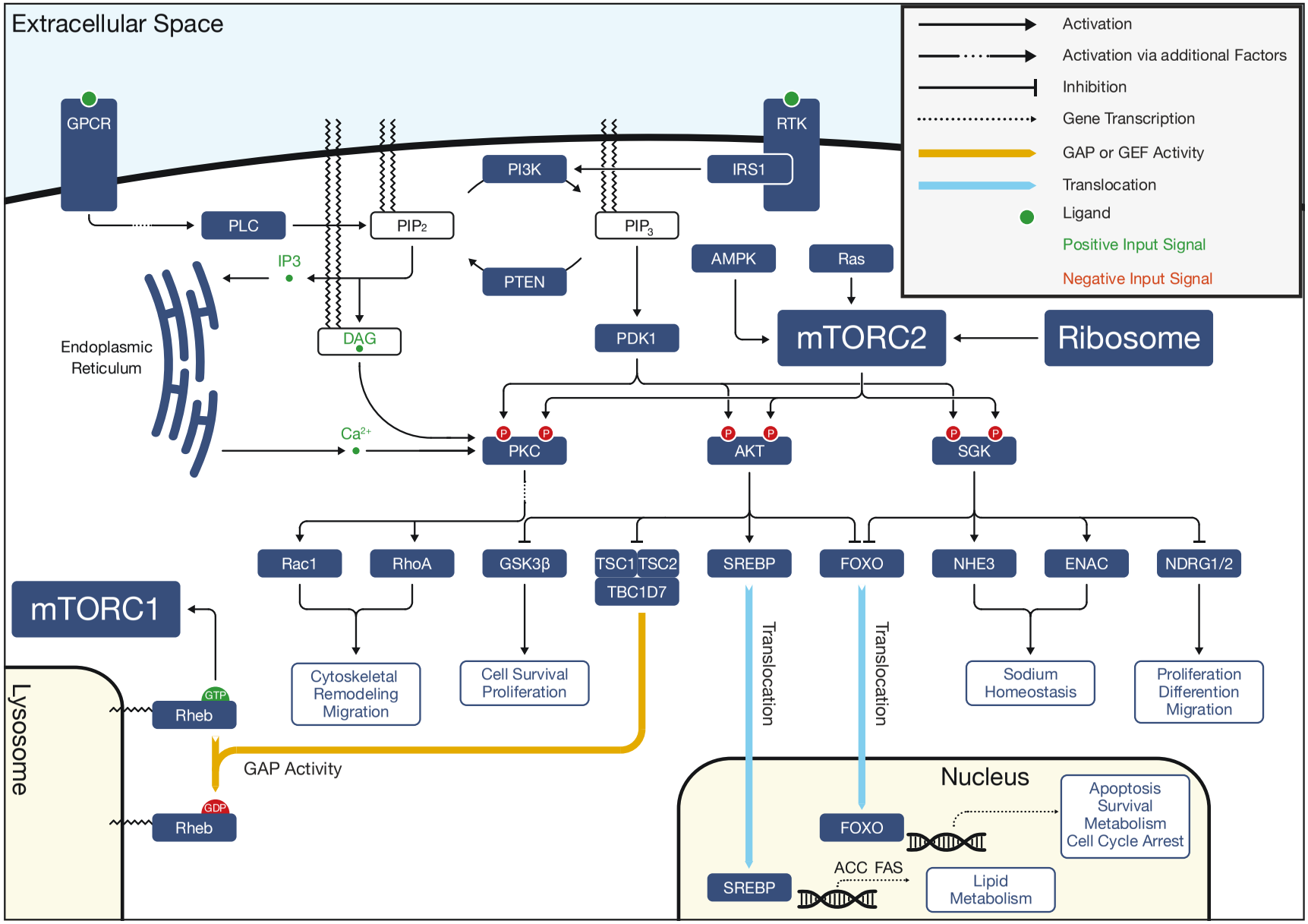
Extracellular Space
Activation
Activation via additional Factors
Inhibition
Gene Transcription
GAP or GEF Activity
Translocation
Ligand
Positive Input Signal
Negative Input Signal
GPCR
RTK
PI3K
IRS1
PLC
PIP2
PIP3
IP3
PTEN
AMPK
Ras
Endoplasmic Reticulum
DAG
PDK1
mTORC2
Ribosome
Ca2+
PKC
AKT
SGK
Rac1
RhoA
GSK3β
TSC1 TSC2
TBC1D7
SREBP
FOXO
NHE3
ENAC
NDRG1/2
mTORC1
Translocation
Translocation
Cytoskeletal Remodeling Migration
Cell Survival Proliferation
Sodium Homeostasis
Proliferation Differention Migration
Lysosome
GTP
Rheb
GDP
Rheb
GAP Activity
Nucleus
FOXO
Apoptosis Survival Metabolism Cell Cycle Arrest
SREBP
ACC FAS
Lipid Metabolism

Figure 1.5 mTORC2 signaling pathway
mTORC2 is mainly activated by growth factor stimulation via PI3K signaling. Activated mTORC2 affects a variety of processes as indicated. Through phosphorylation of its substrates AKT, PKC and SGK, mTORC2 promotes cell survival and proliferation, cytoskeletal rearrangement, sodium homeostasis, lipid metabolism and the inhibition of apoptosis. Figure adapted from Imseng,S. PhD Thesis[17].

1.2.8 The AGC family kinases

mTORC2 mainly acts by direct phosphorylation and regulation of several members of the AGC family of protein kinases, including AKT, PKC and SGK. The AGC kinases consists of 63 evolutionary related Ser/Thr protein kinases which are divided into 14 families and 21 subfamilies. The members are PDK1, AKT, SGK, PKC, protein kinase C related kinase (PRK, also termed PKN for protein kinase N), mitogen- and stress-activated protein kinase (MSK), ribosomal S6 kinase (RSK), p70 ribosomal S6 kinase (S6K), cAMP-dependent protein kinase (PKA), cGMP-dependent protein kinase (PKG), myotonin protein kinase (DMPK), myotonic dystrophy kinase-related CDC42-binding kinase (MRCK), ROCK, nuclear DBF2-related kinase (NDR), large tumor suppressor (LATS), citron Rho-interacting kinase (CRIK), microtubule-associated Ser/Thr kinase (MAST), G protein-coupled receptor kinase (GRK), Sugen kinase 494 (SGK494) and RSK-like (RSKL) [170]. AGC kinases share common structural features and 42 out of the 63 members have evolved independent mechanisms of regulation through additional regulatory domains that mediate kinase activity and localization [171]. The AGC members show the typical bilobal kinase fold, that was first identified by the crystal structure of the catalytic domain of PKA[172]. The catalytic domain consists of a small N-terminal lobe and a large C-terminal lobe, with the ATP binding site located in a deep cleft between the two lobes (Figure 1.6).

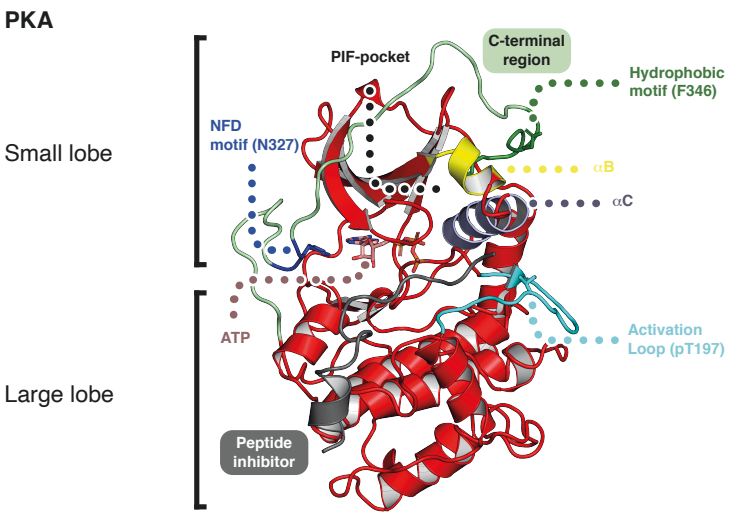

Figure 1.6 Crystal structure of PKA.
The structure of PKA (PDB code 1ATP[173]) shows common features of protein kinases: a small N-terminal lobe and a large C-terminal lobe. Activation loop and hydrophobic motif, important for regulation, are labelled. αB and αC helices, shown in yellow and light blue respectively, are involved in flexibility and dynamics of the two lobes. The peptide inhibitor (in grey) binds between the two lobes.

The big lobe is alpha helical, while the small lobe consists of a five stranded β–sheet and the alpha helix αC, which is contiguous to the alpha helix αB. The activation loop emerges from a DFG-motif and is located between the large lobe and the helix αC in the small lobe. Substrates bind in an extended conformation in the cleft between the two lobes. The presence of a hydrophobic motif (HM) at the C-terminus is characteristic for AGC kinases. The HM has a consensus FTXXFTSTFT sequence and binds into a hydrophobic site in the small lobe of the kinase core, named PIF-pocket after its identification in PDK1[174,175]. In addition, most AGC kinases, except for PDK1, GRKs 1,4-7 and MASTL have a phenylalanine residue in a conserved NFD motif at the C-terminus, which interacts with the adenine of ATP in the catalytic domain. Overall, AGC kinases are very dynamic proteins with a high degree of flexibility. This is due to the activation loop and the αB and αC helices, which contribute to protein flexibility and are targets of activating or inhibitory mechanisms[176]. Indeed, phosphorylation at the activation loop affects the dynamics of the small and large lobes, stabilizing the αC helix and therefore the kinase active conformation[177]. For many but not all AGC kinases, phosphorylation of a conserved Ser or Thr residue on the hydrophobic motif is requisite for full activation[5].

1.2.9 Activation and regulation of the AGC kinases AKT, SGK and PKC

AKT

Since its discovery 25 years ago, the Ser/Thr kinase AKT, also known as PKB, has been extensively studied due to its central role in cell survival and proliferation as one of the primary effectors of PI3K signaling[116]. Mammalian genomes comprise three AKT isoforms, Akt1, Akt2 and Akt3, that play distinct roles in discrete subcellular localization as well as regulation of migration and metastasis in cancer[178-180]. With more than 80% sequence identity, the AKT isoforms share a common architecture and activation mechanism. AKT is a 57-kDa protein that consists of an N-terminal PH domain which binds to PIP3 and PIP2 with high affinity[181,182], followed by the conserved kinase domain and the C-terminal tail (Figure 1.7). The C-lobe of

the kinase domain contains the activation loop with its regulatory phosphorylation site at Thr308. The C-tail contains turn motif and the hydrophobic motif.

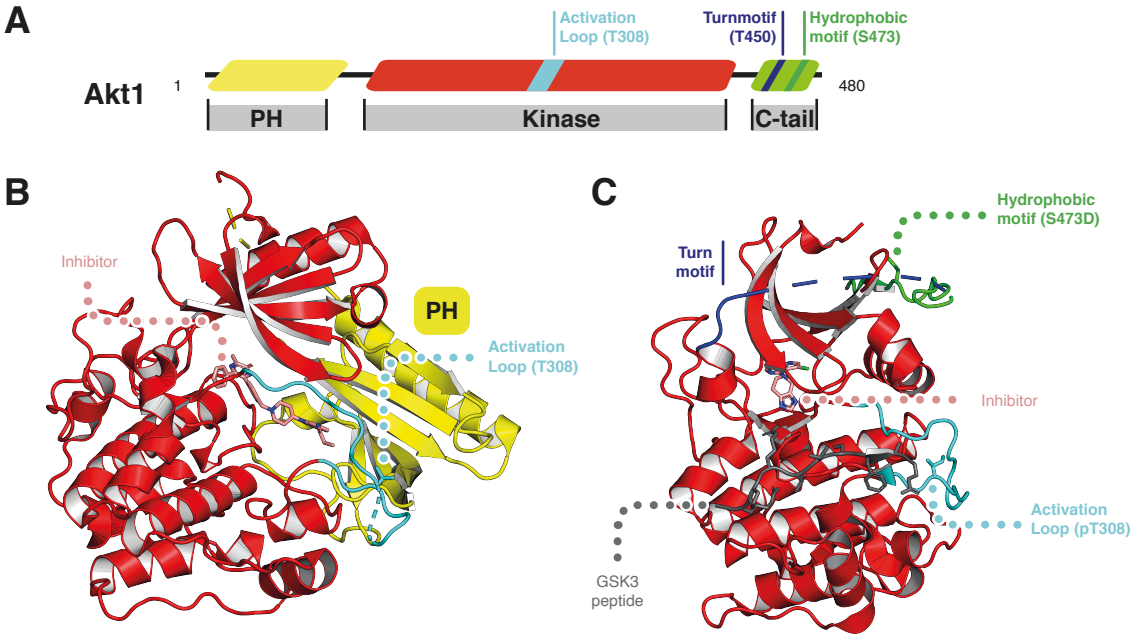

Figure 1.7 Domain architecture and structure of full-length and delta-PH human Akt1
A Schematic domain organization of full-length human Akt1. Activation loop, turn motif and hydrophobic motif are highlighted. **B** Cartoon representation of the crystal structure (PDB code: 3O96) of full-length Akt1 showing the PH domain (in yellow) closing the kinase cleft and inhibiting Akt1. Activation loop (in cyan) and bound inhibitor (in salmon) are highlighted. **C** Cartoon representation of the crystal structure (PDB code: 3CQW[183]) of delta-PH Akt1 in complex with substrate peptide GSK3 (in grey) and inhibitor (in salmon). Activation loop with the conserved phospho-Thr, hydrophobic motif and turn motif are highlighted and color coded.

In the absence of a lipid stimulus, Akt1 is constitutively phosphorylated on Thr450 in the turn motif[184]. It was suggested that the phosphorylated turn motif folds and stabilizes AKT by inducing interaction of the C-tail with the small lobe of the kinase domain by complementary interactions[184]. In the absence of growth factor stimulation, AKT is in an inactive conformation due to autoinhibition by the PH domain[185] (Figure 1.7B). This is supported by a study in which mutations in the PH-kinase domain interface lead to constitutive activation of AKT[186]. PIP3 binds to the AKT PH domain upon growth factor stimulation and PI3K activation, displacing the PH domain from the catalytic cleft, thereby relieving the autoinhibitory conformation[187]. Liberation of the PH domain exposes the activation loop and hydrophobic motif and allows phosphorylation of Thr308 (Akt1) by PDK1 and phosphorylation of Ser473 (Akt1) by mTORC2 [188-190]. Akt1 was initially thought to be activated by PDK1[188,190] but recent studies suggest that phosphorylation of Ser473 by mTORC2 precedes activation loop phosphorylation by

PDK1[191,192]. Thus, maximal activation of Akt1 requires mTORC2 phosphorylation of S473[189] while the dual phosphorylation of the activation loop and of the hydrophobic motif, creates the substrate-binding cleft and reorganize residues of the catalytic domain[193]. Recently, it was shown in *in vitro* studies that Akt1 is directly activated by both PIP3 and PIP2[194,195]. Lucic *et al*. propose a model in which, AKT is released from the plasma membrane upon activation prior to rapidly dephosphorylation and subsequent inactivation by the cytoplasmic PH domain and Leucine rich repeat Protein Phosphatases (PHLPP) and protein phosphatase 2 (PP2A)[195]. This model suggests that substrates phosphorylated by AKT must be restricted to membranes containing PI3K lipid products rather than AKT being released to the cytosol. While the majority of AKT substrates, including TSC2[196], localize to membranes, some targets such as the transcription factor FoxO do not[138]. In conclusion, additional studies are required to fully validate a model in which AKT has a PI3K-indipendent-activation and its localization is limited only to membranes.

PKC

The PKC protein kinases comprises three subclasses, which differ in the N-terminal domains: conventional (PKCα, PKCβ and PKCγ), novel (PKCδ, PKCε, PKCη and PKCθ), atypical (PKCζ and PKCλ)[197]. All PKC isozymes share structural features (Figure 1.8A): An N-terminal regulatory domain linked via a hinge region to the conserved C-terminal kinase domain with the activation loop, followed by the C-tail with the turn and the hydrophobic motif.

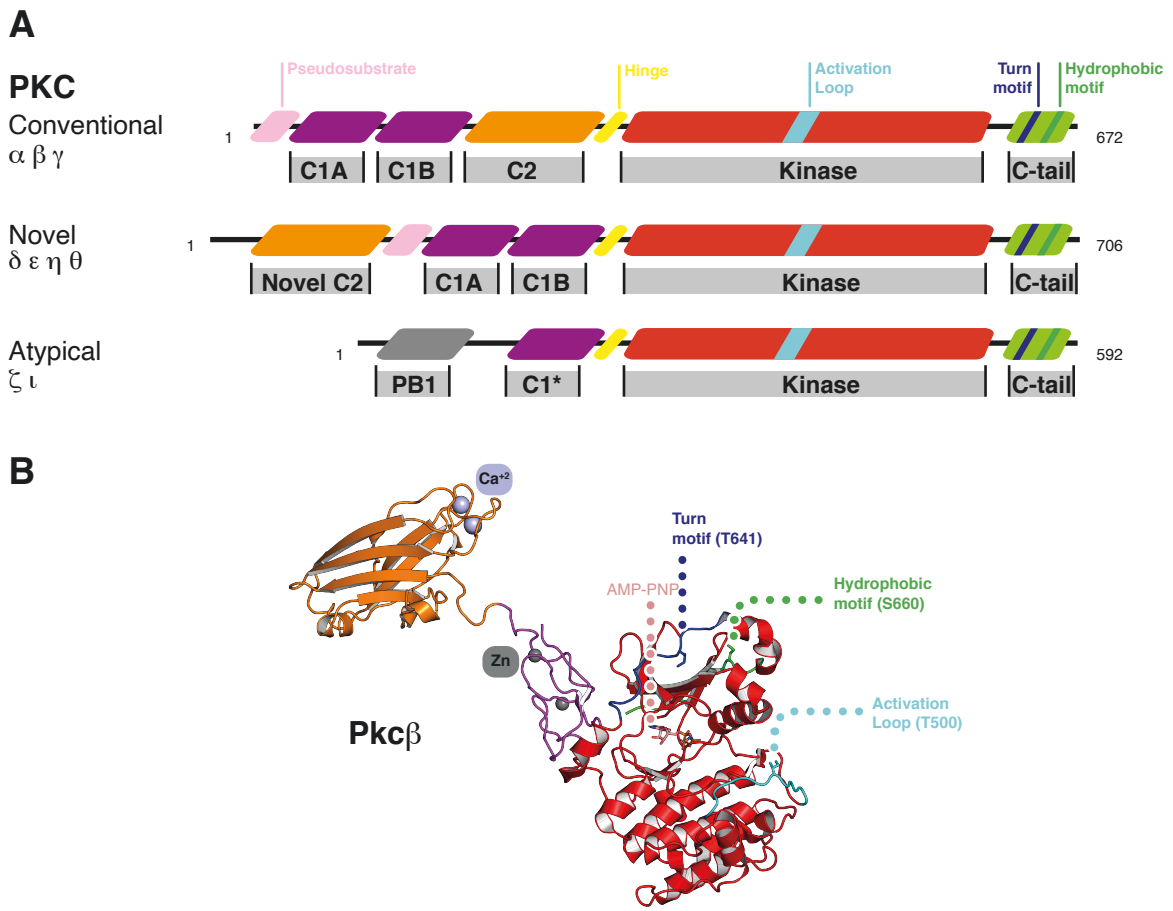

Figure 1.8 Domain architecture of PKC family and structure of full-length Pkcβ.
A The domain architecture of PKC family shows common features: conserved kinase domain (in red) and C-terminal tail (in green). The N-terminus consists of C1 (magenta) and C2 (orange) domains in conventional and novel PKC and a PB1 domain (in grey) in atypical PKC. The pseudosubstrate (in pink) is present in atypical and novel PKC. All subfamilies contain a hinge region (in yellow). Activation loop (in cyan), turn motif (in blue) and hydrophobic motif (in green) are highlighted. *Atypical PKC have an atypical C1 domain. **B** Cartoon representation of the crystal structure (PDB code: 3PFQ[198]) of full-length Pkcβ, comprising the C1B (magenta), C2 (orange), and kinase domain (red). Calcium ions are colored lightblue, AMP-PNP in salmon, turn motif in blue, hydrophobic motif in green and activation loop in cyan. Phospho-Thr500, -Thr641, and -Ser660 are shown as sticks.

PKC kinases have an internal pseudosubstrate, which binds and blocks the catalytic domain due to its sequence similarity to PKC substrates [199]. All PKC isozymes contain a single C1 domain for diacylglycerol binding, whereas conventional and novel PKC isozymes possess a tandem C1 domain (C1A–C1B)[200]. A unique characteristic of conventional PKC isozymes is the presence of a C2 domain that follows the C1 domain and is responsible for Ca^{2+} binding[201] (Figure 1.8). Atypical PKC isozymes contain a Phox and Bem 1 (PB1) domain instead that regulate binding to protein scaffolds[202].

Phosphorylation of PKC in the activation loop and in the hydrophobic motif by PDK1 and mTORC2, respectively[33,44,203], induces an autoinhibited conformation due to binding of the pseudosubstrate to the catalytic domain[199]. The conventional PKC isoforms PKCα/PKCβ, are phosphorylated on Ser657/Ser660 by mTORC2 and on Thr497/Thr500 by PDK1, respectively [5]. Upon binding of agonists to the Gq-coupled receptors (GPCR), phospholipase C (PLC) catalyzes hydrolysis of PIP2 which generates diacylglycerol and releases Ca^{2+}. This induces recruitment of PKC to the plasma membrane and binding of Ca^{2+} to the C2 domain and of diacylglycerol to the C1 domain, followed by conformational changes, and release of the pseudosubstrate and PKC activation[204]. In conclusion, unlike other AGC kinases such as AKT, an acute phosphorylation is not required for the activation of PKC. It is phosphorylated after synthesis to acquire catalytic activity and the sites remain constitutively phosphorylated[205].

SGK

The serum and glucocorticoid kinase (SGK) family of Ser/Thr kinases consists of three isoforms, SGK-1, SGK-2 and SGK-3[5](Figure 1.9 A). All three isoforms share the conserved catalytic domain and the C-terminal tail. The highest variability between isoforms is given by the N-terminus, which determines substrate specificity and turnover of the protein[206] (Figure 1.9 A). Sgk1 has four splicing isoforms which differ in length of the N-terminus. Sgk2 and Sgk3 each have two variants, whereas Sgk3 contains a PX domain (Figure 1.9 B, left panel) in the N-terminal region for PIP3 binding and for localization to early endosomes[207,208]. Sgk1, but not Sgk2 or Sgk3, is rapidly ubiquitinylated and degraded through a six amino acid hydrophobic motif at the N-terminus [209]. Similar to AKT, SGK is activated by phosphorylation of its activation loop and of its hydrophobic motif upon insulin and growth factors stimulation. The most studied SGK isoform, Sgk1, is phosphorylated by mTORC2[163] on Ser422 (Figure 1.9 A), which creates a docking site for phosphorylation of PDK1[210] on Thr256, leading to full Sgk1 activation. Unlike AKT, Sgk1 and Sgk2 do not require association with the cell membrane for their activation since they do not have a membrane binding domain[207](Figure 1.9). SGK phosphorylates substrates in a RXRXXS/T motif, similar to AKT, [211]. Indeed SGK and AKT have a certain substrate promiscuity: they both phosphorylate NDRG1[212,213], NEDD4L[214] and FOXO3A[215].

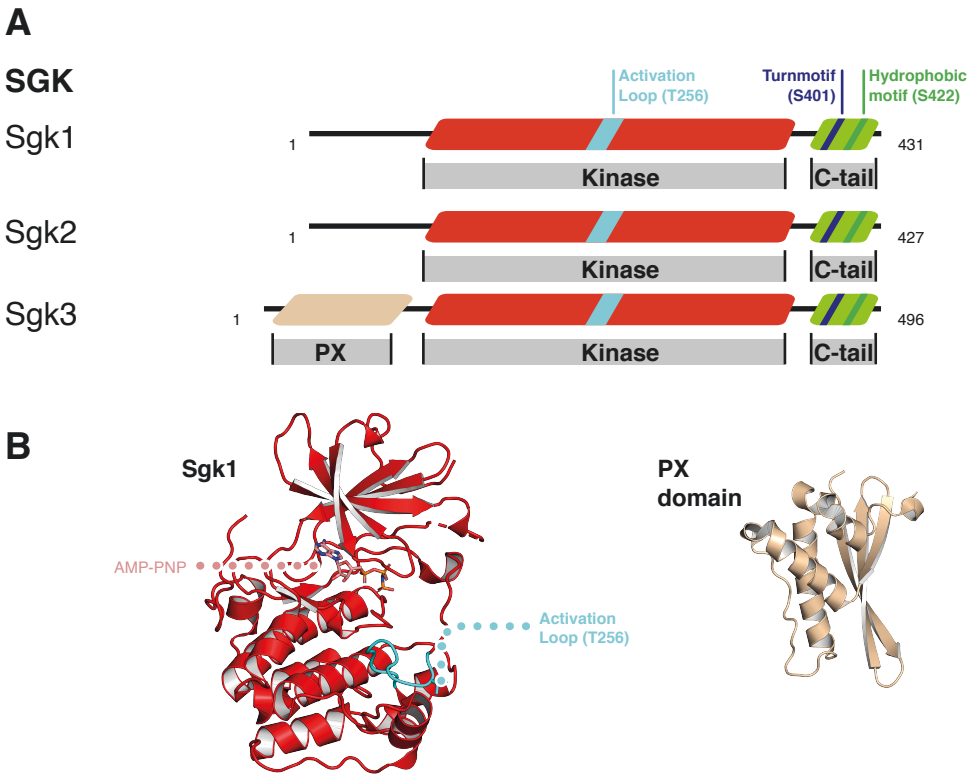

Figure 1.9 Domains in SGK kinases and structure of Sgk1 and Sgk3 PX domain
A The domain architecture of the SGK family shows common features: a conserved kinase domain (in red) and the C-terminal tail (in green). Sgk1 and Sgk2 only differ in four residues difference. Sgk3 contains at its N-terminus a PX domain. **B** On the left, cartoon representation of the crystal structure (PDB code: 2R5T[216]) of Sgk1in complex with AMP-PNP. On the right, cartoon representation of the crystal structure (PDB code: 6EDX[217]) of the PX domain of Sgk3.

1.2.10 mTOR in cancer

The central role of mTOR in cell growth and metabolism is underlined by the link between mTOR dysregulation and disease, including cancer. Mutations in mTOR itself have been identified only in few cancers[218]. Instead, the PI3K–AKT pathway and the Ras-driven MAPK pathway, in which mTOR is a downstream effector and upstream regulator, are most frequently mutated[55]. Hence, mTOR is a promising target for cancer therapy. The first drug targeting mTOR, rapamycin, was approved by the FDA in 1999 for prevention of allograft rejection after organ transplantation and has been widely used ever since[219]. Two rapamycin derivatives (also known as rapalogs), temsirolimus and everolimus, were approved and used since 2007 and 2009, respectively, to treat advanced renal cell carcinoma (RCC)[220]. Everolimus is also prescribed for treating pancreatic neuroendocrine tumors and advanced breast cancer[220]. However, rapalogs failed in cancer treatment, probably due to a lack of complete blocking of 4E-BP-dependent translation and lack of inhibition of mTORC2-AKT

pathway[221]. In addition, the negative feedback regulation of PI3K-signaling by S6K is lost upon mTORC1 inhibition, leading to the stimulation of PI3K-Akt signaling and ultimately inhibition of apoptosis via FoxO[220]. A second generation of catalytic mTOR inhibitors (e.g. Torin1 and PP242) competes with ATP to occupy the kinase active site, thereby inhibiting both mTORC1 and mTORC2[222,223]. These catalytic mTOR inhibitors, however, showed toxicity and in long-term treatment elicited AKT reactivation without input from mTORC2[224]. Currently, a third class of mTOR inhibitors are in clinical trials: the dual mTOR/PI3K inhibitors have effect on the full PI3K-AKT-mTOR pathway and thus, target loss of negative feedback regulation[225].

1.2.11 Structural characterization of the mTOR complexes

Owing to challenges in producing sufficient amounts of purified mTORC1 and mTORC2, the first structures of mTOR were protein fragments obtained by X-ray crystallography. The first crystal structure of the isolated mTOR FRB domain in complex with rapamycin and FKBP12 was solved in 1996 and visualized the binding mode of FKBP12 to mTOR[226]. Other studies solved the crystal structures of the catalytic FATKIN region of mTOR in complex with mLST8[52] and isolated Raptor from the fungus *Chaetomium thermophilum*[50]. The crystal structure of Raptor allowed the interpretation of the cryo-EM reconstruction of mTORC1, resulting in the first description of mTORC1 at a pseudo-atomic model[50]. An intermediate cryo-EM reconstruction at 6.1 Å resolution describes the Tor-Lst8 heterodimer from *Kluyveromyces marxianus* and revealed a conservation of the core scaffold of TOR complexes between yeast and higher eukaryotes [51]. The first high-resolution reconstructions of mTORC1 in the apo form (Figure 1.10) and in complex with its activator Rheb where determined at 3 Å and 3.4 Å resolution, respectively[42].

mTORC1 is a 1 MDa homodimer of heterotrimers that adopts a dimeric, rhomboid formed shape with a central cavity(Figure 1.10). It possesses two-fold (C2) symmetry with the axis of symmetry passing through the central cavity. The FATKIN region of each monomer is located near the central cavity, coming close to each other but not engaging in direct interactions. The HEAT repeats of each mTOR subunits form two distinct helical solenoids, one termed bridge/M-HEAT and the other one horn/N-HEAT[42,50,51]. Dimerization occurs along the mTOR HEAT repeats and the mTOR–Raptor interface[51].

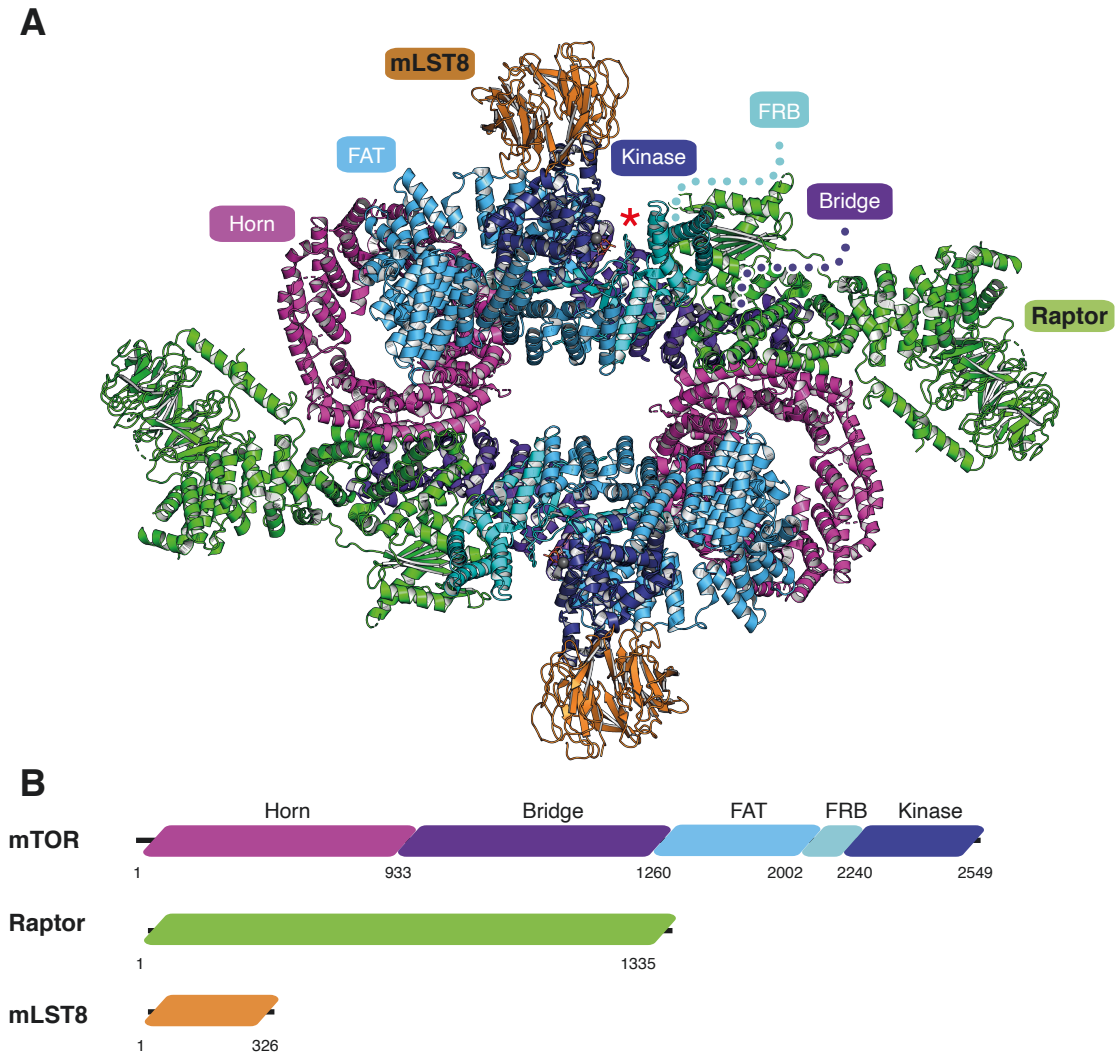

Figure 1.10 Cryo-EM structure of mTORC1
A Cartoon representation of cryo-EM reconstruction of mTORC1 at 3.0Å resolution. mTORC1 adopts a rhomboid-shaped dimer with a central cavity (PDB code: 6BCX[42]). Raptor is located close to the active site, confirming its role in substrate recognition and mTOR regulation. Raptor is in green, and mLST8 in orange. mTOR is colored according to different domains: Horn in magenta, Bridge in purple, FAT in light blue, FRB in cyan and the kinase domain in deep blue. The active site is indicated by a red asterisk. **B** Sequence-level domain organization of mTOR. mTOR, Raptor and mLST8 are color coded according to the structure. Residue numbers are indicated.

The active site is located at the bottom of a deep catalytic cleft, enclosed by the FAT domain, suggesting that, the complex is relatively inactive in its apo-form. The presence of the small GTPase Rheb in the HEAT repeats induces a structural rearrangement, which positions key residues of the mTOR active site into catalytic position[42].

Raptor binds to mTOR through α–helical interactions: the armadillo domain of Raptor forms an α-solenoid stack with the mTOR horn/N-HEAT of one monomer and the bridge/M-HEAT

of the monomer, contributing to the mTORC1 dimer interface[42,51]. However, Raptor is dispensable for mTORC1/TORC1 dimerization since mTOR alone forms a dimer[51,227]. Raptor is required for substrate recruitment and binding[37,64,69]. Raptor binds TOS motif substrates through a region that is located in a cleft between the RNC and the ARM domains[42]. In addition, Raptor is responsible for the recruitment of mTORC1 to the lysosomal surface through binding of the active Rag heterodimer[67]. Recent cryo-EM reconstructions of RagA-GTP/RagC-GDP in complex with mTORC1[70] or with Raptor-Ragulator[71] characterizes the binding interface between Raptor and the Rags.

Structural information on (m)TORC2 is limited to intermediate resolution cryo-EM reconstructions[228-230]. mTORC2 shares certain structural features with mTORC1: The C2 symmetry formed by the mTOR-mLST8 core, the two deep catalytic clefts and the binding site for the subunits Rictor and Raptor, respectively. Chen *et al*.[229] report a 4.9Å resolution cryo-EM reconstruction of mTORC2 (Figure 1.11). Available models of mTOR and mLST8(PDB: 6BCX[42]) were fitted into the EM-density. The density for Rictor and SIN1 could not be unambiguously assigned. However, models were built based on secondary structure predictions, XL-MS and immunoprecipitation assays. According to secondary structure prediction and biochemical analyses, the authors assigned the first 86 residues of N-terminal of SIN1 as a Poly-alanine model to the density on top of the mTOR FRB domain. Based on this, they attributed the mTORC2 insensitivity towards acute rapamycin treatment to SIN1. The other cryo-EM reconstructions of (m)TORC2 at intermediate resolution interpret the extra density on a secondary structure level [228,230].

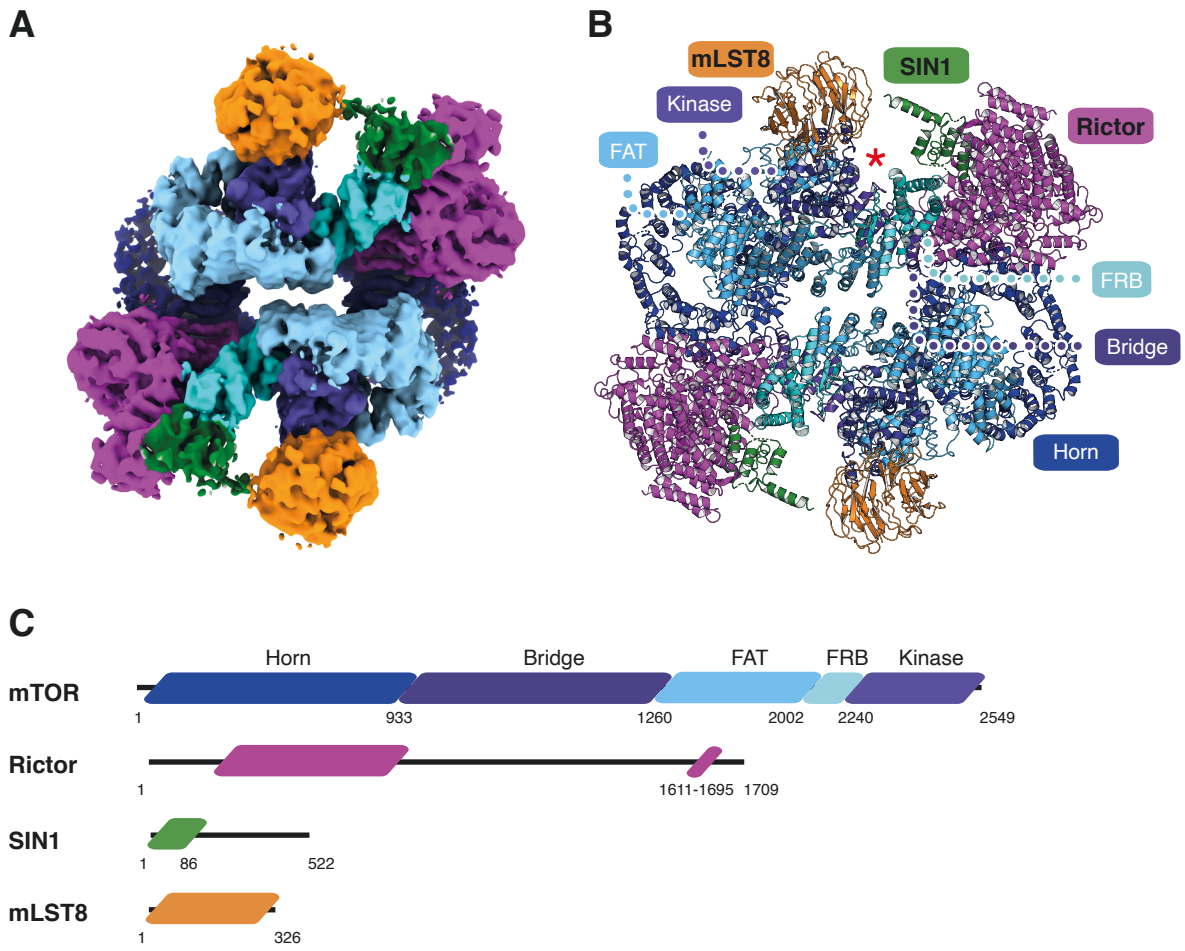

Figure 1.11 4.9Å cryo-EM reconstruction of mTORC2
A Density of the cryo-EM reconstruction of mTORC2 at 4.9Å resolution colored according to protein subunits and mTOR domains as indicated (EMDB code: 6913[229]). **B** Cartoon representation of mTORC2 (PDB code: 5ZCS[229]) mTORC2 adopts a rhomboid-shaped dimer, similar to mTORC1. mTOR and mLST8 structural models are derived from mTORC1 [42] (PDB code: 6BCX[42] and 6BCU[42]). mTOR domains, Rictor, SIN1 and mLST8 are labelled. The active site is indicated by a red asterisk. **C** Sequence-level domain organization of mTOR. For Rictor and SIN1 only the modelled regions are displayed in full color magenta and green respectively. mLST8 is colored in orange.

Structural data on mTORC2 accessory proteins are restricted to the fission yeast Sin1 CRIM domain[231,232] and the human SIN1 PH domains[233]. Structural studies on Sin1 CRIM domain reveal that it contains an acidic loop that appears to be essential for substrates binding[231]. To date structural information that elucidates mTORC2 functions such as activation and substrate recruitment are missing.

1.3 Aims of the thesis

The atypical serine/threonine kinase mTOR is a master regulator of cell growth and proliferation. mTOR signaling is often activated in tumors, metabolic and neurodegenerative diseases. mTORC2 plays a crucial role in metabolic regulation and dysregulation of this complex signaling is linked to metabolic disorder, including type 2 diabetes mellitus, and cancer. However, our understanding of mTORC2 is far from complete. Despite its pivotal role in the cell, mechanistic insights in central mTORC2 functions such as activation and substrate recruitment are scarce.

The key to deeper understanding of the functional role of mTORC2 and its components is the knowledge of their structure. This allows to derive mechanistic models as a basis for new functional experiments. Currently, structural information on the subunits Rictor and SIN1 are limited to intermediate resolution (5-10Å) cryo-EM reconstructions, where the atomic models are likely to be error prone. Structural information on Rictor, fold and secondary structure, is derived from non-atomic model and covers less than 50% of the protein. Structural data on SIN1 are restricted to two isolated domains: the NMR structure of fission yeast CRIM domain and the crystal structure of the human PH domains. However, knowledge, at the molecular level, on the interaction between Rictor and SIN1 is completely missing.

The central aim of this was to obtain mechanistic insights into key mTORC2 functions, in order to understand fundamental processes in mTORC2 biology based on its structure. More specifically:

Aim 1: What is the functional role of Rictor and SIN1 in mTORC2?

My aim was to understand how the two mTORC2-specific subunits Rictor and SIN1 are involved in central mTORC2 functions, such as activation, localization and substrates recruitment. I was aiming to elucidate which regions and structural features of Rictor and SIN1 are involved in the interaction with mTOR and mLST8. Of special interest was the identification of Rictor regions that may provide a platform for regulatory proteins. Moreover, I was aiming to identify which subunit is responsible for the insensitivity of mTORC2 to acute rapamycin treatment.

Aim 2: How are mTORC2 substrates recognized? My goal was to understand how substrates are recognized and how they bind to mTORC2. Further points of interest were to examine if the mTORC2 substrates have a common recognition motif and if SIN1 CRIM domain is the determinant of substrate specificity.

Aim 3: Is mTORC2 in an activated state? Of primary interest was the determination of the activation state of mTORC2. Additionally, I set out to understand the requirements for mTORC2 activation by exploring the possibility of an activator.

1.4 Declaration of own project contribution

I have cloned the mTORC2 substrates Akt1, Pkcα and Sgk1 along with mTORC2 mutants, Rictor mutants and SIN1 mutants. I have reassembled the mTORC2 complex, produced virus and expressed all of the above proteins in *Sf21* insect cells. I purified all the proteins and further characterized them. I have prepared samples for MS study of mTORC2 and analyzed the results. I have characterized mTORC2 WT, mTOR and Rictor mutants by optimizing and conducting *in vitro* activity assays and thermal stability assays. I wrote the "The 3.2Å resolution structure of human mTORC2" manuscript and contributed to preparation of figures and animations. A full list of contributions for all authors is found at the end of the manuscript.

2 The 3.2Å resolution structure of human mTOR complex 2

Reproduced from:

The 3.2Å resolution structure of human mTORC2

Alain Scaiola*, Francesca Mangia*, Stefan Imseng, Daniel Boehringer, Karolin Berneiser, Mitsugu Shimobayashi, Edward Stuttfeld, Michael N. Hall, Nenad Ban, & Timm Maier

*Authors contributed equally to this work

Preprint available on BioRxiv
https://www.biorxiv.org/content/10.1101/2020.04.10.029835v1

2.1 Abstract

The protein kinase mammalian target of rapamycin (mTOR) is the central regulator of cell growth. Aberrant mTOR signaling is linked to cancer, diabetes and neurological disorders. mTOR exerts its functions in two distinct multiprotein complexes, mTORC1 and mTORC2. Here we report a 3.2 Å resolution cryo-EM reconstruction of mTORC2. It reveals entangled folds of the defining Rictor and the substrate-binding SIN1 subunits, identifies the C-terminal domain of Rictor as the source of the rapamycin insensitivity of mTORC2, and resolves mechanisms for mTORC2 regulation by complex destabilization. Two novel small molecule binding sites are visualized, an inositol hexakisphosphate (InsP6) pocket in mTOR and an mTORC2-specific nucleotide binding site in Rictor which also forms a zinc finger. Structural and biochemical analyses suggest that InsP6 and nucleotide binding do not control mTORC2 activity directly but rather have roles in folding or ternary interactions. These insights provide a firm basis for studying mTORC2 signaling and for developing mTORC2-specific inhibitors.

2.2 One Sentence Summary

The structure of mTORC2 reveals the basis of its rapamycin insensitivity and rationalizes how mTORC2 stability controls activity.

2.3 Main Text

mTORC2 is activated by insulin and phosphoinositide 3-kinase (PI3K) signaling[55,56] and acts on cell survival and proliferation[57] by phosphorylating the AGC family kinases: Akt, PKC and SGK [57,59,163,189,234]. mTORC2 also promotes tumorigenesis via upregulation of lipid biosynthesis[58].

mTOR inhibitors played a major role in the elucidation of mTOR signaling and are used in cancer treatment[235]. The polyketide rapamycin specifically inhibits mTORC1[36,37] by forming a complex with the cellular protein FKBP12 that then binds the mTOR FKBP-rapamycin binding (FRB) domain (Figure 2.1)[226]. ATP-like inhibitors target the ATP-binding site in the kinase catalytic domain of eith both mTORCs or the mTORCs and structurally related PI3K[220]. Recently, mTORC2-selective inhibitors were identified, but their mechanism of action remains unknown[236,237]. Several intermediate resolution reconstructions of (m)TOR complexes[50,51,228-230]and high resolution reconstructions of human mTORC1[42] have been reported, but no high-resolution information on mTORC2 is available. Of the mTORC2 accessory proteins, only the isolated pleckstrin homology (PH) and CRIM domains of SIN1

have been structurally characterized[231-233]. For Rictor, fold- and secondary structure-based models have been proposed based on intermediate resolution cryo-electron microscopy (cryo-EM) reconstructions[228-230].

To investigate the high resolution structure of mTORC2 and the mechanism of its regulation we co-expressed recombinant components of human mTORC2 (mTOR, mLST8, Rictor and SIN1) in Spodoptera frugiperda cells. The assembled complex, purified using tag-directed antibody affinity followed by size exclusion chromatography, was analyzed by cryo-EM (Figure 2.1B, and Figs. S1 and S2) in the presence of ATPγS and either the full-length substrate Akt1 (Figure S2.3) or an Akt1 variant missing the PH domain (ΔPH-Akt1), or in the absence of Akt1 with and without ATPγS (Figure S2.2). The sample prepared in the presence of ATPγS and ΔPH-Akt1 yielded the highest overall resolution of 3.2 Å (Density A in Figure S2.2).

mTORC2 forms a rhomboid-shaped dimer (Figure 2.1C) as observed in lower resolution mTORC2 reconstructions[228-230]. The mTOR kinase forms the core of mTORC2 with mLST8 on the periphery, close to the active site cleft, similar to mTOR in mTORC1[42,50]. In the overall reconstruction, as a consequence of EM refinement of a flexible molecule, one half of the dimer showed better local resolution (Figure 2.1B and Figs. S4A-C and Movie S1). Therefore, focused refinement on a unique half of the assembly improved the resolution to 3.0 Å (Density C in Figure S2.2), and these maps were used for structural modelling (Figure S2.4D-F). Previous mTORC2 and yeast TORC2 reconstructions[228-230] revealed that the two mTOR FAT domains are in closer proximity to each other than in mTORC1[42,50,52] and in the current structure, the distance between the mTOR FAT domains is further reduced (Figure S2.5A). Irrespective of these structural differences between the two mTORCs, the catalytic site in mTORC2 closely resembles the catalytic site in mTORC1 without Rheb-mediated activation[42], suggesting that mTORC2 may further be activated by a yet to be defined control mechanism.

Previous studies of mTORC2 subunits Rictor and SIN1 or their yeast orthologs were not of sufficient resolution to allow de novo model building, resulting in ambiguous or inconsistent interpretations[228,229,238]. Here we unambiguously model all structured regions of Rictor and the N-terminal region of SIN1 (Figure 2.2A-C), whereas the middle and C-terminal part of SIN1 retain high flexibility and are not resolved. The fold of Rictor differs substantially from previous interpretations[229] (Figure S2.5B-C). Rictor is composed of three interacting stacks of α-helical repeats, here referred to as the ARM domain (AD), the HEAT-like domain (HD), and the C-terminal domain (CD) (Figure 2.2A-C and Figure S2.6A). The N-terminal AD (residues 26-487)

forms a large superhelical arrangement of nine ARM repeats (Figure 2.2A-B) that structurally separates the HD and CD. The HD (residues 526-1007), interpreted as two separate domains in previous lower resolution studies[228,229], is composed of ten HEAT-like repeats. In sequence space, the HD and CD of Rictor are separated by an extended stretch of residues (1008-1559) that are predicted to be disordered[239] and are not resolved in our reconstruction. We refer to this region as the phosphorylation-site region (PR) because it contains most of Rictor's phosphorylation sites[240]. The two ends of the PR are anchored by the two-stranded β-sheet at the top of the HD, which is thus termed the PR anchor (Figure 2.2B-C and Figure S2.6A). From here, a partially flexible linker wraps around the AD and the mTOR FRB domain extending towards the CD (Figure 2.2B and Figure S2.6C).

The structured parts of the CD form a four-helix bundle and a zinc finger, with bound Zn^{2+}, in the vicinity of the Rictor N-terminus (Figure 2.2A and Figure S2.6B). Residues coordinating the zinc ion are highly conserved in metazoan Rictor (Figure S2.6F). In earlier work, this domain had been interpreted as representing the SIN1 domain[229]. The complete CD is absent in sequences of fungal Rictor orthologs. Nevertheless, other segments of large extensions in yeast Rictor and SIN1 sequences may occupy this location in mTORC2 as observed in an intermediate resolution reconstruction of budding yeast TORC2[230] (Figure S2.6D-E). Increased levels of Zn^{2+} have been reported to stimulate Akt S473 phosphorylation in cells[241-243], but no direct involvement of mTORC2 activatoin has been demonstrated.

Contacts between Rictor and mTOR are made by the Rictor AD, which sits between the proximal mTOR central HEAT domain and the N-terminal HEAT repeat domain, of the distal mTOR subunit (Figure 2.2B). Due to its positioning on top of the mTOR FRB domain, the CD of Rictor blocks binding of FKBP12-rapamycin to mTORC2, thereby explaining mTORC2's insensitivity to rapamycin[43,44,238,244] (Figure 2.2D).

The SIN1 subunit of mTORC2 exhibits an unexpected structural organization. The N-terminal region (residues 2-137), contrary to earlier interpretations, does not form an independently folding domain but interacts tightly with Rictor and mLST8 in an extended conformation (Figure 2.2A-C and 3A-E). The CRIM, RBD and PH domains of SIN1, however, remain flexibly disposed. The N-terminus of SIN1 is inserted into a deep cleft at the interface of the AD and HD of Rictor. The N-terminal Ala2 with a structurally resolved acetylated N-terminus, and Phe3 of SIN1 are buried in a hydrophobic pocket of Rictor (Figure 2.3C,D and Figure S2.7A). The anchored N-terminal region of SIN1 forms two short helices (residues 6 to 33) inserted into grooves on the surface of the Rictor AD (Figure 2.3D) and then continues with a flexible sequence segment toward the Rictor CD (Figs. 2B-C and 3C and Figure S2.7B). Protruding

from the Rictor CD, SIN1 forms a helical segment, referred to as the “traverse”, that spans the distance to mLST8 across the mTORC2 kinase cleft (Figure 2.3C and Figure S2.7B-C). The next region of SIN1 interacts with the fourth strand of the second blade of the mLST8 propeller by β-strand complementation, leading to displacement of an mLST8 loop relative to the structure of mLST8 in mTORC1 (Figure 2.3C,E and Figure S2.7D). SIN1 then follows the surface of the mLST8 propeller, finally forming an α-helix anchored between the first and seventh blades of mLST8.

SIN1 integrates into the Rictor fold, and connects Rictor with mLST8 suggesting a direct role in stabilizing mTORC2. To test the relevance of the anchoring of the N-terminus of SIN1 on Rictor we extended the N-terminus of SIN1. Insertion of residues impairs critical interactions observed for the acetylated N-terminus of SIN1 and prevents Rictor integration into mTORC2, as observed in Baculovirus-mediated expression of mTOR components followed by pull-down assays (Figure 2.3B and Figure S2.8). Therefore, SIN1 acts as an integral part of the Rictor structure that critically stabilises interdomain interactions, explaining the difficulties observed in purifying isolated Rictor[229].

These observations are also consistent with the locations of post-translational modifications or mutations that affect mTORC2 activity. SIN1 phosphorylation at Thr86 and Thr398 has been reported to reduce mTORC2 integrity and kinase activity toward Akt Ser473[245]. Thr86 in SIN1, which is a target for phosphorylation by S6 kinase[245], is bound to a negatively charged pocket of the Rictor CD (Figure 2.3C and Figure S2.7C). Phosphorylation of Thr86 would lead to repulsion from this pocket, destabilizing the interaction between Rictor and mTOR/mLST8 and presumably the entire mTORC2 assembly, in agreement with earlier in vivo and in vitro observations[245]. The importance of SIN1 in connecting Rictor to mLST8 and, therefore also indirectly to mTOR, is also consistent with the requirement of mLST8 for mTORC2 integrity[35,246].

A poorly resolved density linked to the SIN1 helix anchored to mLST8 is observed in all reconstructions. In previous structural studies of yeast TORC2, a similar region of density was associated to the CRIM domain of Avo1, the yeast SIN1 ortholog [230,238]. Most likely, it represents the mobile substrate-binding CRIM domain that directly follows the helix in the SIN1 sequence and has a matching shape based on the solution structure of the S. pombe SIN1 CRIM domain [231,232] (Figure 2.3C-F and Figure S2.9A,C). The positions of the SIN1 RBD and PH domains remain unresolved. In the dataset collected for samples with added full-length Akt1 (Dataset 2 in Figure S2.2), we observe additional low-resolution density (Figure 2.3F and Figure S2.9B-C) between the hypothetic CRIM domain and Rictor AD and CD in the

vicinity of the mTOR active site. This density, not of sufficient resolution to assign specific interactions, may represent parts of bound Akt1 or SIN1 domains (Figure S2.9C).

A proposed regulatory mechanism for mTORC2 involves ubiquitylation of mLST8 on Lys305 and Lys313[247]. Loss of ubiquitylation by K305R and/or K313R mutation, or truncation of mLST8 at Tyr297, leads to mTORC2 hyperactivation and increased Akt phosphorylation[247]. Indeed, mLST8 Lys305 is proximal to the SIN1 helix anchoring the CRIM domain. Ubiquitylation of Lys305 would prevent association of the SIN1 helix, leading to dislocation of the SIN1 CRIM domain required for substrate recruitment (Figs. 3C and 4C). Ubiquitylation of Lys313, which is found on the lower face of mLST8 (Figs. 3C and 4C), presumably also interferes with positioning of the CRIM domain (Figure S2.9).

We observed two novel, small molecule binding sites outside the mTOR catalytic site, which is itself occupied by ATPγS. The first (A-site) (Figure 2.4A and Figure S2.10B) is located in the HD of Rictor and is thus specific to mTORC2. The second (I-site) (Figure 2.4B and Figure S2.10C) is located in the FAT domain of mTOR and is thus common to mTORC1 and mTORC2.

The density of the small molecule in the A-site matched that of an ATP molecule and was confirmed to be ATP (or ATPγS) through a comparison of cryoEM reconstructions of mTORC2 with and without ATPγS added at a near physiological concentration of 2mM (Datasets 1 and 4, Figure S2.2 and S10A). The A-site doesn't resemble any known ATP binding site. Positively charged amino acids (Lys541, Arg575, Arg576, Arg572) of the A-site are conserved in Rictor orthologs from human to yeast (Figs. S6E and S11). Other residues are not conserved, hinting at the possibility for interactions with alternative negatively charged ligands. The A-site is located approximately 100 Å from the mTOR catalytic site. Ligand binding to the A-site causes neither long-range allosteric change affecting the kinase site nor local structural perturbations (Figure S2.12).

To investigate the effect of ligand binding to the A-site, we generated a series of Rictor variants with a mutated A-site (Table S2.1). Variants with three or four mutated residues (A3 and A4) assembled into mTORC2 (Figure S2.13B) while variant A5 was defective in assembly (Figure S2.13B-D). Cryo-EM reconstructions of variants A3 and A4 in the presence of ATPγS (Figure S2.12B-C,E-F) confirmed that the chosen mutations abolish ligand binding under near physiological conditions (Figs. S10A and S12C-F). Purified mTORC2 containing Rictor variants A3 or A4 exhibited thermal stability and kinase activity in an Akt1 in vitro phosphorylation assay comparable to wild-type mTORC2. (Figs. S14B and S15A,B). Complementation of a Rictor knockout (KO) in HEK293T cells by transfected Rictor-WT, or

Rictor variant A3 yielded comparable levels of AKT-S473 phosphorylation (Table S.21 and Figure S2.16). Altogether, the above analyses indicate that ligand binding to the A-site does not directly influence mTORC2 kinase activity, suggesting rather a role in the interaction with other, yet unidentified, partner proteins of mTORC2.

The I-site is formed entirely by the FAT domain of mTOR, where a large, positively charged, pocket is lined by six lysine and two arginine residues to bind an extended ligand (Figure 2.4B and Figure S2.10C). The I-site was still partially occupied in our reconstruction of mTORC2 prepared without addition of exogeneous ATPγS or other relevant ligands (Data Figure S2.10A). The co-purified molecule was identified by map appearance and by ion mobility spectrometry-mass spectrometry (IMS-MS) as inositol hexakisphosphate (InsP6) (Figs. S17 and S18A-F). InsP6 binds in a region, which is incomplete in related PI3Ks[248], but generally conserved in members of the PIKK family of kinases[30]. Indeed, InsP6 was previously reported to associate with DNA-PKcs[249]. Recently, structure determination of the PIKK family pseudo-kinase SMG1 revealed InsP6 binding in a region corresponding to the I-site and led the authors to postulate a corresponding binding site in mTOR but involving both the kinase domain and FAT domain[30]. InsP6 has previously been observed as a structural component of multi-subunit assemblies, including the splicesome[250] and proteasome activator complex[251], and helical repeat regions have been identified as InsP6 interaction sites[252].

To investigate the function of Ins6P interaction, we purified recombinant mTORC2 containing mTOR I-site mutations (Table S2.1). mTOR variants with two and three mutations, I2 and I3, yielded intact mTORC2 complexes (Figure S2.13A), while a variant with five mutations, I5, failed to assemble into mTORC2 (Figure S2.13A-C). mTORC2 containing mTOR variants I2 and I3 displayed normal kinase activity toward Akt1 in vitro (Figure S2.14A). Notably, the mutations in I2 are equivalent to those reported previously to abolish completely the kinase activity of an N-terminally truncated ‘naked’ mTOR fragment toward a C-terminal peptide of Akt1[30]. A possible explanation for this apparent discrepancy is provided by a reduced stability of mTORC2 assembled using the I2 variant (but not the I3 variant) (Figure S2.15A). This destabilizing effect might be more pronounced in an mTOR fragment, than in the context of an assembled mTORC2 (Figure S2.15A).

To investigate a possible role of InsP6 metabolism on mTORC2 activity in HEK293T cells, we knocked down (KD) and knocked out (KO) Inositol-pentakisphosphate 2-kinase (IPPK) and Multiple inositol polyphosphate phosphatase 1 (MINPP1), respectively. The former enzyme generates InsP6 whereas the latter degrades it (Figure S2.19). These manipulations of InsP6

metabolising enzymes did not alter mTORC2 kinase activity in non-stimulated cells or in cells stimulated with FCS and insulin (Figure S2.19A-H). These biochemical results are consistent with the observed stable binding of InsP6 to mTORC2 and suggest a role of InsP6 in mTOR folding or mTOR complex assembly, rather than as an acute transient metabolic input signal to mTORC1 or mTORC2.

Here, we describe a bona fide structure of mTORC2. We visualized how SIN1 stabilizes and tethers Rictor to the mTOR/mLST8 core. SIN1 further uses mLST8 as a platform for positioning its substrate-recruiting CRIM domain, revealing a new functional role for mLST8 and rationalizing the impact of SIN1 and mLST8 modifications on mTORC2 activity. We also provide the structural basis for how the Rictor CD determines mTORC2's rapamycin insensitivity by a mechanism different from those inferred from previous structural data[228,229]. We identified and functionally characterized two ligand binding sites in mTORC2. The I-site on mTOR is common to mTORC1 and 2, binds Ins6P and presumably functions in mTOR folding or assembly rather than acting as a sensor site for acute changes in cellular InsP6 concentration. The mTORC2 specific A-site of Rictor binds ATP. It doesn't affect mTORC2 activity by allostery, but may be involved in linking partner protein interactions to cellular nucleotide triphosphate concentrations. Altogether, the data presented here provide a firm basis for further analysis of the function of mTORC2 and its interplay with partner proteins for controlling subcellular localization[113] and regulation of activity[43,57-59]. Interaction sites of Rictor and mLST8 with SIN1 provide an opportunity for the development of inhibitors specific for mTORC2.

2.4 Figures

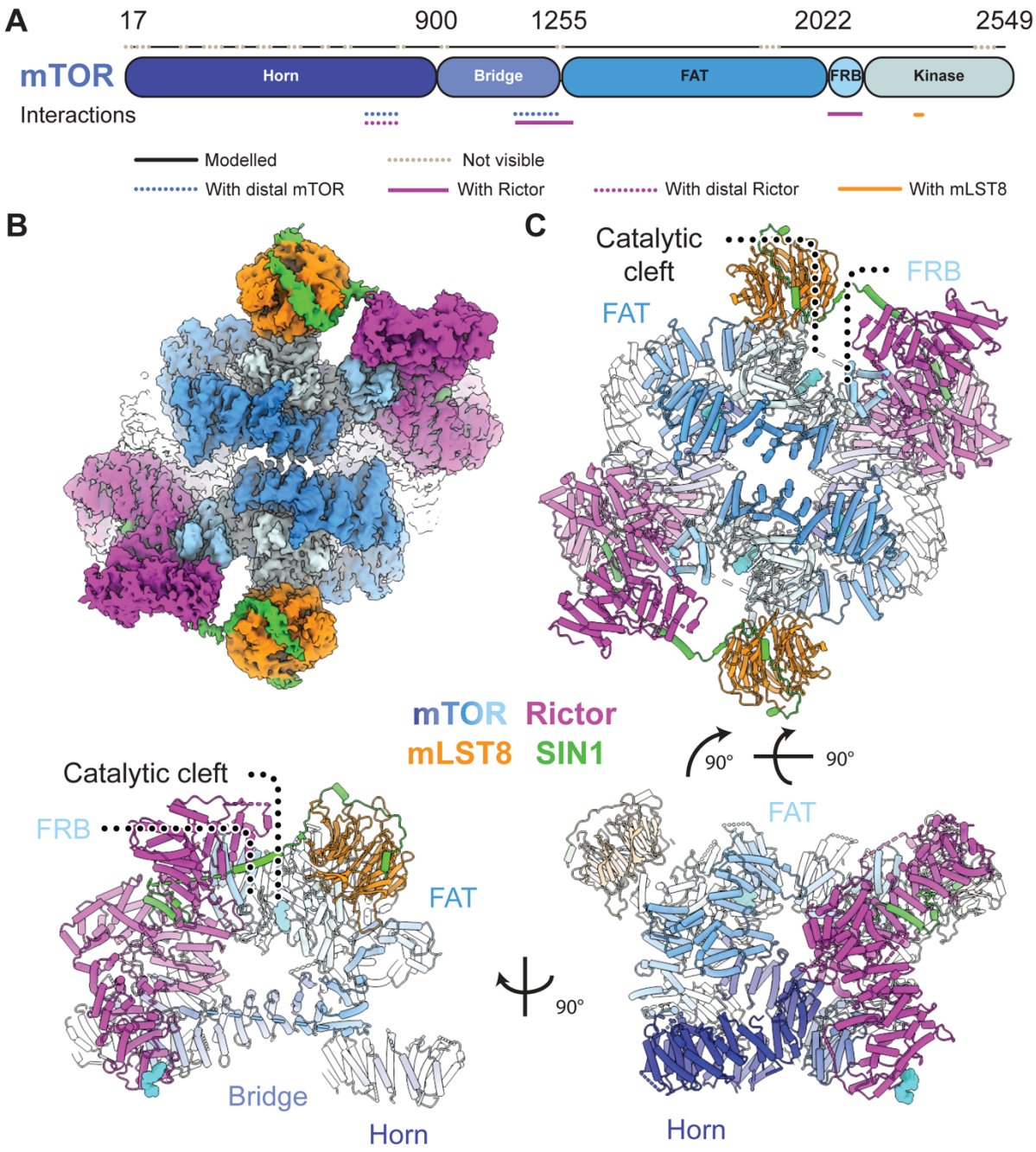

Figure 2.1 Structure of mTOR complex 2
A Sequence-level domain organization of mTOR. Modelled and unresolved regions are indicated as dotted lines. Interactions with other proteins in the complex are highlighted below the sequences. **B** Density of the overall cryo-EM reconstruction of mTORC2 colored according to protein subunits and mTOR domains as indicated. The top half is better resolved than the lower one, most likely due to conformational flexibility. **C** Cartoon representation of mTORC2 in three different orientations. The proteins Rictor (magenta) and SIN1(green) are unique to mTORC2, while mTOR (colored by domain) and mLST8 (orange) are common to both mTORC1 and mTORC2. Bound ligands are represented as cyan spheres.

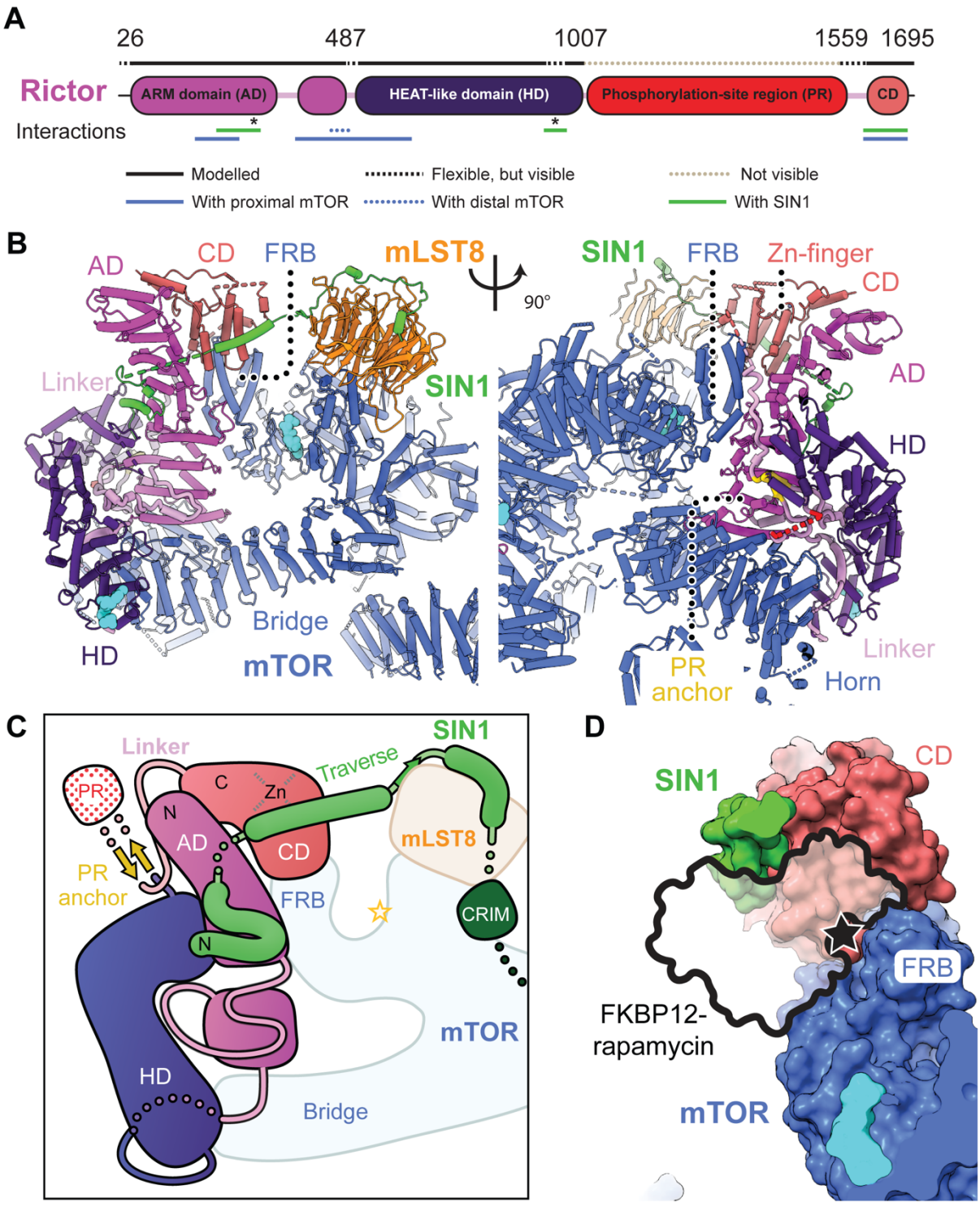

Figure 2.2 The architecture of Rictor

A Sequence-level domain organization of Rictor. Flexible and unresolved regions are indicated as dotted lines. Interactions with other proteins in the complex are highlighted below the sequences. Asterisks indicate residues interacting with the N-terminal region of SIN1. **B** Two views of Rictor, colored by domains. The structured part of Rictor forms three domains: an N-terminal Armadillo repeat domain (AD, magenta), a HEAT-like repeat domain (HD, dark magenta), and a C-terminal domain (CD, light red), the phosphorylation site region

(PR) remains disordered. The sequences flanking the non-resolved PR are highlighted in red, the PR anchor is colored in gold. Bound ligands are shown as cyan spheres. **C** Schematic representation of Rictor and SIN1 domain topology. **D** The Rictor CD occupies the FRB domain and sterically blocks FKBP-rapamycin binding[50].

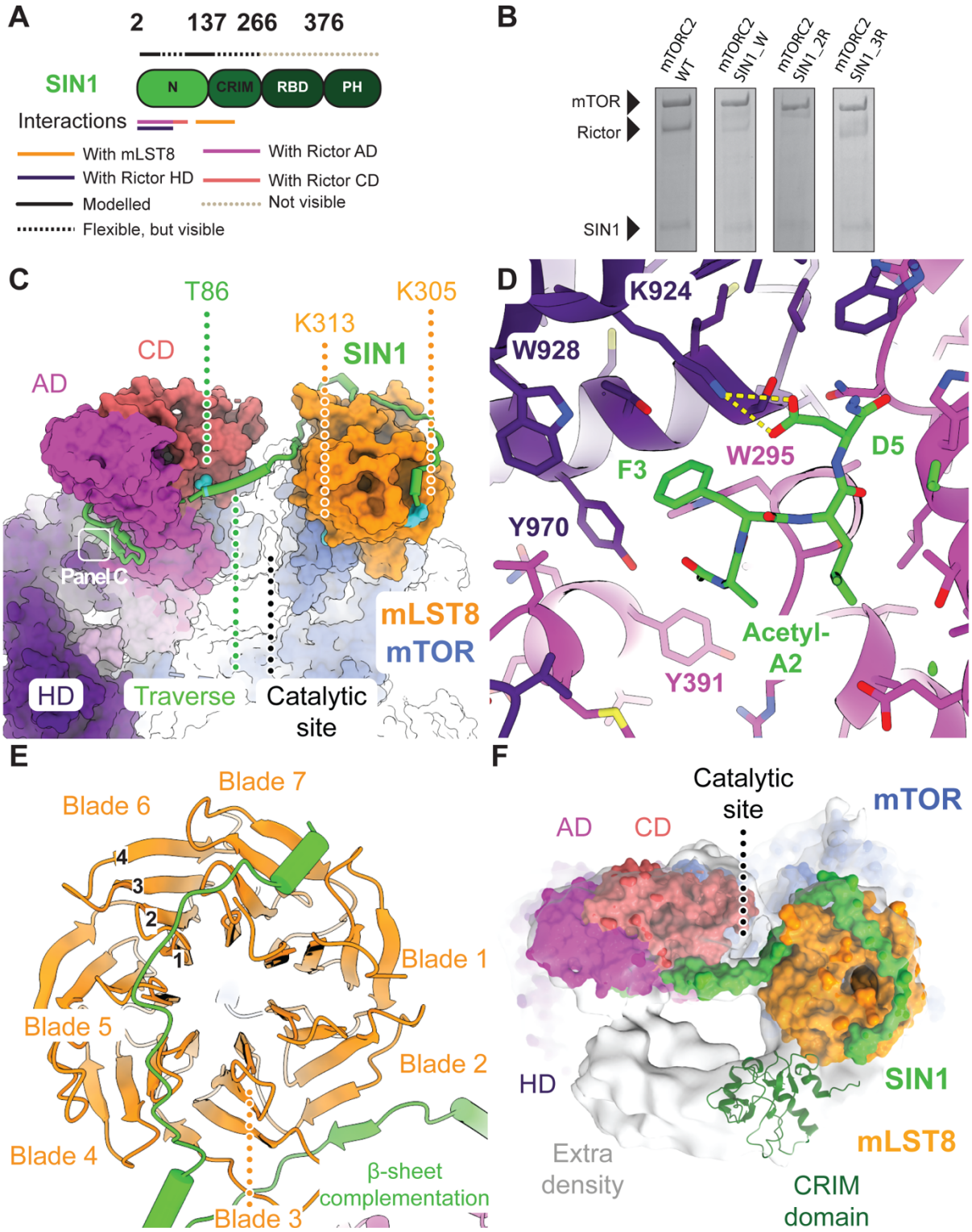
A
2
137
266
376
SIN1
N
CRIM
RBD
PH
Interactions
With mLST8
With Rictor HD
Modelled
Flexible, but visible
With Rictor AD
With Rictor CD
Not visible
B
mTORC2 WT
mTORC2 SIN1_W
mTORC2 SIN1_2R
mTORC2 SIN1_3R
mTOR
Rictor
SIN1
C
T86
K305
K313
SIN1
CD
AD
Panel C
mLST8
mTOR
HD
Traverse
Catalytic site
D
K924
W928
W295
D5
F3
Y970
Acetyl-A2
Y391
E
Blade 7
Blade 6
Blade 1
Blade 5
Blade 2
Blade 4
Blade 3
β-sheet complementation
F
Catalytic site
mTOR
AD
CD
HD
SIN1
mLST8
Extra density
CRIM domain

Figure 2.3 The SIN1 N-terminal region is an integral component of mTORC2
A Sequence-level domain organization of SIN1. Flexible and unresolved regions are shown above each domain representation as dotted lines in two colors as indicated. Interactions with other proteins in the complex are indicated below the domain representation. **B** Extension of the processed SIN1 N-terminus disrupts assembly of Rictor and SIN1 with mTOR/mLST8 into mTORC2. SDS-polyacrylamide gel of a FLAG bead pulldown from lysates of insect cells expressing mTORC2 comprising SIN1 variants. Levels of Rictor are drastically reduced in the mTOR-based pulldown for mTORC2 carrying variants of SIN1 N-terminally extended by a tryptophan (mTORC2 SIN1_W), two consecutive arginines (mTORC2 SIN1_2R) and three consecutive arginines (mTORC2 SIN1_3R) **C** Surface representation of mTORC2. SIN1 (shown as green cartoon) interacts via two N-terminal helices with Rictor, winds around Rictor, traverses the catalytic site cleft and winds around mLST8. The field of view of subpanel C is indicated. **D** Close-up view of the SIN1 N-terminal residues, which are deeply inserted between Rictor AD and HD. Acetylated Ala2 and Phe3 are bound in a hydrophobic pocket, while Asp5 interacts via salt bridges (yellow dashes). **E** Top view of mLST8 β-propeller (orange) and the interaction regions with SIN1 (green). The nomenclature for WD40 β-propeller repeats is indicated. **F** Top view of the catalytic site with the structure shown as surface together with the density of a subclass (light grey). The lower resolution extra density is consistent with a placement of the SIN1 CRIM domain, here shown in dark green (PDB: 2RVK). Unassigned extra density protrudes from the CRIM domain to the mTOR active site and Rictor.

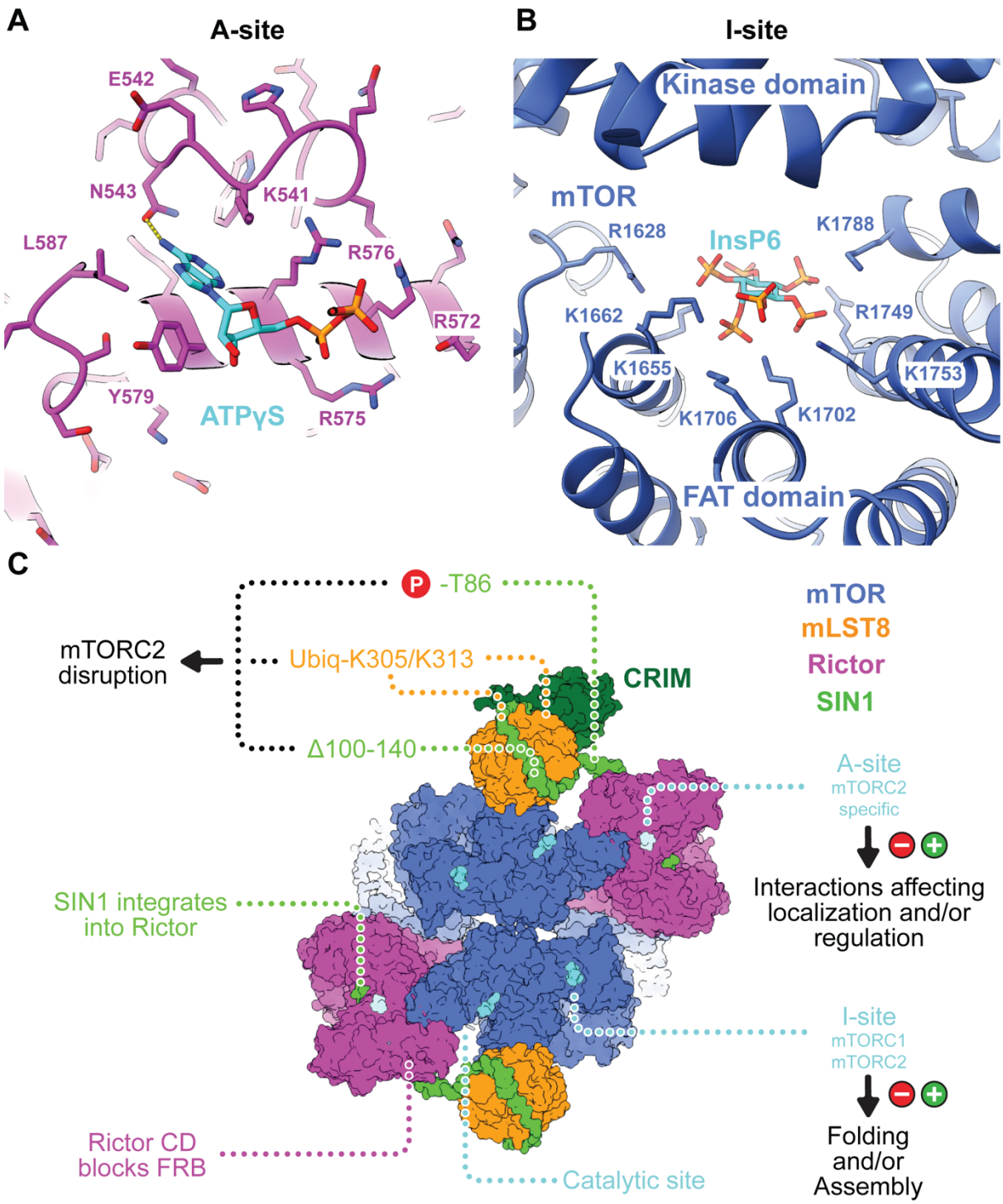
A
A-site
E542
N543
K541
L587
R576
R572
Y579
ATPγS
R575
B
I-site
Kinase domain
mTOR
R1628
InsP6
K1788
K1662
R1749
K1655
K1753
K1706
K1702
FAT domain
C
P -T86
mTORC2 disruption
Ubiq-K305/K313
Δ100-140
CRIM
mTOR
mLST8
Rictor
SIN1
A-site
mTORC2 specific
Interactions affecting localization and/or regulation
SIN1 integrates into Rictor
I-site
mTORC1
mTORC2
Folding and/or Assembly
Rictor CD blocks FRB
Catalytic site

Figure 2.4 Small molecule binding sites of mTORC2 outside the active site region
A Close-up view of the A-site on the periphery of the Rictor HD with bound ATPγS. A hydrogen bond between ATPγS and Asn543is shown as dashed yellow lines. **B** Close-up view of the I-site in the FAT domain of mTOR. InsP6 is surrounded by a cluster of positively charged amino acids. It only directly interacts with residues of the FAT domain. **C** Overview of mTORC2 architecture and ligand interaction sites. Each half of the dimeric mTORC2 has three small molecule binding sites. The kinase active site and the A-site, which is located in the peripheral region of Rictor, bind to ATP (or ATP analogues). The I-site in the middle of the FAT domain of mTOR binds InsP6. The indicated modifications on SIN1 and mLST8 affect mTORC2 assembly. Extra-density region following the CRIM domain is indicated as a grey outline

2.5 Acknowledgements

We thank T. Sharpe at the Biophysics facility and A. Schmidt at the Proteomics Core Facility of Biozentrum and the sciCORE scientific computing facility, all of University of Basel. We thank M. Leibundgut for advice with model building, A. Jomaa and S. Mattei for advice on cryoEM data processing, the ETH scientific center for optical and electron microscopy (ScopeM), and in particular M. Peterek and P. Tittmann for technical support. We are indebted to E. Laczko and J. Hu of the Functional Genomics Center Zürich for the help with the mass spectrometry. We thank Iva Lučić and Thomas Leonard (Max F. Perutz Laboratories, Vienna) for providing (Delta-PH) Akt1 protein.

2.6 Funding

F.M. is supported by a Fellowship for Excellence from the Biozentrum Basel International PhD program. This work was supported by the Swiss National Science Foundation (SNSF) via the National Center of Excellence in RNA and Disease (project funding 138262) to N. Ban and M. N. Hall and SNSF project funding 179323 to T. Maier.

2.7 Author contributions

AS designed the experiments, prepared the sample for cryoEM, carried data processing and structure modelling. AS and DB performed data collection. FM designed the experiments, cloned Akt1, mTORC2 mutants and Rictor mutants, expressed and purified proteins, performed the activity assays and the nanoDSF measurements. ES established the mTORC2 purification procedure. SI cloned mTORC2, contributed to data analysis and manuscript preparation. MS performed the in-cell analysis of mTORC2 activity. KB and MS performed the KO/KD of MINPP1 and IPPK. AS, FM, DB, SI, NB, MNH and TM participated in the writing of the manuscript.

2.8 Competing interest

The authors declare no competing interests.

2.9 Data and materials availability

The high resolution cryo-EM map of the half (Density C) and full-mTORC2 (Density A) has been deposited in the Electron Microscopy Data Bank as EMD- XXX and EMD-YYYY respectively, while the corresponding model are in the Protein Data Bank as PDB ID WWW and ZZZ. Additionally, the density of mTORC2 in absence of ATPγS (Density F), as well as the densities showing extra density (Density G and H) were deposited in the Electron Microscopy Data Bank as EMD-AAAA, EMD-BBBB, and EMD-CCCC respectively.

2.10 Supplementary Materials

2.10.1 Materials and Methods

Protein expression and purification

Insect cell vectors from the 'MultiBac' Baculovirus expression system[253] (Geneva Biotech, Geneva, Switzerland) have been used to clone internally FLAG-tagged pAceBAC-mTOR (FLAG after Asp258), pIDK-Rictor, pIDC-mLST8, and pAceBAC1-SIN1 using Gateway Cloning (Thermo Fisher Scientific, US). Rictor was originally amplified from myc-Rictor, which was a gift from David Sabatini[44] (Addgene plasmid #11367). Site-directed mutagenesis was used to generate mTORC2 A- and I- site variants. The following set of A-site mutants with pIDK-Rictor as template was created: Rictor_R572E_R575E_R576E (A3), Rictor_R572E_R575E_R576E_Y579A (A4), Rictor_R572E_R575E_R576E_Y579A_L587W (A5). The following I-site mutants with FLAG-tagged pAceBAC-mTOR were generated: mTOR_K1753E_K1788E (I2), mTOR_R1628E_K1655E_K1662E (I3) and mTOR_R1628E_K1655E_K1662E_K1706E_K1735E (I5). Wild-type Rictor and mutants A3, and A5 were subcloned into a gentamycin resistant-mammalian expression vector under control of a CMV promoter. SIN1 N-terminal variants were generated by inserting a tryptophan (SIN1_W), two consecutive arginines (SIN1_2R) or three consecutive arginines (SIN1_3R) using site-directed mutagenesis and pAceBAC1-SIN1 as template. Plasmids encoding FLAG-tagged mTOR, Rictor and mLST8 were fused to a 'MultiBac' expression plasmid using Cre-recombinase (New England Biolabs, Ipswich, USA) and transposed into a bacmid for baculovirus production. Baculovirus encoding untagged SIN1 was produced separately.

Sf21 insect cells (Expression Systems) were grown in HyClone insect cell media (GE Life Sciences) and Baculovirus was generated according to the Fitzgerald *et al.*, 2006[253]. For the expression of recombinant human WT mTORC2, A- and I- site mTORC2 mutants and mTORC2 carrying SIN1 N-terminal variants, Sf21 cells were infected at a cell density of 1 Mio/ml. Cells were coinfected with 1:100 (v/v) ratio of two undiluted supernatants from cells previously infected with baculovirus encoding FLAG-mTOR, Rictor and mLST8, or infected with baculovirus encoding untagged SIN1, respectively. WT mTORC2, A- site mutants A3, A4 and A5 and I- site mutants I2, I3 and I5 were purified as follows: insect cells were harvested 72 hours post infection by centrifugation at 800 x g for 25 minutes and stored at –80°C until further use. Cell pellets were lysed in 50 mM bicine pH 8.5, 200 mM NaCl, 2 mM $MgCl_2$ by sonication and the lysate cleared by ultracentrifugation. Soluble protein was incubated with 10 ml anti-DYKDDDDK agarose beads (Genscript, Piscataway, USA) for 1 hr at 4°C. The beads were transferred to a 50 ml gravity flow column (BioRad) and washed four times with 200 ml of wash buffer containing 50 mM bicine pH 8.5, 200 mM NaCl, 2 mM EDTA. Protein was eluted by incubating beads for 30 min with 10 ml wash buffer supplemented with 0.6 mg/ml synthetic DYKDDDDK peptide (Genscript, Piscataway, USA). The eluate was combined with three additional elution steps using 0.1 mg/ml synthetic DYKDDDDK peptide and five minutes incubation time. The eluted protein was concentrated using a 100,000 Da molecular mass cut off centrifugal concentrator (Amicon) of regenerated cellulose membrane and purified by size-exclusion chromatography on a custom-made Superose 6 Increase 10/600 GL gel filtration column equilibrated with 10 mM bicine pH 8.5, 150 mM NaCl, 0.5 mM EDTA, 2 mM TCEP. Purified WT mTORC2 was concentrated in gel filtration buffer to a final concentration of 3-3.5 mg/ml determined by A280 absorption using a NanoDrop 2000; Thermo Scientific. Sample was supplemented with 5% (v/v) glycerol and stored at -80 °C for later cryo-EM use. Purified mTORC2 variants with A- and I-site mutants were concentrated in gel filtration buffer to a final concentration of 0.4-2 mg/ml as determined by absorption at 280nm wavelength using a NanoDrop 2000 (Thermo Scientific). The resulting samples were supplemented with 5% (v/v) glycerol and stored at -80 °C for later use.

The coding sequence for Akt1[254], was cloned into a pAceBAC1 expression vector (Geneva Biotech, Geneva, Switzerland) with an N-terminal His10–Myc–FLAG tag by Gateway cloning. Baculovirus was produced as described for mTORC2. Akt1 was purified with anti-DYKDDDDK agarose beads as described for mTORC2. The eluted protein was concentrated using a 10,000 Da molecular mass cut off centrifugal concentrator (Amicon) of regenerated cellulose membrane and further purified by size-exclusion chromatography with a Superdex

75 Increase column equilibrated with 10 mM bicine pH 8.5, 150 mM NaCl, 0.5 mM EDTA, 2 mM TCEP. Purified Akt1 was concentrated in gel filtration buffer, supplemented with 5% (v/v) glycerol and stored at -80 °C for further experiments. Dephosphorylated Akt1 was obtained after overnight incubation of 4.5 mg of protein with 6 µg of λ-protein phosphatase (New England Biolabs) in presence of PMP buffer (New England Biolabs) and 1mM $MnCl_2$ prior to size exclusion chromatography. Successful Akt1 dephosphorylation was confirmed by Western Blot with antibodies against phospho-Akt-Ser473 (#4060 Cell Signaling Technologies, Beverly, USA) and phospho-Akt-Thr450 (#9267 Cell Signaling Technologies, Beverly, USA). Human (Delta-PH)-Akt1 protein (residues 144-480, mono-phosphorylated on T450), as described in Lucic *et al.*[195] (therein referred to as Akt1KD), was provided by T. Leonard (Max-Perutz Labs, Vienna).

Expression and assembly analysis via immunoprecipitation

A-site mutants A3, A4, A5, and I- site mutants I2, I3, I5 and mTORC2 carrying SIN1 N-terminal variants extended by a tryptophan (SIN1_W), two consecutive arginines (SIN1_2R) and three consecutive arginines (SIN1_3R) inserted between the processed Met1 and Ala2, were immunoprecipitated in small-scale using FLAG beads. Five grams wet weight of pellets from insect cells expressing A- and I- site mutants and SIN1 N-terminal variants were lysed in 50 mM bicine pH 8.5, 200 mM NaCl, 2 mM $MgCl_2$ using a Dounce homogenizer. The lysate was cleared by ultracentrifugation for 45 minutes at 35,000 x g. Soluble protein was incubated with 125 µl of anti- DYKDDDDK agarose beads (Genscript, Piscataway, USA) for 1 h at 4°C. The beads were transferred to a 5 ml gravity flow column (Pierce Centrifuge Columns, Thermo Scientific) and washed with 50 ml of buffer containing 50 mM bicine pH 8.5, 200 mM NaCl, 2 mM EDTA. Protein was eluted by 30 minutes incubation of the beads with 400 µl wash buffer supplemented with 0.6 mg/ml synthetic DYKDDDDK peptide Genscript, Piscataway, USA). Total lysate, soluble supernatant after ultracentrifugation, flowthrough from FLAG column, buffer wash and elution fraction were loaded onto a 4-15% SDS polyacrylamide gel (Bio-Rad Laboratories). Additionally, total lysate, supernatant after ultracentrifugation and elution fraction of mTORC2 WT, SIN1 N-terminal variants and mutants A5 and I5 were analysed by immunoblotting using antibodies against mTOR (#2972; Cell Signaling Technologies, Beverly, USA), SIN1 (Bethyl A300-910A), Rictor (Bethyl A300-458A) and actin (MAB1501; Merck Millipore).

Assay for mTORC2 kinase activity

mTORC2 kinase activity assays were conducted in 100 mM HEPES pH 7.4, 1 mM EGTA, 1 mM TCEP, 0.0025% Tween-20, 10 mM $MnCl_2$ using dephosphorylated Akt1 as a substrate. In a 60 µl reaction volume, 0.05 µM of either WT or A- and I- sites mutant mTORC2 were mixed with 1 µM Akt1 and, where indicated, either DMSO or 25 µM Torin1. The mixture was preincubated for five minutes at room temperature and the reaction was initiated by the addition of 10 µM ATP. After 20 minutes at 37°C the reaction was terminated by the addition of 60 µl 2x Laemmli sample buffer. The reactions were analysed by western blotting using primary antibodies against phospho-Akt-Ser473 (#4060; Cell Signaling Technologies, Beverly, USA), phospho-Akt-Thr450 (#9267; Cell Signaling Technologies, Beverly, USA), Akt (#4685), and mTOR (#2972; Cell Signaling Technologies, Beverly, USA), anti-FLAG antibodies (Sigma-Aldrich F1804), SIN1 (Bethyl A300-910A), Rictor (Bethyl A300-458A) at a dilution of 1:1000. A goat anti-rabbit HRP-labeled antibody (ab6721; Abcam, Cambridge, UK) was used as the secondary antibody at a dilution of 1:3000. Signals were detected using the Enhanced Chemiluminescence (ECL) kit SuperSignal™ West Femto Maximum Sensitivity Substrate (Thermo Scientific). Images were acquired using a Fusion FX (Vilber) imaging system.

Thermal stability assay

Thermal unfolding was monitored by Differential Scanning Fluorimetry (DSF) based on internal tryptophane fluorescence on a Prometheus NT.48 instrument (NanoTemper Technologies). Purified WT MTORC2 or mTORC2 containing mutations in A- or I- site were diluted to 0.1 mg/mL in 10 mM bicine pH8.5, 150 mM NaCl, 0.5 mM EDTA, 2 mM TCEP. High precision capillaries (NanoTemper Technologies) were filled with 10 µL sample and placed on the sample holder. A temperature gradient of 0.1°C/min from 22 to 65 °C was applied and fluorescence intensity at 330 and 350 nm was recorded. A plot of the ratio of fluorescence intensities at those wavelengths (F350/F330) was generated using a Python script. The experiment was repeated two times with five replicates per sample run each time. Melting points were calculated using PR.ThermControl software version 2.1.2. Data were analyzed using GraphPad Prism version 8.0.0 (GraphPad Software, San Diego, California USA) to generate the mean and SD of the melting points. One outlier, likely resulting from capillary handling, for sample A4 was excluded from data analysis.

In cell analysis of mTORC2 activity for A-site mutants

HEK293T cells were cultured and maintained in DMEM high glucose with 10% FCS, 4 mM glutamine, 1 mM sodium pyruvate, 1x penicillin/streptomycin. RICTOR knockout cells were

generated as described in Bossler *et al.*, 2019[255]. 4 µg of plasmids harboring RICTOR-WT, RICTOR-A_3, and RICTOR-A_5 were transfected with JetPRIME (Polyplus). 24 hours after transfection, cells were starved for serum for overnight and stimulated with 10% FCS and 100 nM insulin for 15 min. Total cell lysates were prepared in lysis buffer containing 100 mM Tris-HCl pH7.5, 2 mM EDTA, 2 mM EGTA, 150 mM NaCl, 1% Triton X-100, complete inhibitor cocktail (Roche) and PhosSTOP (Roche). Protein concentration was determined by a Bradford assay, and equal amounts of protein were separated by SDS-PAGE, and transferred onto nitrocellulose membranes (GE Healthcare). Antibodies used were as follows: AKT (Cat#2920, Cell Signaling Technology), AKT-pS473 (Cat#4060, Cell Signaling Technology), RICTOR (Cat#2040, Cell Signaling Technology), ACTIN (Cat#MAB1501, Millipore), IRDye 800CW goat anti-rabbit IgG (Cat#926-32211, LI-COR), and IRDye 680RD goat anti-mouse IgG (Cat#926-68070). Signals were detected by LI-COR Fc (LI-COR Biosciences).

In cell analysis of the dependence of mTORC2 activity on IPPK and MINPP1

HEK293T cells were cultured and maintained in DMEM high glucose with 10% FCS, 4 mM glutamine, 1 mM sodium pyruvate, 1x penicillin/streptomycin. For knockdown of IPPK and MINPP1, 0.1 x 106 cells/well were seeded in a 6-well plate and transfected with 100 nM siRNA using the jetPRIME (Polyplus) system. After 32h, cells were washed twice with PBS (-/-) and starved for serum for 16 hours. 48 hours post-transfection, cells were incubated at 37 °C with PBS (+/+) for 10 min followed by stimulation with 10 % FCS and 100 nM insulin for 15 min at 37 °C. Cells were washed with ice-cold PBS (-/-) and harvested for SDS-PAGE or RNA isolation for qPCR analysis. Knockout experiments were conducted as described above, using generated KO cells instead of transfection with siRNA. Total cell lysates were prepared in M-PER lysis buffer (ThermoFisher) containing complete inhibitor cocktail (Roche) and PhosSTOP (Roche), and protein concentrations determined by Bradford assay. Equal amounts of protein were separated by SDS-PAGE, transferred onto nitrocellulose membranes (GE Healthcare), and signals were detected by LI-COR Fc (LI-COR Biosciences). Antibodies used were as follows: AKT (Cat#2920, Cell Signaling Technology), AKT-pS473 (Cat#4060, Cell Signaling Technology), ACTIN (Cat#MAB1501, Millipore), IRDye 800CW goat anti-rabbit IgG (Cat#926-32211, LI-COR), and IRDye 680RD goat anti-mouse IgG (Cat#926-68070).

For qPCR, total RNA was isolated using the RNeasy kit (Qiagen). RNA was reverse-transcribed to cDNA using iScript cDNA synthesis kit (BIO-RAD). Semiquantitative real-time PCR analysis was performed using fast SYBR green (Applied Biosystems). Relative

expression levels were determined by normalizing each CT values to POLR2A using the ΔΔCT method. The sequence for the primers used in this study was as follows. IPPK-fw: 5'-AATGAATGGGGGTACCACGG-3', IPPK-rv: 5'-AACTTCAGAAACCGCAGCAC-3'; MINPP1-fw: 5'-AGCTACTTTGCAAGTGCCAG-3', MINPP1-rv: 5'-TGCATGACCAAACTGGAGGA-3'.
Knockout cells were generated using the LentiCRISPR system as described in Sanjana *et al.*, 2014[256]. gRNAs against IPPK and MINPP1 were expressed from LentiCRISPRv2 (kind gifts from Feng Zhang; Addgene plasmids no. 49535 and no. 52961) by transfection of HEK293T cells with 1µg DNA using jetPRIME. The following gRNA target sequences were used: IPPK gRNA 5'-TCGGCCGGTGCTCTGCAAAG-3', MINPP1 gRNA 5'-ATCCAGTCCGCGTACCACAA-3'. Following transfection, cells were selected with puromycin, propagated, and screened for loss of target protein by qPCR. DNA sequencing of PCR products confirmed insertions or deletions leading to interrupted sequencing reactions. Pools of knockout cells were used to avoid clonal variation. HEK293T cells transfected with empty vector were used as control.

Sample preparation for LC-MS analysis

10 µg of mTORC2 I- site mutants I2, I3 and A- site mutants A3, A4, and A5 were dissolved in 50 µl digestion buffer (1% sodium deoxycholate (SDC), 0.1 M TRIS, 10 mM TCEP, 15 mM chloroacetamide (CAA), pH = 8.5) using vortexing for trypsin digestion. For endoproteinase GluC and chymotrypsin digestion, the same protein aliquots were dissolved in 20 ul of a digestion buffer consisting of 1 M urea, 0.1 M ammoniumbicarbonate, 10 mM TCEP and 15 mM CAA. Samples were either incubated for 10 min at 95°C (trypsin) or 1h at 37°C (GluC and chymotrypsin) to reduce and alkylate disulfide bonds. Protein aliquots were digested over night at 37°C by incubation with sequencing-grade modified trypsin, GluC and chymotrypsin (all 1/50, w/w; Promega), respectively. Then, the peptides were cleaned up using iST cartridges (PreOmics, Munich) according to the manufacturer's instructions. Samples were dried under vacuum and dissolved in LC-buffer A (0.1 % formic acid) at a concentration of 0.05 µg/ul.

Targeted PRM-LC-MS analysis to confirm presence of mutations

To enhance the sensitivity of the LC-MS analysis, a label-free targeted LC-MS approach was carried out. Therefore, three lists of peptides considering the cleavage specificity of the three proteases used and containing all mutation sites was generated. The peptide sequences were imported into the Skyline (version 20.1 (https://brendanx-

uw1.gs.washington.edu/labkey/project/home/software/Skyline/begin.view) to generate a mass isolation list of all doubly and triply charged precursor ions for each protease. These were then loaded into a Q-Exactive plus LC-MS platform and analyzed using the following settings; The setup of the µRPLC-MS system was as described previously[257]. Chromatographic separation of peptides was carried out using an EASY nano-LC 1000 system (Thermo Fisher Scientific), equipped with a heated RP-HPLC column (75 µm x 30 cm) packed in-house with 1.9 µm C18 resin (Reprosil-AQ Pur, Dr. Maisch). Peptides were analyzed per LC-MS/MS run using a linear gradient ranging from 95% solvent A (0.15% formic acid, 2% acetonitrile) and 5% solvent B (98% acetonitrile, 2% water, 0.15% formic acid) to 45% solvent B over 60 minutes at a flow rate of 200 nl/min. Mass spectrometry analysis was performed on Q-Exactive plus mass spectrometer equipped with a nanoelectrospray ion source (both Thermo Fisher Scientific). Each MS cycle consisted of one MS1 scan followed by high-collision-dissociation (HCD) of the selected precursor ions in the isolation mass lists. Total cycle time was approximately 2 s. For MS1, 3e6 ions were accumulated in the Orbitrap cell over a maximum time of 50 ms and scanned at a resolution of 35,000 FWHM (at 200 m/z). MS2 scans were acquired at a target setting of 3e6 ions, accumulation time of 110 ms and a resolution of 35,000 FWHM (at 200 m/z). The normalized collision energy was set to 27%, the mass isolation window was set to 0.4 m/z and one microscan was acquired for each spectrum.

The acquired raw-files were converted to the mascot generic file (mgf) format using the msconvert tool (part of ProteoWizard, version 3.0.4624 (2013-6-3)). Using the MASCOT algorithm (Matrix Science, Version 2.4.1), the mgf files were searched against a decoy database containing normal and reverse sequences of the predicted SwissProt entries of Homo sapiens (www.ebi.ac.uk, release date 2019/12/09), the mTOR and Rictor mutations and commonly observed contaminants (in total 41,556 sequences for Homo sapiens) generated using the SequenceReverser tool from the MaxQuant software (Version 1.0.13.13). The precursor ion tolerance was set to 10 ppm and fragment ion tolerance was set to 0.02 Da. The search criteria were set as follows: full tryptic specificity was required (cleavage after lysine or arginine residues unless followed by proline), 3 missed cleavages were allowed, carbamidomethylation (C), was set as fixed modification and oxidation (M) as a variable modification. Next, the database search results were imported to the Scaffold Q+ software (version 4.3.2, Proteome Software Inc., Portland, OR) and the protein false identification rate was set to 1% based on the number of decoy hits. Specifically, peptide identifications were accepted if they could be established at greater than 97.0% probability to achieve an FDR

less than 1.0% by the scaffold local FDR algorithm. Protein identifications were accepted if they could be established at greater than 65.0% probability to achieve an FDR less than 1.0% and contained at least 1 identified peptide. Protein probabilities were assigned by the Protein Prophet program[258]). Proteins that contained similar peptides and could not be differentiated based on MS/MS analysis alone were grouped to satisfy the principles of parsimony. Proteins sharing significant peptide evidence were grouped into clusters. Finally, a spectral library (*.blib) was generated from the assigned MS/MS spectra and imported to Skyline together with the acquired raw data files. Only precursor ions confidently identified by database searching and present in the spectral library were employed for quantitative analysis. Quantitative result reports were further analyzed by Microsoft Excel and PRISM (GraphPad Software, San Diego, US).

EM Sample preparation and data collection

Different conditions were screened for mTORC2 in the presence and absence of substrates (Figure S2.2). For all conditions, freshly thawed mTORC2 aliquots were used to prepare samples with an mTORC2 concentration of 0.37 mg/mL. Shortly before grid preparation, the samples were diluted to reach a final mTORC2 concentration of 0.12 mg/mL.

For each grid, a small piece of continuous carbon was floated on top of the sample for one minute[259]. The carbon was then picked with a Quantifoil R2/2 holey carbon copper grid (Quantifoil Micro Tools), which was swiftly mounted in a Vitrobot (Thermo Fischer Scientific) whose chamber was set to 4°C and 100% humidity. 5 µL of buffer was then added on top of the grid on the side showing the carbon covered with particles, which was immediately blotted with a setting of 0 to 6 seconds blotting time and rapidly plunge-frozen in a mixture 2:1 of propane:ethane (Carbagas)[260].

Data were collected using a Titan Krios (Thermo Fisher Scientific) transmission electron microscope equipped with either a K2 Summit direct electron detector (Gatan), a K3 direct electron detector (Gatan) or a Falcon 3EC direct electron detector (Thermo Fisher Scientific) using either EPU (Thermo Fisher Scientific) or SerialEM[261] (Figure S2.2). Cameras were used in counting and/or super-resolution mode. During data collection, the defocus was varied between -1 and -3 µm and four exposures were collected per holes. Stacks of frames were collected with a pixel size of 0.84 Å/pixel and a total dose of about 70 electrons/Å2.

Data processing

For all datasets, the initial processing was done in similar fashion. First, the stacks of frames were aligned and dose-weighted using Motioncor2[262]. GCTF[263] was used to estimate the contrast transfer function (CTF) of the non-dose weighted micrographs. After a selection of good micrographs using both the quality of the power spectra and the quality of the micrographs themselves as criteria, particles were picked using batchboxer from the EMAN1.9 package[264] using particle averages from manually picked particles as references. Particles were extracted using Relion3.0[265], followed by two rounds of 2D classification using cryoSPARCv2 (Structura Biotechnology Inc.)[266] (Table S2.2). The first reference was generated by ab-initio reconstruction using cryoSPARCv2. Good particles from 2D classification were then used for a homogeneous 3D refinement followed by non-uniform refinement using cryoSPARCv2. Two masks were then generated manually around each half of the pseudo-dimeric mTORC2 using UCSF Chimera[267] and two focused refinements around each half of the complex using cryoSPARCv2 were performed using those masks. For the dataset 1 which contained ΔPH-Akt1, the resolution was further improved by performing Bayesian particle polishing[268] followed by CTF refinement using Relion3.1. Those particles were again subjected to a round of non-uniform refinement and local refinement using cryoSPARC v2. For each reconstruction, the maps were sharpened using phenix.auto_sharpen[269] or were transformed to structure factors using phenix.map_to_structure_factors[270] and sharpened in COOT[271].

Further 3D classifications without alignment for local structural variability close to the catalytic center were performed using the particles from the datasets containing the purified Akt1 and, independently, the ones from the dataset with ΔPH-Akt1 using Relion3.0[265] and using a mask manually created in UCSF Chimera[267]. After classification, the particles were used for refinement using cryoSPARCv2 (Structura Biotechnology Inc.). To compare the density of the sample with and without ATPγS, the final density (Volume A) was filtered to 4.2 Å and compared to the density without ATPγS (Volume F). Difference density was calculated using UCSF ChimeraX[272].

Modelling and docking

First, mTOR and mLST8 models were taken from the EM structure of mTORC2 (PDB : 5ZCS[229] and each fold was rigid-body fitted into the better half of the density. Minor changes in mTOR conformation were done manually to fit the density, then Rictor and SIN1 were manually built de novo using COOT[271]. Map quality enabled direct model building for structured regions, lower resolution density provided connectivity information for assigning

and linking regions of Sin1 and Rictor as shown in Extended Data Fig. 5c and 6b. The second half of mTORC2 was made by copying and rigid-body fitting each chain of the first half in the second one. Finally, the structure of either one-sided or two-sided mTORC2 were refined using phenix.real_space_refine[269] (Table S2.1), using Ramachandran and secondary structure restraints. As the horns of mTOR were flexible and their local resolution were significantly lower, additional reference restraints were applied, using PDB: 6BCX[42] as reference. The model was then validated by comparing the FSCs calculated for the experimental density and the models (Figure S2.3). In addition, both the half and full structure were also refined in their respective half map (half map 1) and the FSC of this structure against the same half map (half map 1), the other half (half map 2) and the full map were compared. The similarity of the curves shows that the structure was not overfitted[273].

Ligand identification via mass spectrometry

Inositol hexakisphosphate (InsP6) (Sigma-Aldrich) was directly dissolved in 10 mM ammonium acetate (pH8.5) and diluted to 50 µM. mTORC2 in cryo-EM buffer was buffer exchanged and concentrated in 10 mM ammonium acetate (pH8.5) using an Amicon Ultra 0.5 mL – MWCO 100kDa. The concentrated complex was mixed with an equal volume of Phenol at pH8, thoroughly vortexed for 30 seconds and incubated at room temperature for 30 minutes. The tube was then centrifuged for 5 min at 15000 xg. The aqueous phase was then used for mass spectrometry. A sample containing only buffer and no protein was subjected to the same treatment for reference. The samples were then mixed with four volumes of injection buffer (90% Acetonitrile, 9% Methanol, 50 mM ammonium acetate (pH7) and directly injected using a Hamilton syringe in a Synapt G2-SI HDMS (Waters) in negative mode and using the T-Wave IMS.

Figure generation

All density and structure representations were generated using UCSF ChimeraX[272]. Difference densities were calculated in ChimeraX using the “volume subtract” command. Local resolutions were estimated using cryoSPARC v2 (Structura Biotechnology Inc.). The electrostatic surface representation of Rictor was generated using APBS (Adaptive Poisson–Boltzmann Solver[274]). Multiple sequence alignment was performed using Clustal Omega[275] and visualized with Espript[276]. Conservation analysis was done with AL2CO[277] and visualized in UCSF ChimeraX[272].

2.10.2 Supplementary Figures

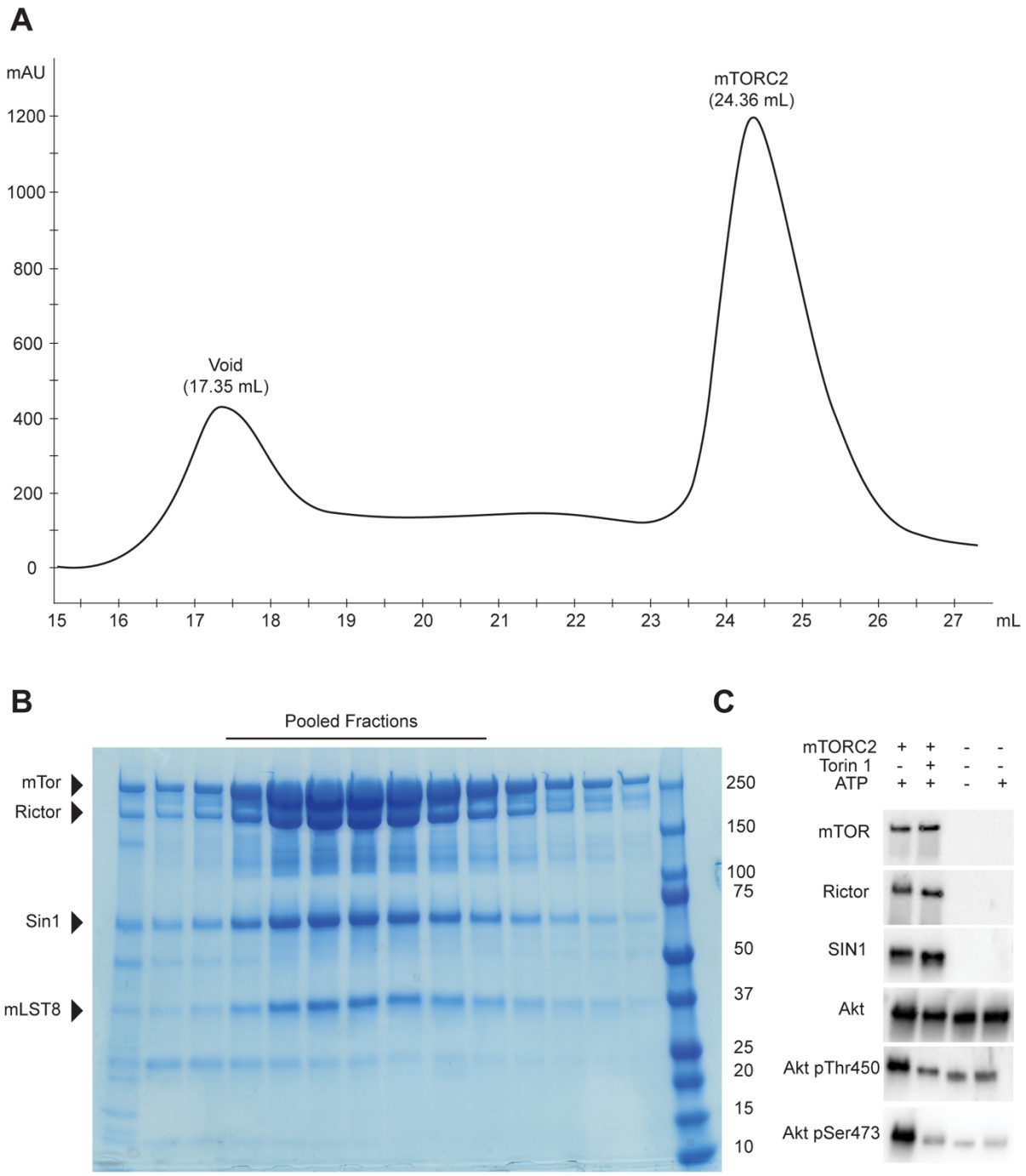

Figure S2.1 mTORC2 purification and characterization.
A Size exclusion elution profile of mTORC2 from a custom made Superose 6 Increase 10/600 GL column at a flow rate of 0.1 mL/min. The void and the mTORC2 peaks are indicated. **B** SDS-polyacrylamide gel of the fractions of the size exclusion chromatography. Fractions pooled for further analysis are indicated. **C** Kinase activity assay of purified mTORC2 using Akt1 as a substrate. Western blots showing the phosphorylation state of Akt1 in the presence and absence of mTOR inhibitor Torin1, ATP and mTORC2. Akt1 phosphorylation is detected

by phospho-specific antibodies as described in Methods. Unprocessed gels are shown in the Supplementary Data.

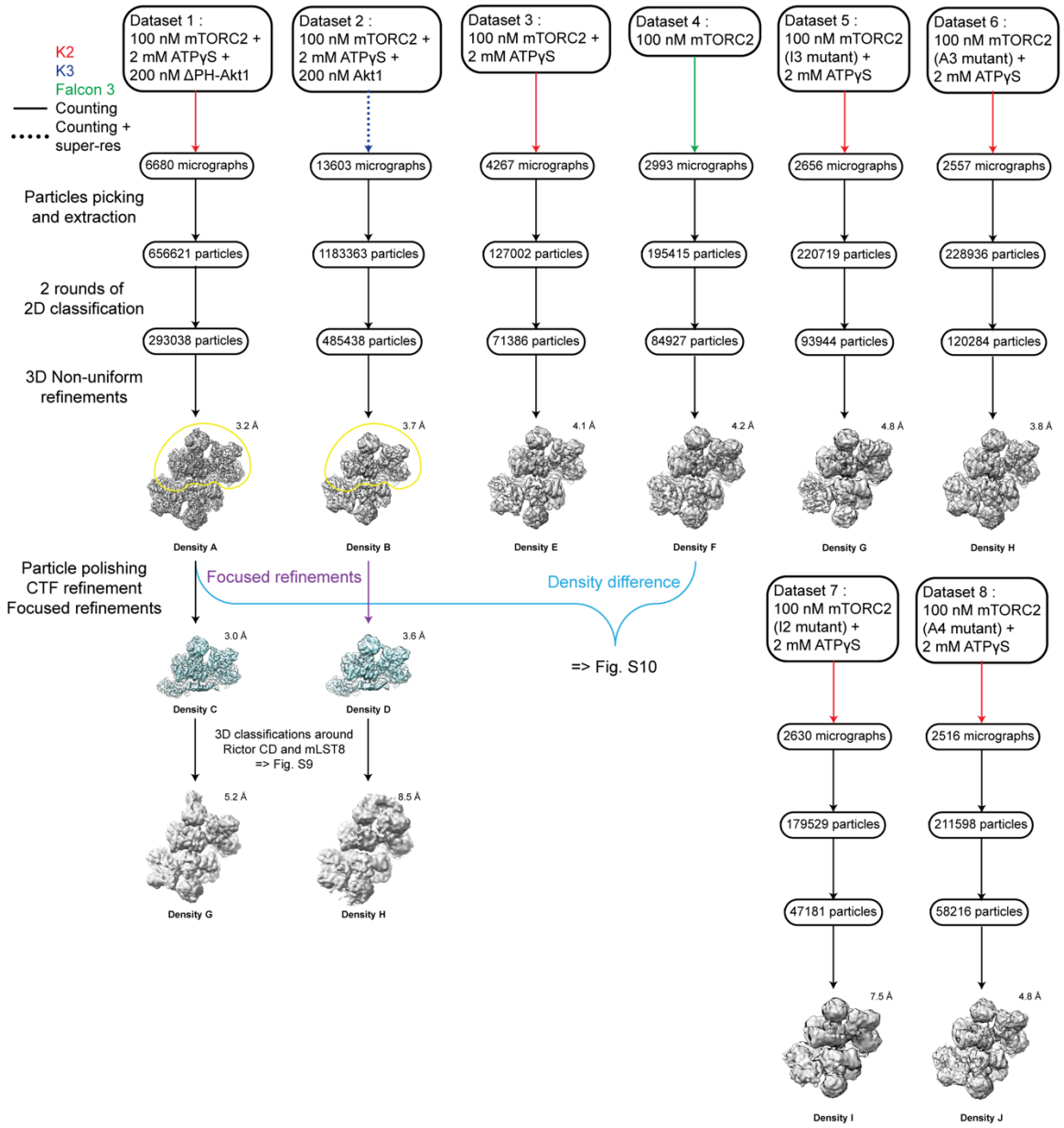

Figure S2.2 CryoEM data processing scheme.
Four datasets were collected with different conditions: with full-length Akt1 (dataset 2), ΔPH-Akt1 (dataset 1) and without Akt1 (dataset 3) in the presence of ATPγS, and dataset 4 without addition of ATPγS. Dataset 1 reached the highest resolution and was used for further processing using CTF parameter refinement and Bayesian particle polishing to reach the highest resolution of this study, Density C, with a resolution of 3.0Å. Both datasets 1 and 2 were used for 3D classifications in the proximity of mLST8 after a refinement focused on the better half. Four further datasets (datasets 5-8) were collected for mTORC2 containing mutant variants of mTOR and Rictor, respectively, to analyze the impact of mutations

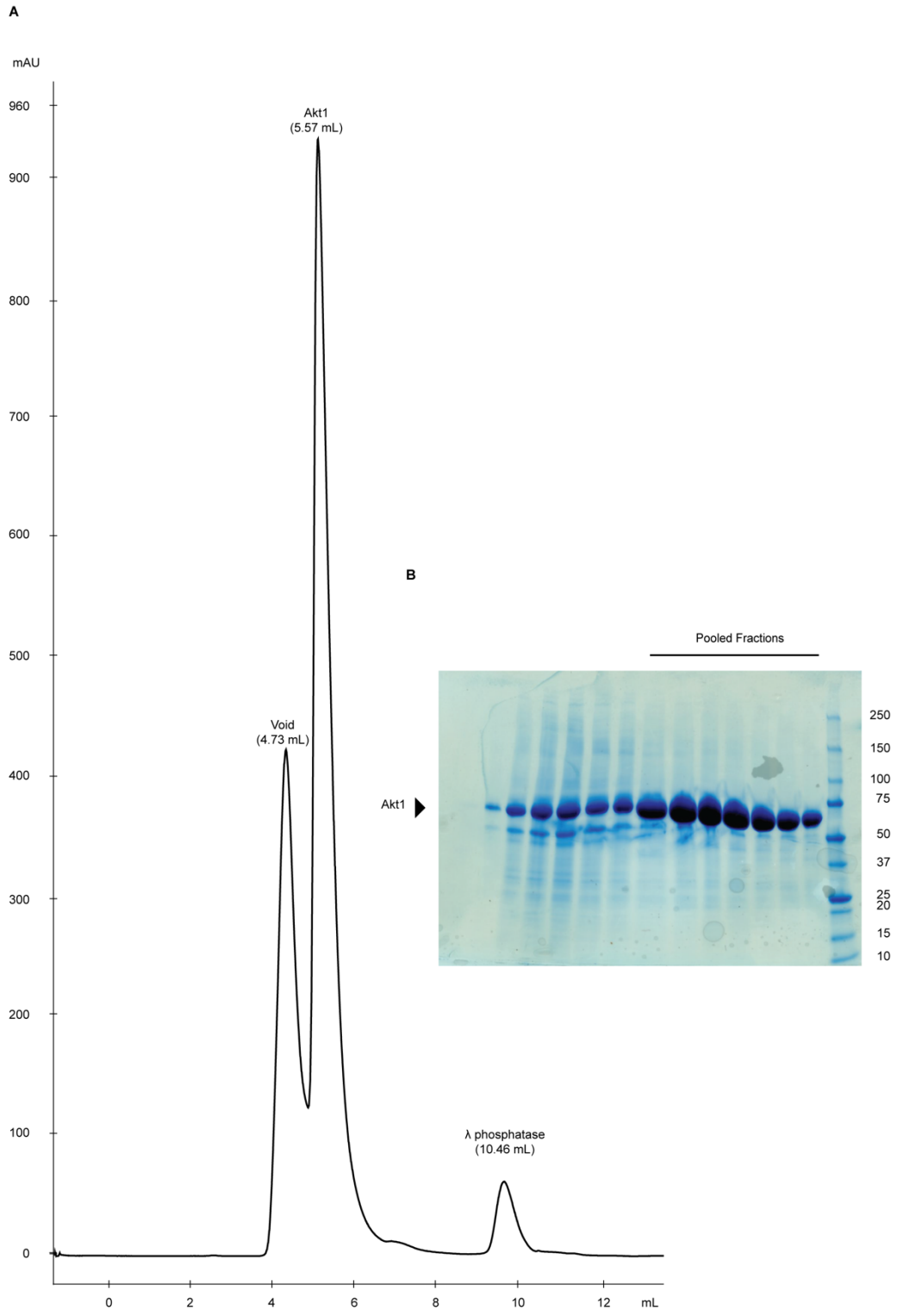

Figure S2.3 Purification of Akt1.
A Elution profile of Akt1 after dephosphorylation by λ-phosphatase in size exclusion chromatography on Superdex 75 Increase. The void, the Akt1 and λ-phosphatase peaks are indicated. **B** SDS-polyacrylamide gel of the fractions of the size exclusion elution. Fractions pooled for the final sample are indicated.

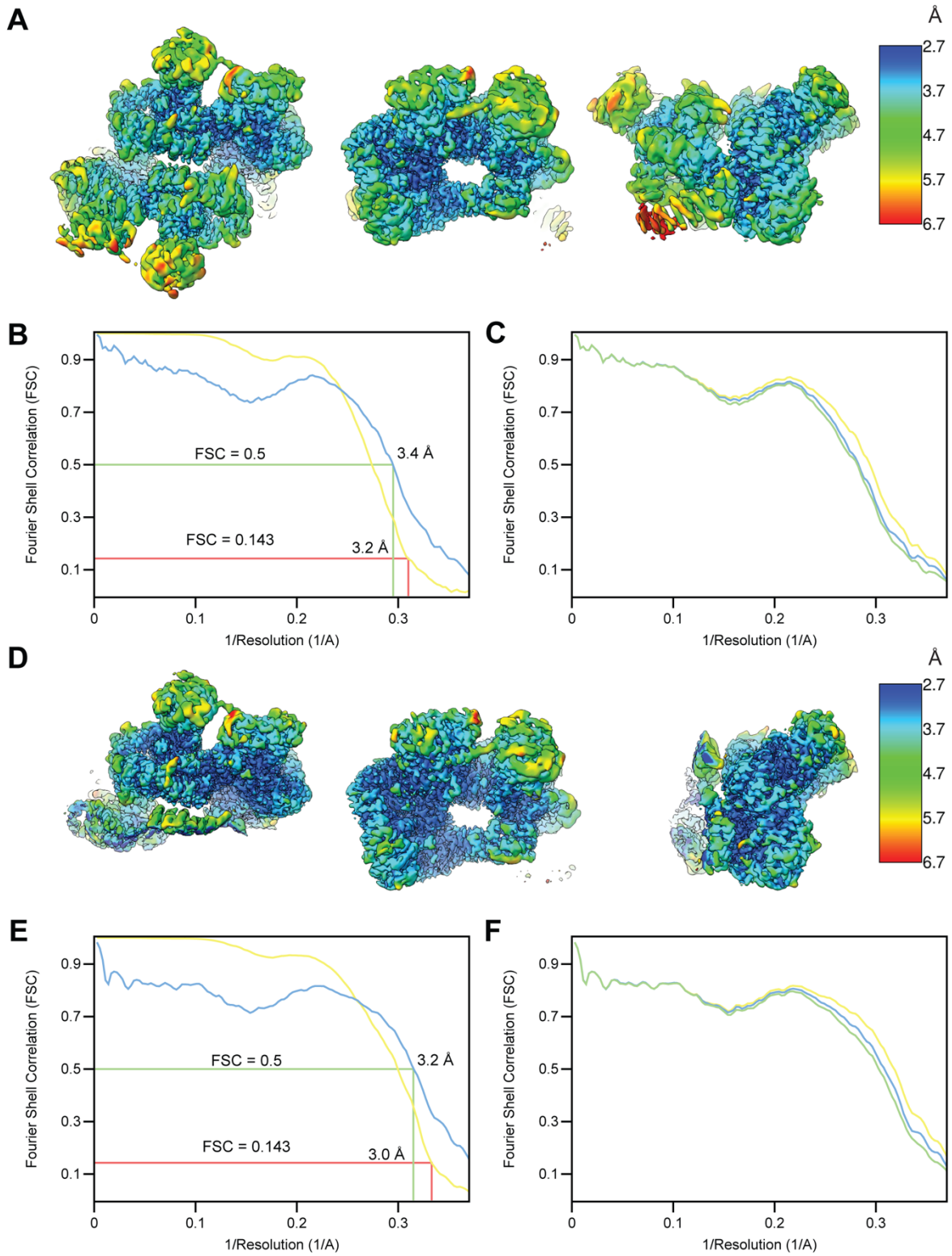

Figure S2.4 Resolution of cryo EM reconstructions of mTORC2.
A Three views of local resolution heatmaps for non-uniform refinement (Density A). Local resolution varies between ~2.7 Å in the core of one half and 6-7 Å for the flexible region of the second half. **B** FSC curves calculated between the two half maps (yellow) and between the model and the non-uniform refinement map (blue). The overall resolution of the map is 3.2 Å (FSC=0.143) and is close to the 3.4 Å resolution of model versus map (FSC=0.5). The

large local resolution differences (Panel A) are most likely responsible for the deviation between half-map and model-based resolution. **C** FSC curves calculated between the model refined in the half map 1 versus the half map 1 (blue), the half map 2 (green), and the full map (yellow). **D** Same as panel **A** but for the good half (Density C), which was used for model building and refinement. **E** and **F** similar to **B** and **C** respectively, but for maps calculated with a mask around the good half.

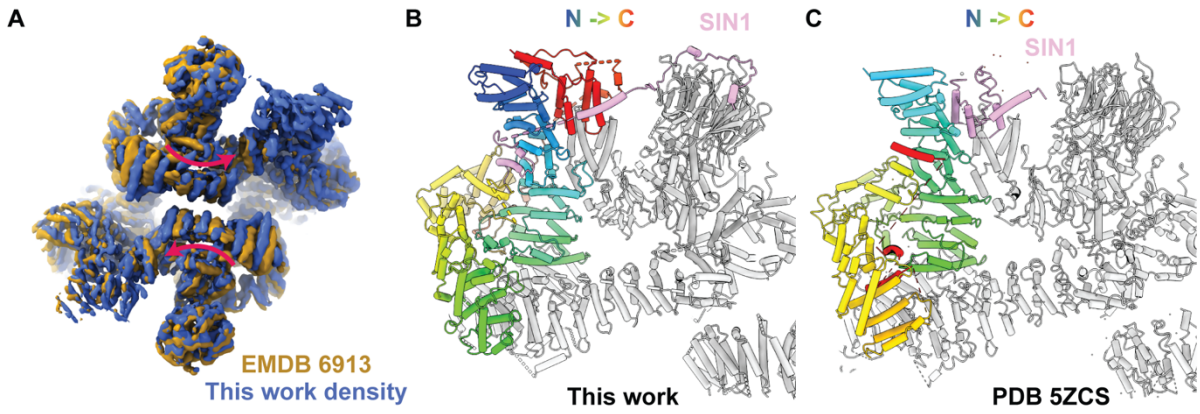

Figure S2.5 Comparison of current and previous mTORC2 structures.
A Overlay of mTORC2 density A (blue) filtered down to 4.9 Å to match the resolution of an earlier mTORC2 reconstruction (EMDB 691328) showing the inward rotation of the FAT region in the current reconstruction. A similar mode of rotation is apparent when comparing to an earlier intermediate resolution structure of human mTORC2 (EMDB 392730). **B** and **C**, Overview of Rictor and SIN1 topology in the current structure (B) and a previous mTORC2 model (PDB: 5ZCS28) (C). SIN1 is coloured in pink and Rictor is coloured by sequence from blue (N-terminus) to red (C-terminus).

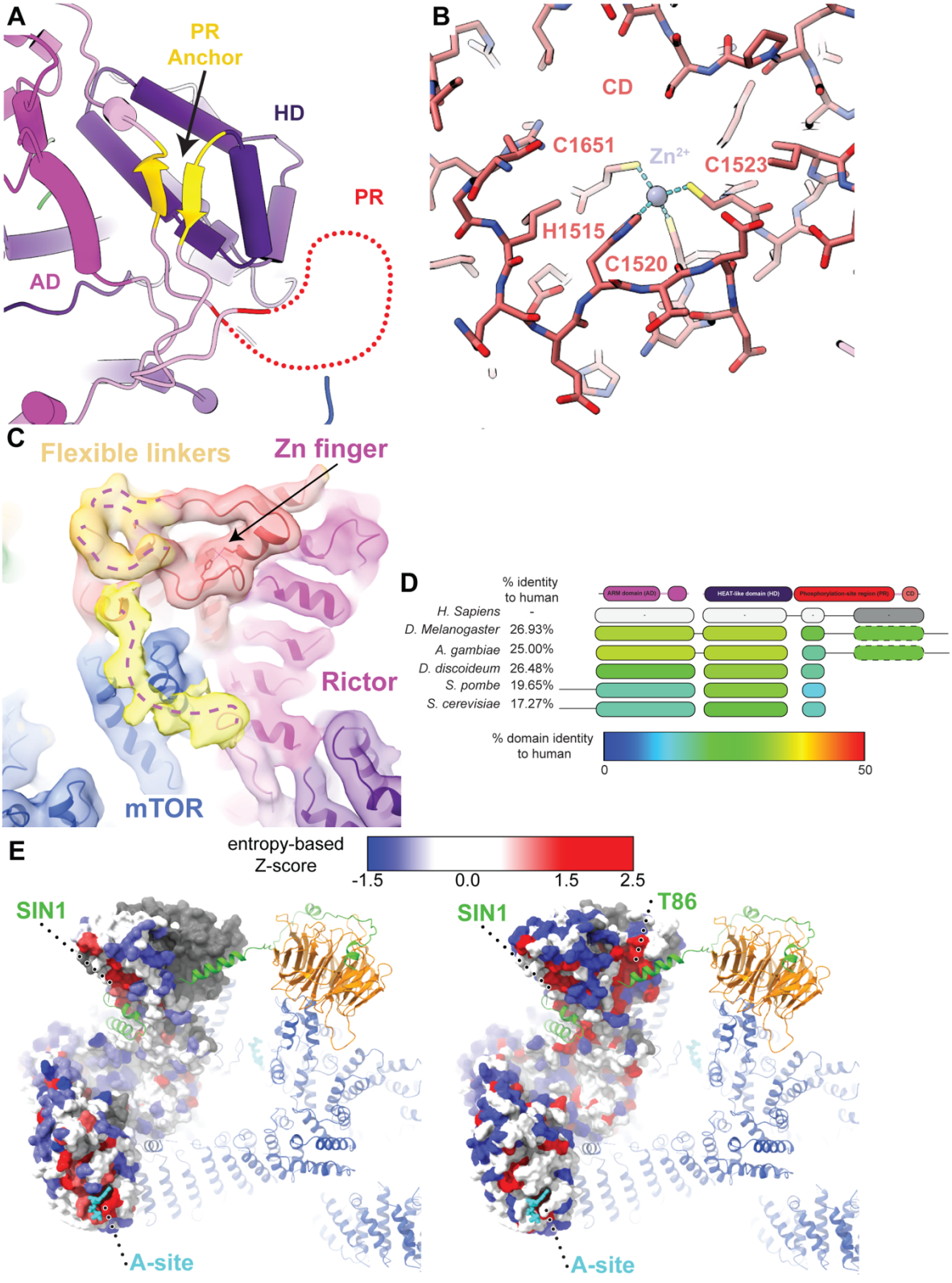
A
PR
Anchor
HD
PR
AD
B
CD
C1651
Zn2+
C1523
H1515
C1520
C
Flexible linkers
Zn finger
Rictor
mTOR
D
% identity
to human
H. Sapiens -
D. Melanogaster 26.93%
A. gambiae 25.00%
D. discoideum 26.48%
S. pombe 19.65%
S. cerevisiae 17.27%
ARM domain (AD)
HEAT-like domain (HD)
Phosphorylation-site region (PR)
CD
% domain identity
to human
0
50
E
entropy-based
Z-score
-1.5
0.0
1.5
2.5
SIN1
A-site
SIN1
T86
A-site
F
SP|Q6R327|RICTR_HUMAN
SP|Q6R327|RICTR_HUMAN
TR|Q7YU91|Q7YU91_DROME
TR|Q7PSX6|Q7PSX6_ANOGA

Figure S2.6 PR anchor and Zn^{2+} binding site in Rictor.
A Close-up view of the antiparallel-strands (gold) which are located in sequence before and after the PR of Rictor, anchoring the PR to the top of HD. **B** Close-up view of the Rictor CD zinc finger, which is part of the four-helix bundle and is formed by His1515, Cys1520, Cys1523, and Cys1651. **C** An overall mTORC2 reconstruction filtered to 6Å resolution reveals flexible linker segments (dashed line) and the connectivity in the CD region. The map is shown at 4σ contour level and flexible linkers are highlighted in orange (3.5σ contour level). Another linker visible at lower contour level (shown at 2.5σ contour level in yellow) shows the connectivity to the preceding structured segment of Rictor. **D** Sequence conservation in Rictor. A multiple sequence alignment of Rictor orthologs is analysed by AL2CO75 (entropy based conservation measure, independent counts) which shows four conserved blocks colored according to their respective percent identity relative to H. sapiens Rictor. The fourth block, corresponding to the end of the PR and the CD, is only conserved in metazoans. **E** Surface representation of Rictor coloured by residue conservation within eukaryotes (left) and metazoans (right). Blue represents poorly conserved residue, while red shows high conservation. Conserved patches are found around the A-site and the region interacting with Sin1. Grey regions are not found in all species compared. **F** Multiple sequence alignment of metazoan homologs of Rictor around the Zinc finger. The residues coordinating the zinc are underlined with a star.

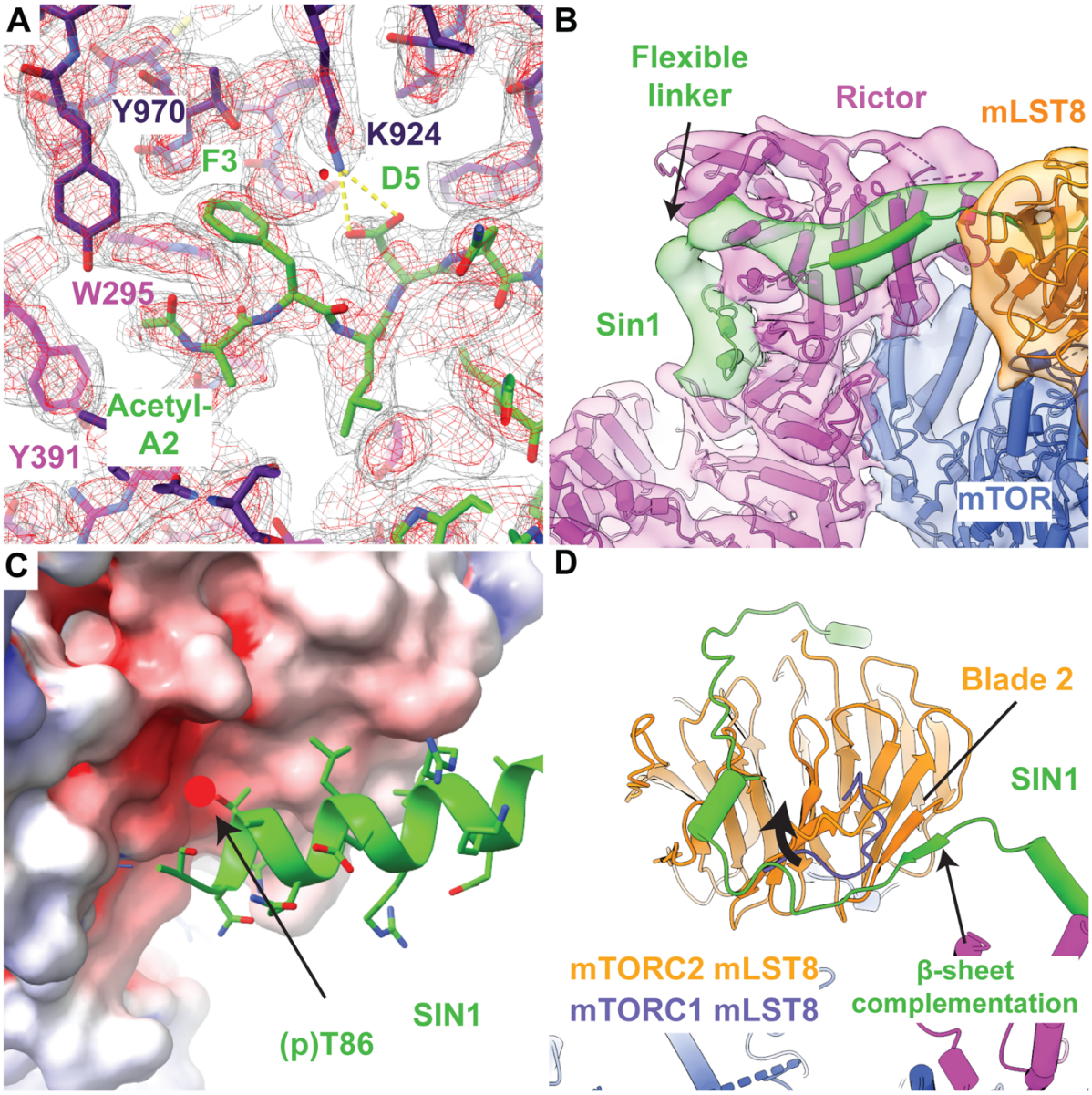

Figure S2.7 Local structural features and interactions of SIN1.
A Close-up view of the N-terminal end of SIN1 (green), which is found deeply inserted between the AD (magenta) and the HD (dark magenta) of Rictor. Possible hydrogen bonds are indicated as a dashed yellow line. **B** Overview of the poorly ordered SIN1 linker between its N-terminal region and the traverse shown using a map filtered to 10Å resolution. **C** Close-up view of Thr86 of SIN1. Rictor is shown as a surface and coloured according to the electrostatic potential. Thr86 is inserted into a negatively charged pocket and phosphorylation (red circle) is likely incompatible with insertion into this pocket. **D** Different conformations of the linker between sheet three and four of the third blade of mLST8 are observed in mTORC2 (orange) and mTORC1 (blue). SIN1 extends towards the second blade of mLST8 and interacts via β-strand complementation.

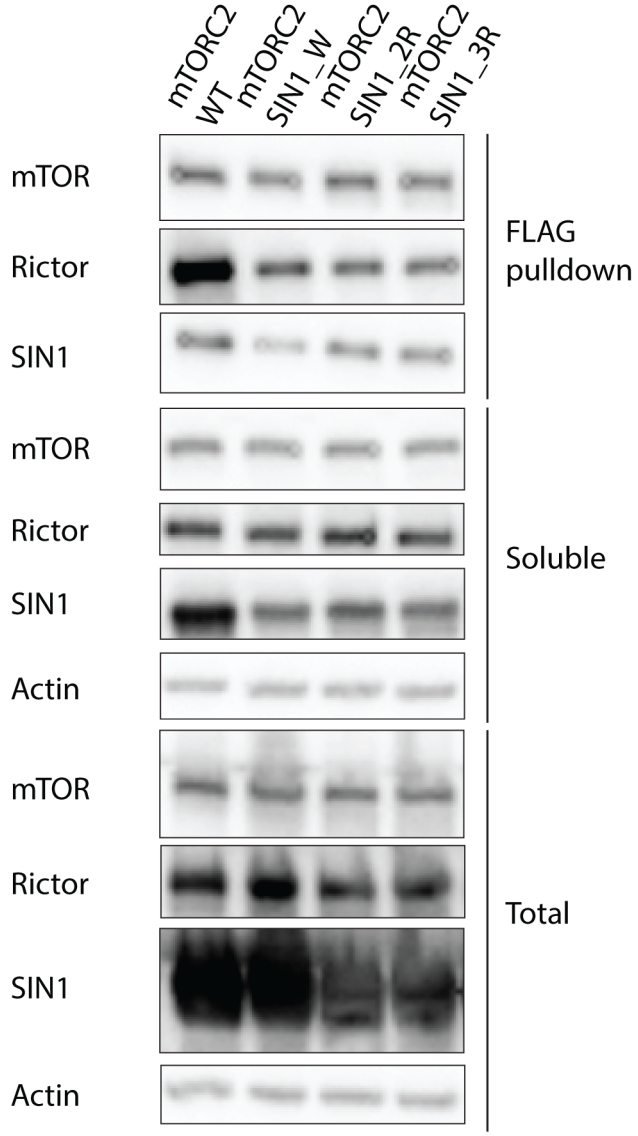

Figure S2.8 Analysis of expression and mTORC2 integration of SIN1 variants.
Western blot from lysate and mTOR-based FLAG-bead pulldown of in insect cells recombinantly overexpressed mTORC2 WT and mTORC2 carrying variants of SIN1 with insertion of a tryptophan (mTORC2 SIN1_W), two consecutive arginines (mTORC2 SIN1_2R) and three consecutive arginines (mTORC2 SIN1_3R) at its processed N-terminus. Total lysate, soluble input protein after centrifugation and Flag-bead pulldown were blotted with immunodetection for mTOR, Rictor and SIN1. Actin was used as loading control. mTOR, Rictor and SIN1 expression levels are comparable in the WT and SIN1 N-terminal variants, but Rictor and SIN1 pull-down is lower in mutant variants than in mTORC2 WT.

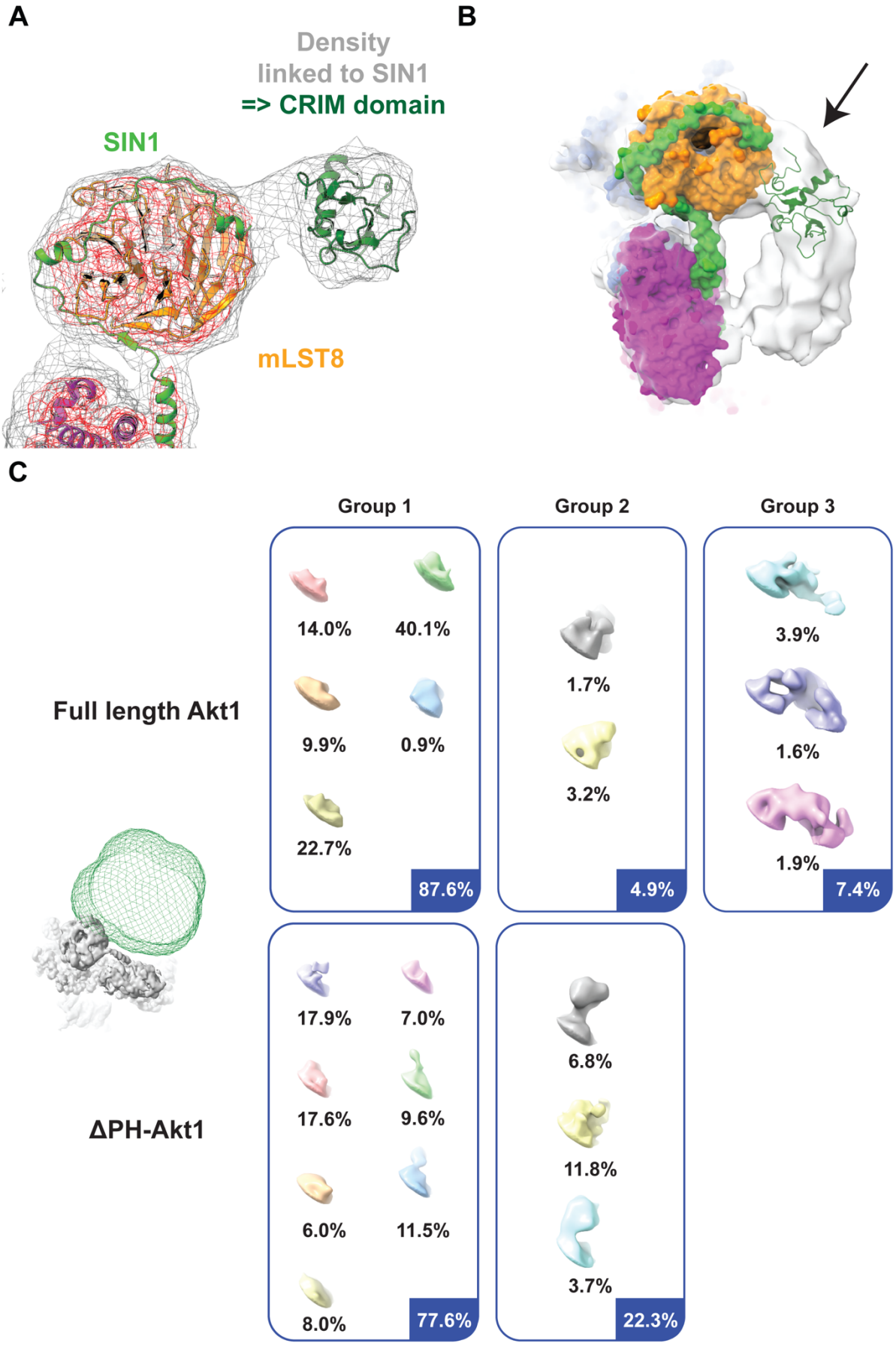
A
Density
linked to SIN1
=> CRIM domain
SIN1
mLST8
B
C
Group 1
Group 2
Group 3
Full length Akt1
14.0%
40.1%
9.9%
0.9%
22.7%
87.6%
1.7%
3.2%
4.9%
3.9%
1.6%
1.9%
7.4%
ΔPH-Akt1
17.9%
7.0%
17.6%
9.6%
6.0%
11.5%
8.0%
77.6%
6.8%
11.8%
3.7%
22.3%

Figure S2.9 Local structural features and substrate recognition by SIN1.
A Overview of Sin1 and mLST8 in density G, shown at two different contour levels (red and grey), highlights the extra density found in the continuation of Sin1. **B** View of the structure above the catalytic site shown within density H showing the visible arch of extra density found between mLST8 and Rictor. The structure of the CRIM domain (PDB 5RVK) was fitted into the density, explaining part of the arch. The second part cannot be explained unambiguously. **C** Local classification without alignment around the SIN1 CRIM domain in density G. Top view of 3D classes calculated with a mask around Rictor CD and mLST8. (show on the left in green relative to the high-resolution reconstruction). The top ten classes are calculated from datasets collected for samples containing full length Akt1, while the bottom ten classes are of samples containing ΔPH-Akt1. Classes showing small extra density, probably corresponding to the CRIM domain were put in group 2, while the classes showing a more “arch”-like structure were put in the group 3.

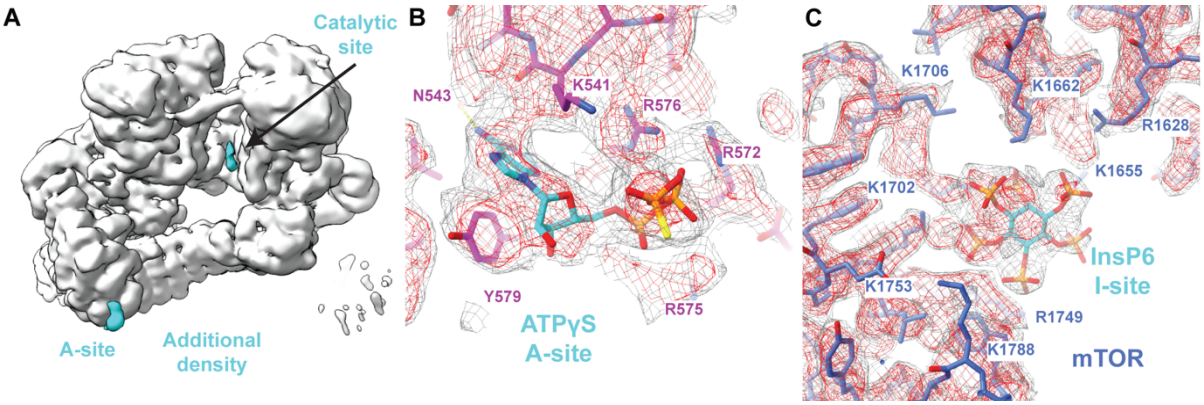

Figure S2.10 Overview of mTORC2 ligand binding sites.
A Difference densities between the reconstructions in presence (Density A, low pass filtered to 3.9Å) and absence of ATPγS (Density D, showed in grey) are shown in light blue (shown at 4σ) in the A-site and the catalytic site, highlighting the similarity of differences in both site. **B** Close-up view of ATPγS in the A-site in Rictor. **C** Close-up view of InsP6 bound to the I-site in the FAT domain of mTOR (blue). For panel (B), and (C), density for the focused refinement around one protomer is shown in mesh style at two contour levels (grey and red). (Density D).

Figure S2.11 Sequence conservation of Rictor
Multiple sequence alignment of Rictor orthologs showing conservation and secondary structure. Blue boxes represent region of BLOSUM62 similarity score above 0.1, while the one highlighted in red are strictly conserved among the shown sequences.

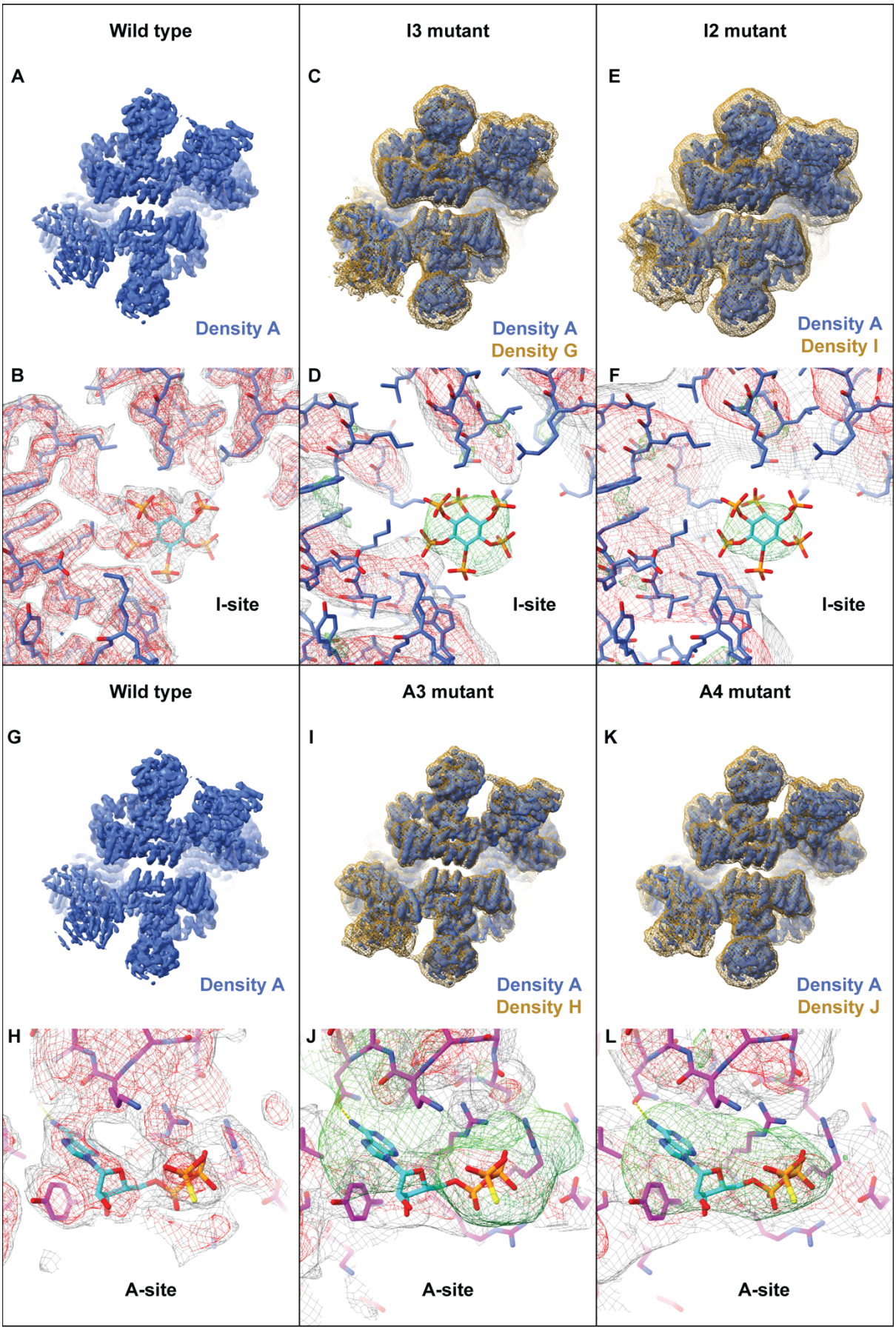
Wild type
A
Density A
B
I-site
I3 mutant
C
Density A
Density G
D
I-site
I2 mutant
E
Density A
Density I
F
I-site
Wild type
G
Density A
H
A-site
A3 mutant
I
Density A
Density H
J
A-site
A4 mutant
K
Density A
Density J
L
A-site

Figure S2.12 Comparison of reconstructions of wild type mTORC2 and I-site or A-site variants

A and **G** Overall cryoEM reconstruction of wt-mTORC2 in presence of ATPγS and ΔPH-Akt1 for the indicated variants of mTORC2. **D** Close-up view of the I-site in the wt-mTORC2. **E**, **F**, **K**, and **L** Overlay of mTORC2 density A (blue) filtered down to 4.9 Å with mutant mTORC2 reconstruction. **E**,**F**. Close up-view of the I-site of the mTOR mutants (grey and red) with the difference density with the wt-mTORC2 (green). **J** Close-up view of the A-site in the wt-mTORC2. **K**,**L**. Close up-view of the A-site of the mutant Rictor mutant (grey and red) with the difference density with the wt-mTORC2 (green).

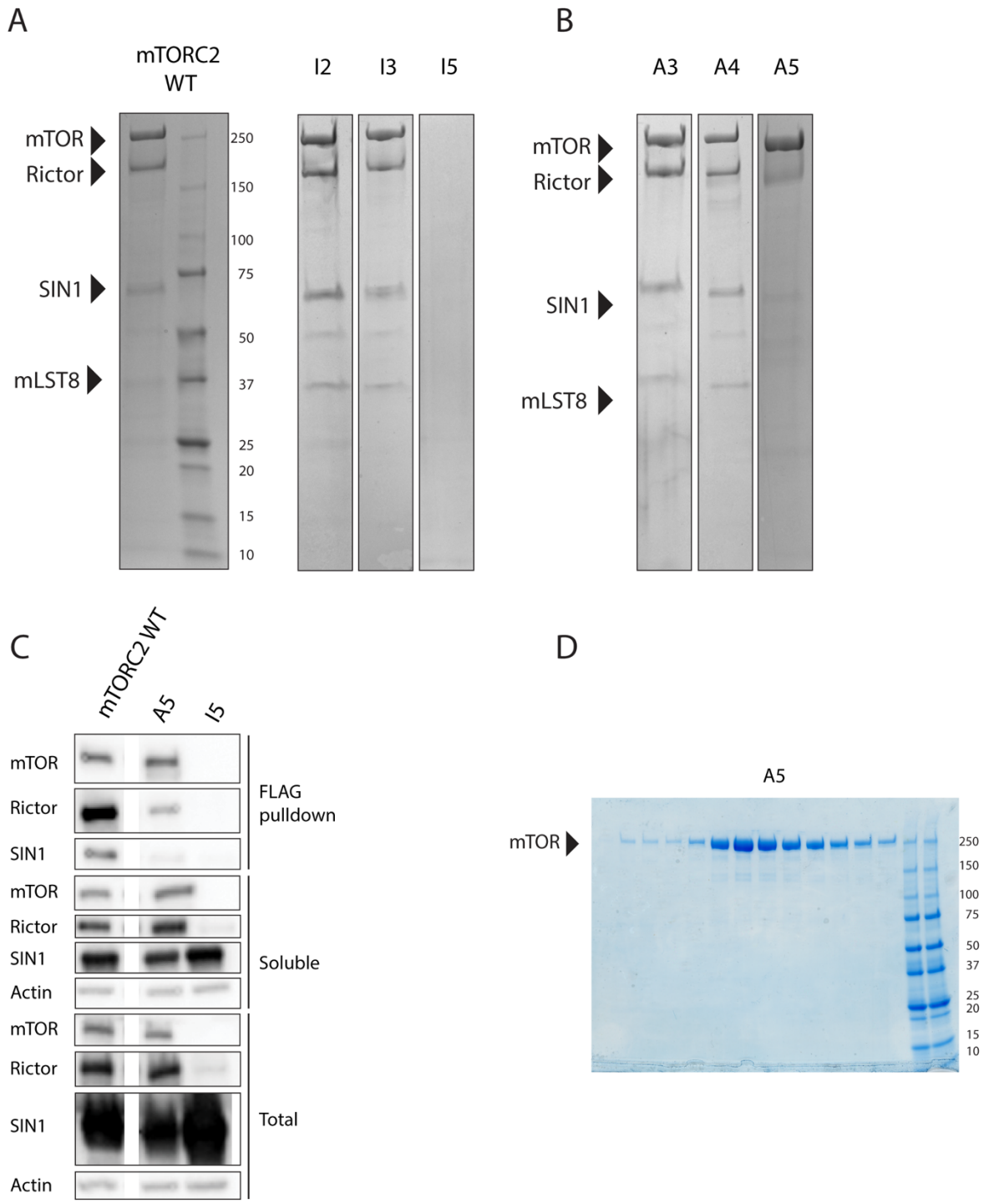

Figure S2.13 Expression and assembly of A- and I- site mutants into mTORC2
A Coomassie-stained SDS-polyacrylamide gel analysis of mTOR-based FLAG bead pulldown from recombinant overexpression in insect cells for mTORC2 WT and two variants with mutations in the I-site. mTOR mutants I2 and I3 assemble into mTORC2 complexes, for mutant I5, neither mTOR nor other mTORC2 subunits are pulled down. **B** Coomassie-stained SDS-polyacrylamide gel of a small-scale mTOR-based FLAG bead pulldown of four Rictor A-site mutants. Mutants A3 and A4 assemble into mTOR complexes. Mutant A5 shows lower

level of pulled down Rictor and SIN1. **C** Analysis of protein levels from recombinant overexpression in insect cells of mTORC2 components for mutant variants I5 and A5, which show no or partial complex assembly. Rictor mutant A5 shows comparable expression levels to WT in the total and input fractions but less SIN1 and Rictor are pulled down, indicative of defective complex assembly. For mTOR mutant I5, mTOR is not detected, Rictor levels are lower than WT, but SIN1 is present at WT levels. **D** SDS-polyacrylamide gel of size exclusion chromatography after up-scaled recombinant insect cell overexpression of mTORC2 with Rictor variant A5. Purification yielded a diminished Rictor content, indicating defective complex assembly.

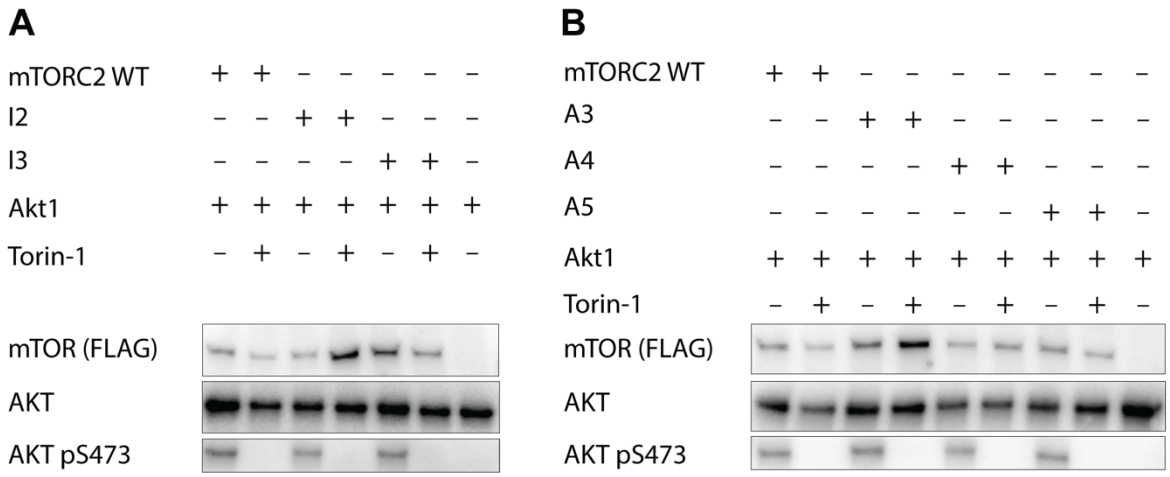

Figure S2.14 Effect of A- and I- site mutations on mTORC2 activity in vitro
In vitro kinase activity assay of purified mTORC2 for two I-site and three A-site variants (A5 purifies as only mTOR) compared to mTORC2 WT, using Akt1 as substrate and immunodetection of AKT pSer473 as readout for activity. Addition of Torin-1 is used for negative control. **A** Analysis of I-site variants I2 and I3, all variants display activity. **B** Analysis of A-site variants A3, A4 and A5 (purified with diminished Rictor content), all variants display activity.

A

	Apparent Melting Point °C		
Sample ID	Mean	SD	Replicates
mTORC2 WT	44.6	0.428	5
I2	42.8	0.354	5
I3	44.4	0.339	5
A3	44	0.563	5
A4	44	0.443	4
A5	Not measurable		

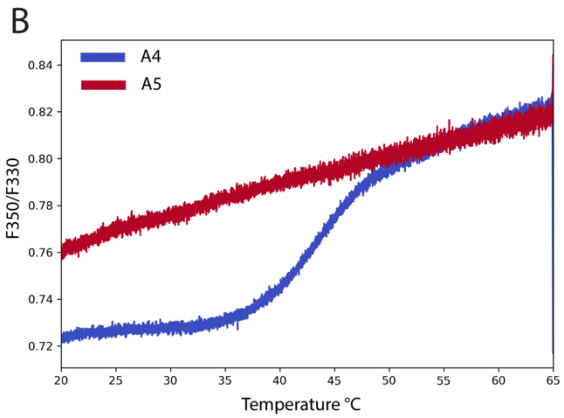

Figure S2.15 Thermal stability of A- and I- site variants of mTORC2.
A Mean and SD of the mean of the melting points of mTORC2 WT and two I-site and two A-site variants, as recorded by nanoDSF measurements. **B** Plot of the ratio of fluorescence at wavelengths 350/330 nm plotted against increasing temperature to determine the Tm of the analyzed protein. Variant A5, which purifies with diminished Rictor content shows no defined melting point, in contrast to variant A4 that contains only one mutation less, indicating exposure of tryptophan residues already at low temperatures.

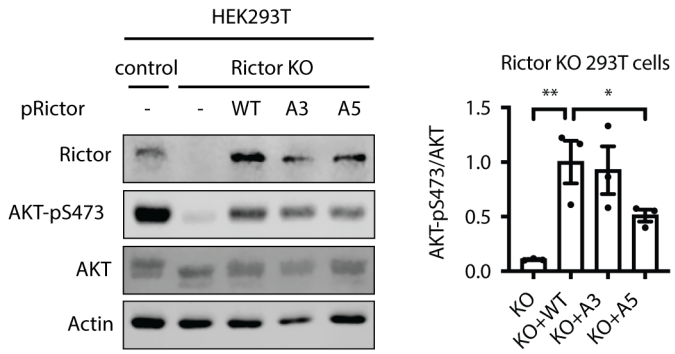

Figure S2.16 In cell mTORC2 activity for mTORC2 A-site variants.
Immunoblots of lysates from control or Rictor knockout HEK293T cells complemented with Rictor-WT, Rictor variant A3, or Rictor variant A5. Cells were starved for serum for overnight and stimulated with 10% FCS and 100 nM insulin for 15 min. Actin serves as a loading control. For quantification, AKT-pS473 signals are normalized to total AKT signals. One-way ANOVA, **$p<0.01$, *$p<0.05$. N=3.

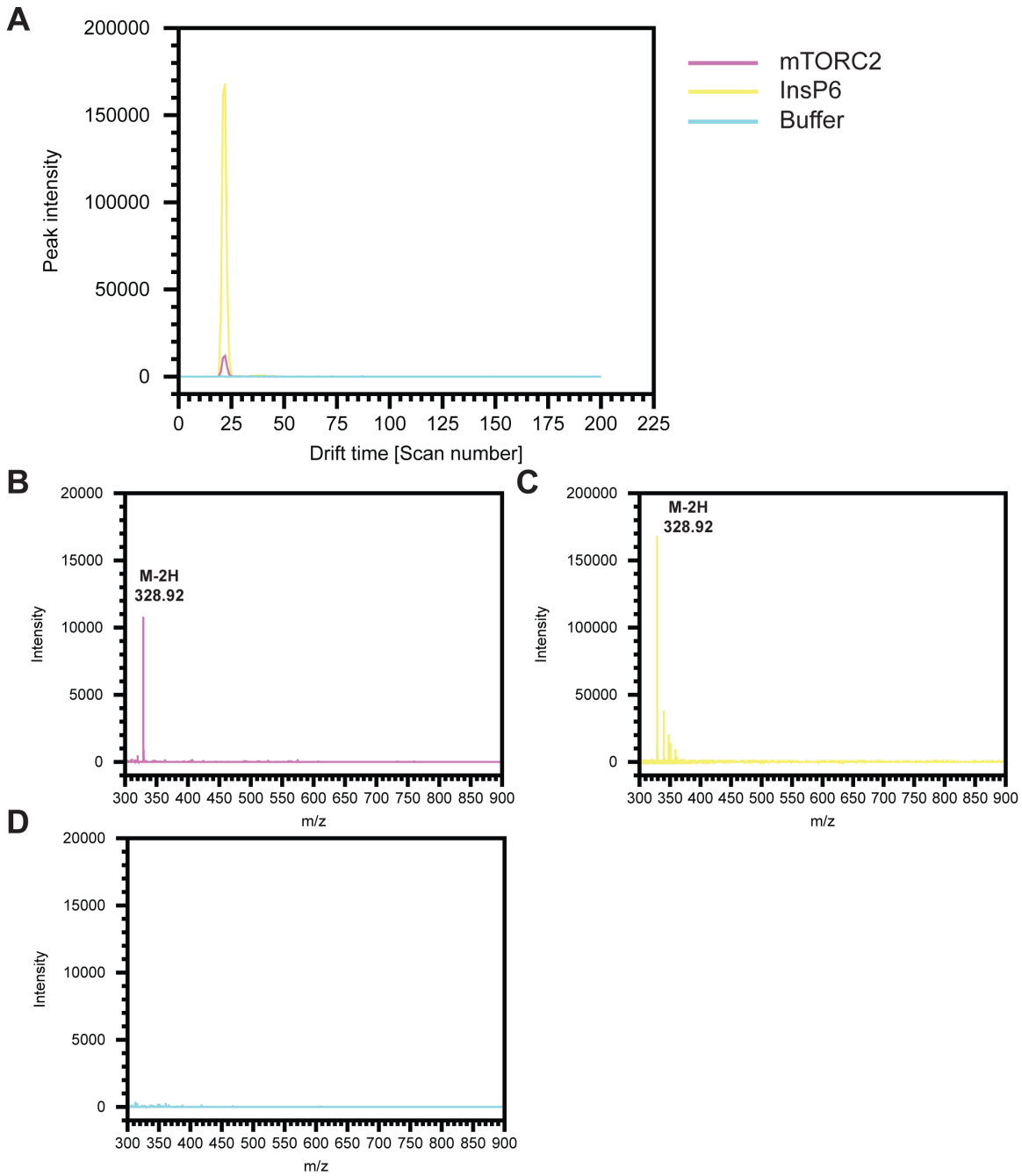

Figure S2.17 Mass spectrometry analysis for ligand identification.
A Ion mobility chromatogram for the m/z 328.92 +/- 0.01 Da. The buffer control curve (blue) which was treated as the sample one (magenta) does not show any peak in this range, while the InsP6 reference (yellow) shows a strong peak around scan 22. The same peak was found in our sample (magenta) at the same drift time. **B** Mass spectra corresponding to the scan 22 in the ion mobility is shown between 300 and 900 Da. Peaks corresponding to the doubly charged InsP6 are observable in the mTORC2 sample (magenta) **B** and in the InsP6 reference sample (yellow) **C** No significant peaks are detected in the buffer control.

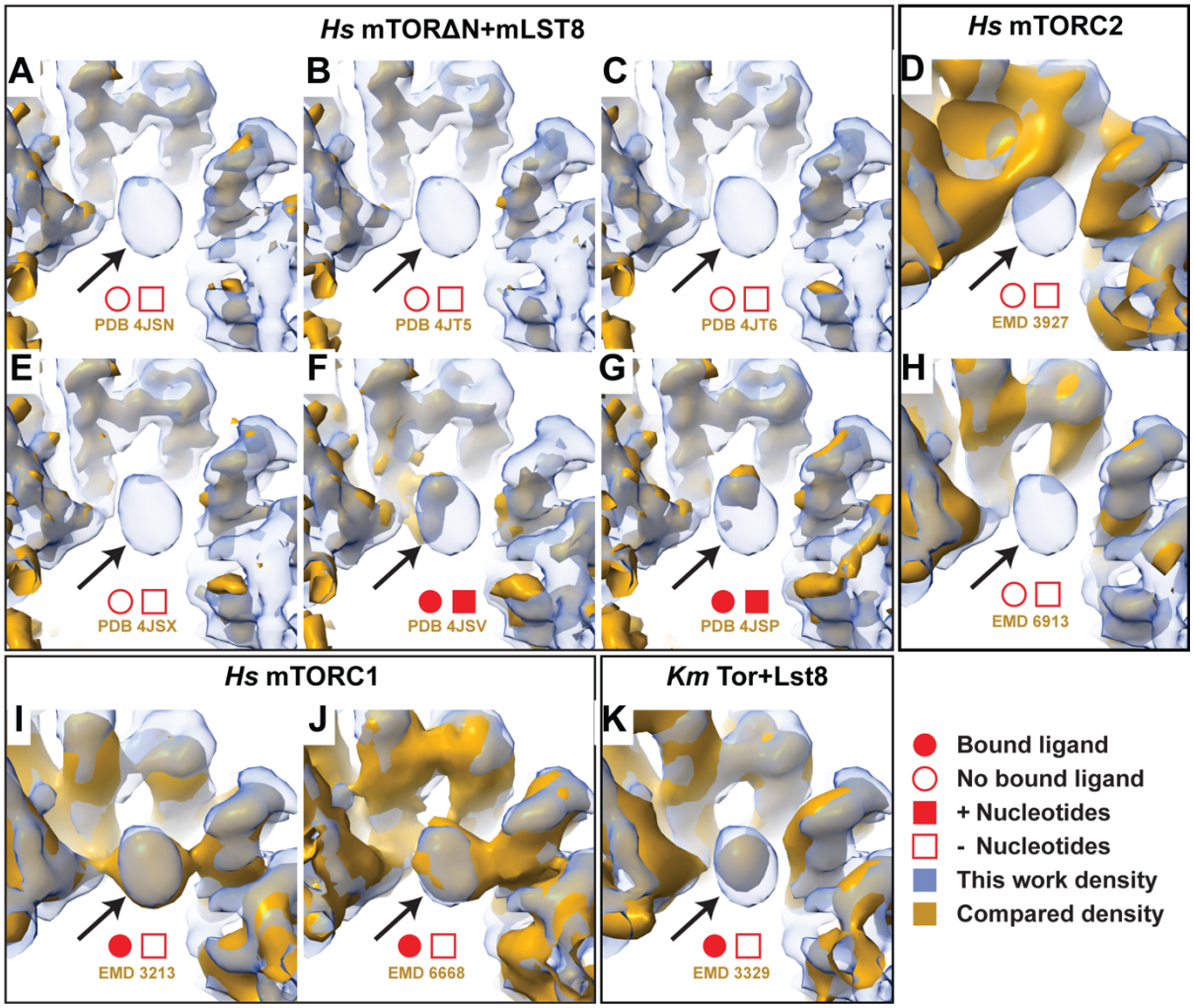

Figure S2.18 Comparison of the I-site in published structures of mTOR complexes
Close up view of the I-site (arrow) in the mTORC2 density (blue mesh) compared with published density maps (dark yellow). **A-C** and **E-G** Densities for crystal structures of human mTOR-mLST8. Extra density can be seen in the I-site in densities corresponding to PDB 4JSV and 4JSP panel F and G. These structures were obtained in presence of ATP analogs. **A,B,C** and **E** structures were obtained in absence of ATP or ATP analogs. **D** and **H**, Comparison to human mTORC2 from EMD3927 and EMD 6913 in which no ligand binding is observed. **I-K** Densities from low and medium resolution cryoEM reconstructions which also show extra density in the I-site. The densities come from **I** human mTORC1 (EMD 3213) and from **J** human mTORC1(EMD 6668) and from **K** fungal Tor-Lst8 (EMD 3329). **I-K** Densities were obtained in absence of ATP analogs. Together these results suggest that InsP6 can be copurified presumably depending on cellular InsP6 concentration and specific purification conditions. Appearance of density in the I-site upon nucleotide analogue supplementation suggests the possibility of alternate binding of nucleotides to the mTOR I-site, when it is not occupied by Ins6P.

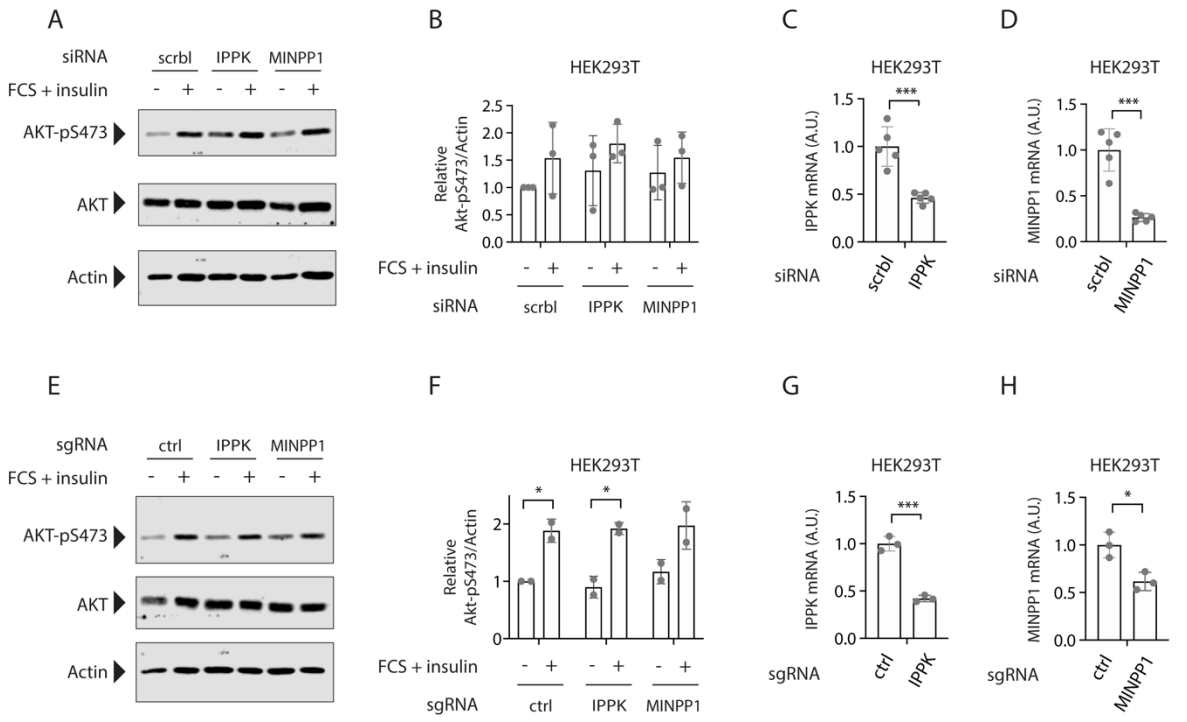

Figure S2.19 Knock-down or knock-out of IPPK or MINPP1 does not alter mTOR-Akt signaling

A Western Blot showing Akt phosphorylation under starving and stimulating conditions. IPPK and MINPP1 knockdown cells were generated using HEK293T cells. n=3 **B** Quantification of western blot in a) and all biological replicates (n=3). **C,D** Knockdown validation via qRT-PCR analysis of IPPK and MINPP1 knockdown cells (n=5). **E** Western Blot showing Akt phosphorylation under starving and stimulating conditions. IPPK and MINPP1 knockout cells were generated using HEK293T cells. n=2. **F** Quantification of western blot in d) and all biological replicates (n=2). **G,H** Knockout validation via qRT-PCR analysis of IPPK and MINPP1 knockouts in HEK293T cells (n=2). Sequencing results of PCR fragments including the sgRNA binding site were interrupted, which suggests successful Cas9 activity and knockout of IPPK and MINPP1.

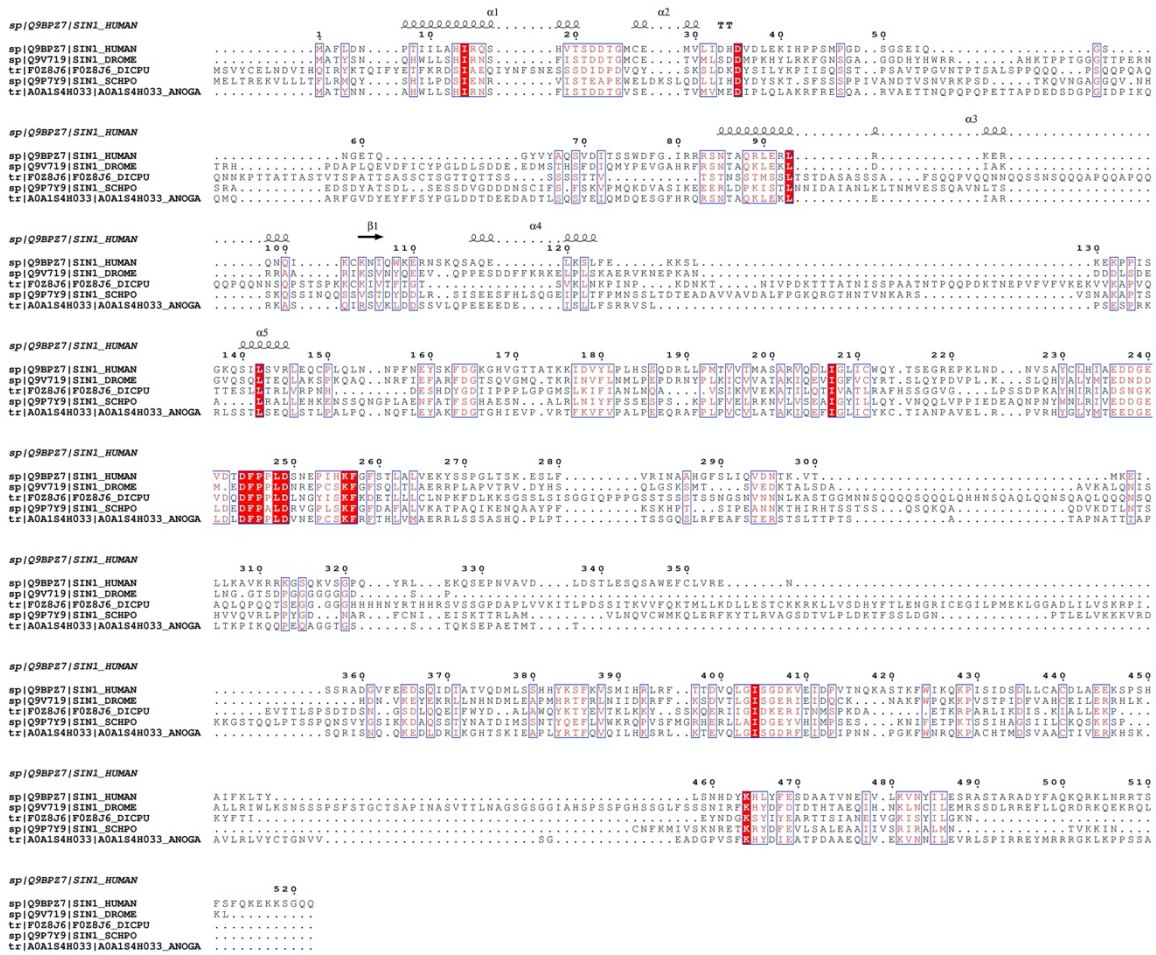

Figure S2.20 Sequence conservation of SIN1.
Multiple sequence alignments of SIN1 homologs showing conservation and secondary structure. The sequence of the S. cerevisiae SIN1-homolog Avo1 was omitted for clarity as it contains several large insertions.

2.10.3 Supplementary Tables

ID	Mutant type	Mutations	Primers
I2	I- site double mutant	mTOR_K1753E_K1788E	Forward: GAGCTTGGAGAGTGGCAGCTGAATCTACA GGGCATCAATGAGAGCACAATCCCCAAAG TGCTGCAGTACTACAGCGCCGCCACAGA GCACGACCGCAGCTGGTACGAGGCCTGG CATG Reverse: CAGGAAGCATCGGGCCATGAGCTTGTGCA GTTCCTGCTTA
I3	I- site triple mutant	mTOR_R1628E_K1655E_K1662E	Forward: GAGATCGTAGAGGACTGGCAGAAAATCCT TATGGTGCGGTCCCTTGTGGTCAGCCCTC ATGAAGACATGAGAACCTGGCTCGAGTAT GCAAGCCTGTGCGGCGAGAGTGGCAGGC TGG Reverse: CTGGCAGCCCTGCAGTCTCTCCCACCAGA T
I5	I- site quintuple mutant	mTOR_R1628E_K1655E_K1662E _K1706E_K1735E	Restriction and ligation of synthetic DNA fragment
A3	A- site triple mutant	Rictor_R572E_R575E_R576E	Forward: GAGTTTGTAGAGGAGCTACTTTATTTTTAC AAGCCCAGCAGTA Reverse: GTGTAACTGTTCATCTTTATAGTTTCTTAG
A4	A- site quadruple mutant	Rictor_R572E_R575E_R576E_Y57 9A	Forward: GAGTTTGTAGAGGAGCTACTTGCATTTTAC AAGCCCAGCAGTAAATTATAT Reverse: GTGTAACTGTTCATCTTTATAGTTTCTTAG
A5	A- site quintuple mutant	Rictor_R572E_R575E_R576E_Y57 9A_L587W	Forward: GAGTTTGTAGAGGAGCTACTTGCATTTTAC AAGCCCAGCAGTAAATGG TATGCCAACCT GGAT Reverse: GTGTAACTGTTCATCTTTATAGTTTCTTAG

Table S2.1

	Non-uniform refinement (EMDB-xxxx) (PDB xxxx)	Focus refinement on one half (EMDB-xxxx) (PDB xxxx)
Data collection and processing		
Magnification	59500x	59500x
Voltage (kV)	300	300
Electron exposure (e–/Å^2)	~70	~70
Defocus range (μm)	1.0-3.0	1.0-3.0
Pixel size (Å)	1.34 (1.6x binned)	1.34 (1.6x binned)
Symmetry imposed	C1	C1
Initial particle images (no.)	656'621	656'621
Final particle images (no.)	293'038	293'038
Map resolution (Å)	3.2	3.0
FSC threshold	0.143	0.143
Map resolution range (Å)	2.7-~7	2.7-~7
Refinement		
Initial model used (PDB code)	5ZCS (mTOR+mLST8)	5ZCS (mTOR+mLST8)
Model resolution (Å)	3.4	3.2
FSC threshold	0.5	0.5
Model resolution range (Å)	3.2 -	3.0 -
Map sharpening *B* factor (Å^2)	97.47	69.09
Model composition		
Non-hydrogen atoms	56947	24994
Protein residues	7437	3126
Ligands	8	4
B factors (Å^2)		
Protein	122.01	42.44
Ligand	132.774	59.92
R.m.s. deviations		
Bond lengths (Å)	0.004	0.002
Bond angles (°)	0.808	0.513
Validation		
MolProbity score	1.57	1.68
Clashscore	3.83	6.22
Poor rotamers (%)	1.59	1.3
Ramachandran plot		
Favored (%)	96.30	96.29
Allowed (%)	3.68	3.71
Disallowed (%)	0.03	0.00

Table S2.2 Refinement statistics for mTORC2 half and complete complex.

3 Discussion and Outlook

3.1 Summary of results

Extensive efforts in sample optimization and a tour-de-force of cryo-EM data collection enabled the determination of cryo-EM structures of mTORC2 at 3.2 Å resolution in the presence of ATPγS and either full-length Akt1 or ΔPH-Akt1, or in absence of Akt1 with and without ATPγS. The high-quality EM map allowed unambiguous *de novo* model building of all structured regions of Rictor and the N-terminal region of SIN1, revealing a Rictor fold substantially different from previous interpretations[229]. Rictor consists of three stacks of α-helical repeats, the ARM domain, the HEAT domain and the C-terminal domain. A disordered phosphorylation region (PR), which is not resolved in our reconstruction, is located between the HEAT domain and the C-terminal domain. The C-terminal domain of Rictor causes the rapamycin insensitivity of mTORC2 by blocking access of FKBP12-rapamycin to FRB domain. SIN1 shows an unexpected elongated fold. Its N-terminus is inserted into a deep cleft of Rictor, SIN1 then bridges the catalytic cleft and wraps around mLST8 and positions the substrate recruiting CRIM domain. The CRIM, RBD and the PH domains of SIN1 show high flexibility and were not resolved. We identified and functionally characterized two ligand binding sites in mTORC2. The I-site in mTOR binds InsP6 and likely has a role in mTOR folding and assembly. The A-site in Rictor binds ATP and could be involved in linking partner protein interactions to cellular nucleotide triphosphate concentrations.

These findings provide the basis to answer mechanistic questions of mTORC2 biology and shed light onto the functional role of the individual subunits in signaling, substrate recruitment and mTORC2 activation.

3.2 Detection of an InsP6 binding site in mTOR

The newly identified I-site in mTOR binds InsP6. Our structural, biochemical and biophysical characterization suggests that the functional role of the I-site may lay in mTOR folding and assembly rather than InsP6 sensing.

Recently, Gat *et al*.[30] reported the structure of the PIKK SMG1 in complex with SMG8 and SMG9, and revealed the presence of InsP6 in a region conserved among PIKK family members. They propose a binding site in mTOR that involves not only the FAT domain but also the kinase domain. The authors suggest that, both in mTOR and SMG1, the InsP6

phosphates interact on one side with positively charged residues of the FAT domain and with several arginines of the kinase domain. They conclude a key role of InsP6 in catalytic activity via stabilization of the kinase lobes. In contrast, we show that InsP6 phosphates interact solely with positively charged residues of the FAT domain and exclude any involvement of the kinase domain. We provided an EM reconstruction of the I-site mutants and a comparison with wild type mTORC2, which does not show a conformational change between the kinase and the FAT domain. This is in agreement with biochemical and biophysical characterization of purified mTORC2 containing two mutations in the I-site. The mutations do not alter the kinase activity, but they lead to reduced stability of mTORC2 instead. Gat *et al* report a reduced kinase activity for the double I-site mutant (K1753E and K1788E). This discrepancy might be attributed to the fact that the authors use a truncated version of mTOR (residues 1376 – 2549) in complex with mLST8, as well as a truncated C-terminal peptide of Akt1(residue 450-480). Our experiments were carried out using a fully assembled mTORC2 and a full-length Akt1, which represent more closely the physiological context. Moreover, the only mTOR I-site mutant which failed to assemble into stable mTORC2, I5, carries five mutations. The I-site tolerates several mutations without changes in catalytic activity *in vitro*. Moreover, alterations of InsP6 metabolizing enzymes in cells did not alter mTORC2 kinase activity.

The presence of InsP6 in mTORC2 raised the question of a functional role in mTORC2. We conclude that InsP6 rather acts as a factor in mTOR folding and complex assembly, than as a metabolic signal. InsP6 is required in maintaining the structural fold of several multi-subunit assemblies, especially in helical repeat regions[250-252]. The fact that the InsP6 is deeply buried in its binding pocket in the FAT domain suggests that it is most likely not involved in mediating binding to other proteins. Furthermore, the unexpected occurrence of InsP6 and other inositol phosphates in the X-ray or EM densities of proteins, interpreted as structural or mechanistic features, suggests a structural role for InsP6 rather than a metabolic function[250,251,278]. As other inositol phosphates, InsP6 is implicated in a variety of functions including DNA-damage repair, cohesin dynamics, RNA-editing, retroviral assembly, nuclear transport and phosphorylation[279]. InsP6 is widely distributed in animal cells, but the molecular mechanisms that regulate its cellular functions in animal cells have not been completely elucidated and shall be addressed by future studies.

3.3 Detection of a novel nucleotide binding site in Rictor

The second binding site outside the mTORC2 catalytic site, the A-site, is occupied by ATPγS in our reconstruction. The A-site does not resemble any known ATP binding site. The residues coordinating the base are not well conserved, whereas the positively charged amino acids around the phosphates are conserved in Rictor orthologs from yeast to human. Thus, the binding site is very likely not specific to adenine, suggesting that the A-site could potentially bind another nucleotide or polyphosphate. In a cellular context, other ligands would be available for binding to the A-site, such as GTP or even inositol polyphosphates.

The nucleotide binding at the A-site is not involved in allosteric regulation of mTORC2 activity regardless of the identity of the nucleotide, as shown by the *in cell* mutant activity assay (Figure S2.16). However, the A-site may be involved in thus far unknown protein-protein interactions mediated by intracellular nucleotide or polyphosphate concentrations.

One approach to identify novel interaction partners would include a Rictor-KO complementation with Rictor A-site variants at both conserved and variable residues followed by a co-IP and a subsequent quantitative proteomics study. Proteins with reduced abundance upon Rictor mutations would be potential candidates for further studies. As co-IP is not performed at equilibrium, transient interactions might evade detection. In order to increase the likelihood of capturing such interactors, *in vivo* cross-linking of lysine residues with membrane-permeable NHS-ester based linkers could be used. Employment of disuccinimidyl sulfoxide (DSSO), a cleavable lysine-lysine linker could be particularly useful, as together with capturing transient interactors it would also allow unambiguous confirmation of a binding interface near the A-site with a cross-linking mass spectrometry workflow. The presence of a nucleotide or polyphosphate binding site in Rictor that is involved in modulating interactions with other proteins, could illuminate the role of Rictor in processes like cytoskeletal rearrangements and cell polarity, where it plays a pivotal role. Many studies have described how deletion or downregulation of Rictor alone, but not of SIN1, impairs actin polymerization and cell polarity[144,280].

3.4 mTORC2 substrate recruitment

The cryo-EM reconstruction of mTORC2 with full-length Akt1 partially elucidates the mTORC2 substrate recruitment mechanisms. We did not find Akt1 bound in a fixed position on mTORC2, which would have allowed visualization of the binding mode of substrates with mTORC2. We did, however, observe additional low-resolution density near the CRIM domain

and the mTOR active site, which may account for parts of bound substrate or for the SIN1 domains RBD and PH.

The exact mechanisms for mTORC2 substrates binding and recruitment are still not understood. To date, no high-resolution structural information on mTORC2 bound to substrates is available. Unlike mTORC1 substrates which use the TOS motif to interact with mTORC1 through Raptor[38,39,42], no TOS motif-like sequence has been identified for mTORC2 substrates yet. However, major mTORC2 substrates share common structural features, as they belong to the same family, the AGC kinases family[5]. mTORC2 phosphorylates its main substrates, AKT, SGK and PKC on a conserved serine in the hydrophobic motif located on the C-terminal tail. The specificity of mTORC2 substrate recruitment depends on the SIN1 CRIM domain[231], which might recognize a conserved and shared region of the substrates. A proposed, but yet uncharacterized, interaction site of the CRIM domain is the kinase catalytic domain of the AGC kinases[231]. Further biochemical and structural work is required to characterize the interaction between SIN1-CRIM and mTORC2 substrates.

The density observed in our mTORC2 reconstruction in presence of full-length Akt1 is not of sufficient resolution to assign specific domains. Akt1 flexibility might have hindered high-resolution structural characterization. Moreover, the interaction might be weak and transient, as the substrates need to be released upon phosphorylation. A transient interaction might therefore translate into a low occupancy of mTORC2-bound substrates in the sample. Cross-linking mTORC2 and Akt1 could trap this labile interaction and enrich a higher number of mTORC2 molecules in a substrate-bound-state. A parallel approach for the identification of a bound substrate would involve structure determination of full-length or fragments of Akt1 bound to the CRIM domain, allowing identification of the interacting residues. This could be achieved by either co-expression of Akt1 and the SIN1 CRIM domain or by complex formation after individual expression and purification. A fusion construct might help to counteract a weak interaction and force the two domains into a stable complex. In addition to X-ray crystallography, substrate binding could also be examined using cryo-EM. Protein complexes smaller than 100kDa have been visualized at near-atomic resolution by using a 200kV microscope and a K3 camera[281]. Additional biophysical techniques such as fluorescence polarization or isothermal calorimetry can be applied to determine the kinetics and thermodynamics of the interaction.

3.5 mTORC2 activation

Structural analysis of our mTORC2 reconstruction has revealed that mTOR resides in an inactive conformation similar to non-activated mTORC1. Thus, mTORC2 might need an activator to induce a structural rearrangement for full activation as in the case of mTORC1.

The activity of kinases in the cell is tightly regulated. Aberrant kinase activity has been implicated in many human diseases, in particular cancer. Currently, the regulatory mechanisms governing mTORC2 activation are not fully understood but its localization at the plasma membrane plays an important role[111,113]. Controversial studies suggest that mTORC2 might be constitutively active at the plasma membrane and that its activation is independent of growth factors/PI3K[113]. Contrastingly, the canonical mechanism of mTORC2 activation suggests a PI3K mediated activation and binding of PIP3 to the PH domain of SIN1 and subsequent mTORC2 recruitment to the plasma membrane[45,111].

It has been proposed that another protein might be required for full (m)TORC2 activation[125,282,283]. The conformation of the mTOR-FATKIN in our mTORC2 reconstruction aligns better with the FATKIN of non-activated mTORC1 (1.2 Å RMSD over 1120 aligned Cα atoms) than with the FATKIN domain of Rheb-bound mTORC1 (3.5 Å RMSD over 1036 aligned Cα atoms)(Figure 3.1). This suggests that apo-mTORC2 is in the same minimum basal activity state as apo-mTORC1 and that an activator would be required for realigning active site residues and thus stimulating kinase activity.

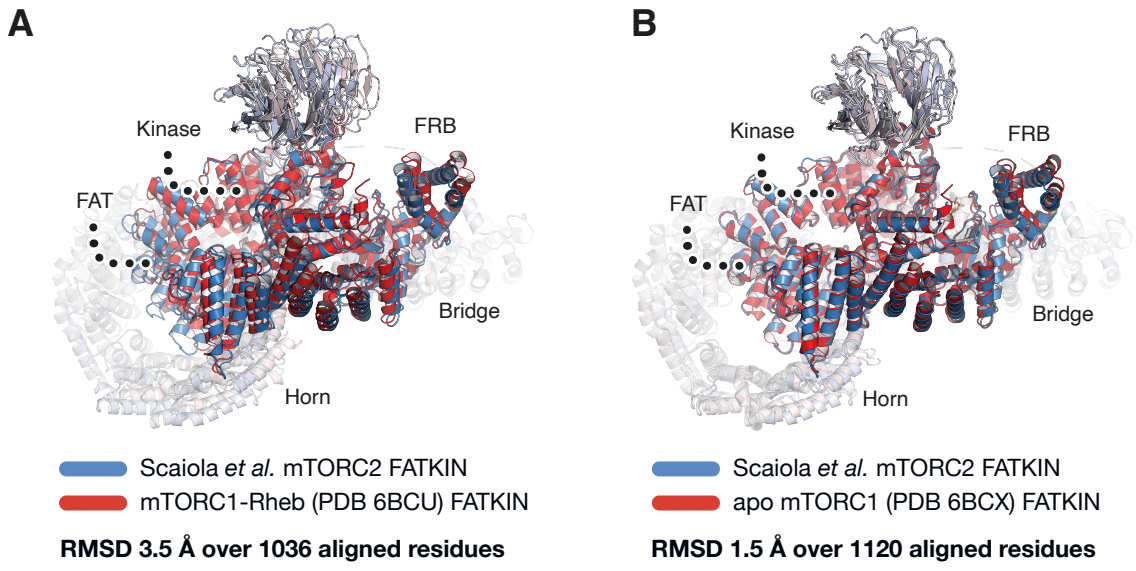

Figure 3.1 Structural comparison of FATKIN conformation in mTORC1 and mTORC2
A Superposition of FATKIN in mTORC2 and FATKIN in activated mTORC1-Rheb (PDB code: 6BCU). The RMSD is 3.5Å. mTORC2 FATKIN is colored in blue, mTORC1 FATKIN in red. The mTOR domains, Horn, Bridge, FAT, FRB and kinase are indicated. **B** Superposition of FATKIN in mTORC2 and FATKIN in activated apo mTORC1 (PDB code: 6BCX). The RMSD is 1.5Å.

mTORC2 FATKIN is colored in blue, mTORC1 FATKIN in red. The mTOR domains, Horn, Bridge, FAT, FRB and kinase are indicated.

A combined proximity-dependent biotin labeling (BioID) proteomics and CRISPR genetics approach identified mutant Ras proximal to mTORC2[125]. Additional experiments by the same group revealed that Ras can directly bind to mTORC2 at the mTOR kinase domain and the SIN1 RBD domain. They conclude that this interaction regulates mTORC2 kinase activity specifically at the plasma membrane. Kovalski *et al.*[125], identified a direct interaction of the mTOR kinase domain with Ras residues near its effector binding domain by XL-MS.
It is possible to speculate on two mechanisms for mTORC2 activation:
I) Kovalski *et al*[125]*.* suggest that Ras binds to the kinase domain of mTOR and to the RBD domain of SIN1 for mTORC2 activation. The binding might induce a structural rearrangement, which is very unique to mTORC2 also due to the involvement of SIN1.
II) Ras or another activator could bind mTORC2 at the same interface as Rheb in the case of mTORC1, which could trigger activation via a similar mechanism. For this case, it would be tempting to speculate that Rheb could activate mTORC2 in an artificial setting, but this might be prevented *in vivo* by different subcellular localizations of mTORC1 and mTORC2 and colocalization of their activators. This might explain the requirement of Ras or other GTPases for mTORC2 activation. Regulation of colocalization of the kinase, the activator and mTORC2 substrates could be a very efficient mechanism to regulate activity based on distinct inputs.
A suitable approach to identify the mTORC2 activator would be an *in vitro* kinase activity assay with purified mTORC2 and Akt1 phosphorylation as a readout in the presence of different GTPases. A cryo-EM reconstruction of mTORC2 and bound activator would then allow determination of the binding site and of the activation. This would ultimately allow comparison between the activation mechanisms of mTORC1 and mTORC2.

3.6 Towards development of mTORC2 specific inhibitors

Deregulation of mTORC2, particularly hyperactivation, is commonly observed in many types of human cancers[55]. Moreover, Rictor has been identified to be highly mutated and overexpressed in certain cancer types including colorectal cancer and non-small cell lung cancer[284,285]. Thus, novel therapeutic strategies based on specific mTORC2 inhibition might yield new options for the treatment of these diseases.
An mTORC2 specific inhibitor has only recently become available. Benavides-Serrato *et al.*[236], identified the mTORC2 inhibitor compound (CID613034) in a yeast two-hybrid screen to

inhibit the interaction between Rictor and mTOR. The optimized compound (JR-AB2-011) showed antitumoral effects in a xenograft model of glioblastoma[236]. However, the molecular mechanism of action remains unclear. Our mTORC2 structure could help to identify the binding site of JR-AB2-011 on either mTOR or Rictor by modelling and would elucidate its mechanism of action. Moreover, determination of the structure of JR-AB2-011 with its target could guide optimization of the compound's potency and drug properties.

We have shown that extension of the SIN1 N-terminus disrupts the Rictor-SIN1 interaction and therefore mTORC2 assembly. Our data paves the way for the development of a novel class of mTORC2 specific inhibitors. These molecules need to be designed to occupy the Rictor hydrophobic pocket, preventing the interaction with SIN1 and leading to defects in mTORC2 complex assembly. An excess of peptide analog of the SIN1 N-terminus could be initially used to test the feasibility of this approach. In case of a positive outcome, design of a high-throughput screening assay in combination with a compound library would allow to identify drug precursors that can be developed into drug candidates.

3.7 General Outlook

Proteins are the functional units of life. During my PhD thesis, I elucidated important functional mechanisms of key proteins involved in cellular metabolism. Our results provide a deeper understanding of how such proteins function and they enable the design of novel therapeutic strategies.

In the past, protein domains were often regarded as individual functional units which are connected by non-functional linkers, like “balls on a string”. One underlying reason for this perspective was that only proteins with a fixed conformation were accessible for structural studies, as non-structured linkers or disordered regions were often removed to ease structure determination. However, in recent years, it has become apparent that also regions without tertiary structure, as well as linker regions connecting domains, are involved in important biological processes. For instance, disordered regions often undergo PTM modifications, determining the functional state of a protein[286] or they allow interaction with structured domain in other proteins by exposing short linear peptide motifs[287]. Technological advances in cryo-EM, such as new detector technologies and new imaging processing algorithms[288], allowed the study of fully assembled, large multi protein complexes at atomic resolution. Additionally, cryo-EM is uniquely suited in visualizing large, dynamic proteins with flexible regions. The importance of seemingly disordered regions in a protein complex are illustrated by the elongated and unexpected structure of SIN1 in mTORC2. SIN1 contributes to the assembly of mTORC2 by inserting into the Rictor core, then running over the surface of mLST8 to position the CRIM domain in proximity of the mTOR catalytic site. Structural and functional characterization of disordered and flexible regions without apparent tertiary structure is crucial and will deepen the understanding of mechanisms and functions of proteins, protein complexes and their contributions to cellular processes.

Ultimately, the mechanistic and functional insights into mTORC2 biology presented in this work, but also into other proteins in general, pave the way for the development of new therapeutic strategies. mTORC2 dysregulation is implicated in numerous diseases, including metabolic diseases and different types of cancer[55], and possibly other diseases which have not been linked to mTORC2 yet. Specific mTORC2 inhibitors would be an effective treatment for certain cancers. Personalized medicine, tailoring therapy with the best possible response and the highest safety margin to individual patients, is becoming a reality and cancer therapies are at the forefront of this revolution. This strategy is applicable to mTORC2 hyperactivated tumors as well. Tumor biopsies from patients could be analyzed for alterations in mTORC2 signaling, and mTORC2-targeted inhibitors could be chosen. However, cancer

cells often develop evasive resistance mechanisms by inactivation of the drug, altering the drug metabolism and especially by increasing the mutation rate and selecting for drug-resistant lines. One of the most common drug resistances due to secondary mutations is the Imatinib resistance in chronic myelogenous leukemia (CML). Point mutations and amino acid substitutions in the kinase domain of the BCR-ABL protein, induce protein conformational changes, which prevent binding of the drug[289]. A possible approach to overcome such cancer resistance mechanisms is the development of chimeric inhibitors, which merge two drug pharmacophores in a single molecule. Generating these types of compounds could reduce the occurrence of evasive mechanisms by requiring two parallel escaping mechanisms. Chimeric inhibitors could be designed for large molecular assemblies, targeting different protein subunits or intra- and inter-domain proteins, linker-protein interactions. Alternatively, they could be designed to interfere with different molecular pathways involved in neoplastic diseases. However, major challenges associated with chimeric inhibitors include altered absorption properties as well as a higher susceptibility to be metabolized due to their increased size. Overall, a profound structural and functional knowledge on a drug target, as shown for mTORC2 in this thesis, is indispensable for the design of novel therapeutic avenues.

4 Acknowledgements

Firstly, I would like to thank my PhD Committee for guiding me during the last years and for their insightful comments and encouragement. My sincere thanks goes to Timm for accepting me in his lab and for the continuous support of my Ph.D. studies and related research. Thank you, Christoph and Olga, for the great scientific discussions and for your helpful advice.
I would like to thank my collaborators in Zurich, Alain, Daniel and Nenad for the productive collaboration and for sharing this great effort.
My sincere thanks also go to the collaborator from the Hall lab, Mitsugu. Special thanks also to Karolin and Asier.
I thank my fellow labmates for the stimulating discussions but mostly for all the fun we had!
Many thanks to my desk neighbor Matzino for being so amazing and patient with me. Thank you for all the wonderful moments we spent together and for reminding me that you might lose your protein without an injection loop.
Thank you Shubi for being the amazing person helping me overcoming the challenges of the PhD! Life would have been tougher and definitely boring without you by my side! I will miss chatting in CR1, CR2 and CR3… I hope life will give us a CR4 not too far from each other. Thank you for being always there for me, whatever the problem, whatever the time of the day or the night. Also, thank you for giving me the chance to shout at someone in Italian style.
Many thanks to Yvvino for always listening to my endless complaints and be target of my jokes. I still have some hope for your clothing style, even after the “gelataio incident”
Many thanks to Eddi for guiding me in the early days of my PhD, you are a wonderful scientist and person. Thank you Malik for the nice chats in the lonely days in the lab and for sharing the chicken video, it was a true gift! Thanks to Roman for being the pillar of the lab, for the laughs and the tears I shared with you. Thank you Florian for being an excellent source of gossips and jokes. Thank you Hugo for the nice chats in the small office and for all the nonsense with fire extinguishers. Thank you Yana for being my patient desk neighbor and for the productive scientific discussions. Thank you Elsa for the silly moments together and for sharing your craziness. Thank you Karo for all the nice moments, the gossips and the laughs. Thank you Sophia for the nice time we spent in the lab and especially in Saas-Fee. Thank you Flurin for being a lovely and funny master student and for all the jokes and the games we played.

4 Acknowledgements

A special thanks goes to my fantastic lizards-ladies for being a constant support throughout my PhD, even when oceans were separating us.
Thank you Anna for being such a charismatic and joyful friend. Thank you for helping me in the tough moments because you also knew what it meant…"And then, there's us!" Thank you for reminding me that there is always a way and a solution and that you will always be there for me.
Thank you Freddy for all the fantastic moments spent together, for the nice jokes and the duck-watching at the Rhine! I have always admired you for your commitment and love for science, for your creativity and I am sure life will bring you far.
Thank you Anja for being a dear skiing companion, for the thousands of laughs and for being such a lovely friend. I will never forget the silly dance moves and finishing bags of chips in Saas-Fee! Thank you for always being there for me and having a nice word.
Thank you Giovi for being such a wonderful friend and supporting me since my master. You have always brightened up my days with your jokes and your positive attitude for the world. I wish life will bring you wherever you want to go.
Thank you Leo, my fellow lizard and fossil, for relentlessly listening to my complaints, stupid jokes and loud shouts at Matzino. Thank you for sharing with me, until the very end, this hard journey. You have made the office a funny place.
Many thanks also to my Italian friends Giulia, Linda, Ire and Paola for supporting me since 2006 and bearing with my craziness. Thanks for the laughs and the wonderful traveling adventures.
Thanks to Stefan who has been a constant source of support and encouragement during the challenges of the PhD and of life. I am truly thankful for having you in my life. Thank you for always being there at times I thought that it is impossible to continue, you helped me to keep things in perspective. Thank you for your trust and for always believing in me. Words would never say how grateful I am to you.

Ringrazio la mia famiglia: i miei genitori Walter e Cecilia, mio fratello Gaetano e mio nonno Francesco per essere la costante della mia vita ed il mio luogo sicuro. Non avrei mai potuto raggiungere certi traguardi senza il vostro supporto. A voi devo tutto e dedico questa tesi perché mi avete sempre insegnato a lavorare duramente per raggiungere i miei obiettivi.

This work is dedicated to my parents, Walter and Cecilia, who have always love me unconditionally and have taught me to work hard for the things I aspire to achieve.

5 References

1 Ardito, F., Giuliani, M., Perrone, D., Troiano, G. & Lo Muzio, L. The crucial role of protein phosphorylation in cell signaling and its use as targeted therapy (Review). *Int J Mol Med* **40**, 271-280, doi:10.3892/ijmm.2017.3036 (2017).

2 Humphrey, S. J., James, D. E. & Mann, M. Protein Phosphorylation: A Major Switch Mechanism for Metabolic Regulation. *Trends Endocrinol Metab* **26**, 676-687, doi:10.1016/j.tem.2015.09.013 (2015).

3 Johnson, L. N. & Lewis, R. J. Structural basis for control by phosphorylation. *Chem Rev* **101**, 2209-2242, doi:10.1021/cr000225s (2001).

4 Ubersax, J. A. & Ferrell, J. E., Jr. Mechanisms of specificity in protein phosphorylation. *Nat Rev Mol Cell Biol* **8**, 530-541, doi:10.1038/nrm2203 (2007).

5 Pearce, L. R., Komander, D. & Alessi, D. R. The nuts and bolts of AGC protein kinases. *Nat Rev Mol Cell Biol* **11**, 9-22, doi:10.1038/nrm2822 (2010).

6 Vezina, C., Kudelski, A. & Sehgal, S. N. Rapamycin (AY-22,989), a new antifungal antibiotic. I. Taxonomy of the producing streptomycete and isolation of the active principle. *J Antibiot (Tokyo)* **28**, 721-726, doi:10.7164/antibiotics.28.721 (1975).

7 Staunton, J. & Wilkinson, B. Biosynthesis of Erythromycin and Rapamycin. *Chem Rev* **97**, 2611-2630, doi:10.1021/cr9600316 (1997).

8 Martel, R. R., Klicius, J. & Galet, S. Inhibition of the immune response by rapamycin, a new antifungal antibiotic. *Can J Physiol Pharmacol* **55**, 48-51, doi:10.1139/y77-007 (1977).

9 Heitman, J., Movva, N. R. & Hall, M. N. Targets for cell cycle arrest by the immunosuppressant rapamycin in yeast. *Science* **253**, 905-909, doi:10.1126/science.1715094 (1991).

10 Brown, E. J. *et al.* A mammalian protein targeted by G1-arresting rapamycin-receptor complex. *Nature* **369**, 756-758, doi:10.1038/369756a0 (1994).

11 Sabatini, D. M., Erdjument-Bromage, H., Lui, M., Tempst, P. & Snyder, S. H. RAFT1: a mammalian protein that binds to FKBP12 in a rapamycin-dependent fashion and is homologous to yeast TORs. *Cell* **78**, 35-43, doi:10.1016/0092-8674(94)90570-3 (1994).

12 Sabers, C. J. *et al.* Isolation of a protein target of the FKBP12-rapamycin complex in mammalian cells. *J Biol Chem* **270**, 815-822, doi:10.1074/jbc.270.2.815 (1995).

13 Keith, C. T. & Schreiber, S. L. PIK-related kinases: DNA repair, recombination, and cell cycle checkpoints. *Science* **270**, 50-51, doi:10.1126/science.270.5233.50 (1995).

14 Bosotti, R., Isacchi, A. & Sonnhammer, E. L. FAT: a novel domain in PIK-related kinases. *Trends Biochem Sci* **25**, 225-227, doi:10.1016/s0968-0004(00)01563-2 (2000).

15 Perry, J. & Kleckner, N. The ATRs, ATMs, and TORs are giant HEAT repeat proteins. *Cell* **112**, 151-155, doi:10.1016/s0092-8674(03)00033-3 (2003).

16 Imseng, S., Aylett, C. H. & Maier, T. Architecture and activation of phosphatidylinositol 3-kinase related kinases. *Curr Opin Struct Biol* **49**, 177-189, doi:10.1016/j.sbi.2018.03.010 (2018).

17 Imseng, S. Structural studies on the target of rapamycin complex 1. 2016, Doctoral Thesis, University of Basel, Faculty of Science. . doi:10.5451/unibas-006769347 (2016).

18 Blackford, A. N. & Jackson, S. P. ATM, ATR, and DNA-PK: The Trinity at the Heart of the DNA Damage Response. *Mol Cell* **66**, 801-817, doi:10.1016/j.molcel.2017.05.015 (2017).
19 Marechal, A. & Zou, L. DNA damage sensing by the ATM and ATR kinases. *Cold Spring Harb Perspect Biol* **5**, doi:10.1101/cshperspect.a012716 (2013).
20 Matsuoka, S. *et al.* ATM and ATR substrate analysis reveals extensive protein networks responsive to DNA damage. *Science* **316**, 1160-1166, doi:10.1126/science.1140321 (2007).
21 Walker, J. R., Corpina, R. A. & Goldberg, J. Structure of the Ku heterodimer bound to DNA and its implications for double-strand break repair. *Nature* **412**, 607-614, doi:10.1038/35088000 (2001).
22 Jette, N. & Lees-Miller, S. P. The DNA-dependent protein kinase: A multifunctional protein kinase with roles in DNA double strand break repair and mitosis. *Prog Biophys Mol Biol* **117**, 194-205, doi:10.1016/j.pbiomolbio.2014.12.003 (2015).
23 Sibanda, B. L., Chirgadze, D. Y., Ascher, D. B. & Blundell, T. L. DNA-PKcs structure suggests an allosteric mechanism modulating DNA double-strand break repair. *Science* **355**, 520-524, doi:10.1126/science.aak9654 (2017).
24 Yin, X., Liu, M., Tian, Y., Wang, J. & Xu, Y. Cryo-EM structure of human DNA-PK holoenzyme. *Cell Res* **27**, 1341-1350, doi:10.1038/cr.2017.110 (2017).
25 Diaz-Santin, L. M., Lukoyanova, N., Aciyan, E. & Cheung, A. C. Cryo-EM structure of the SAGA and NuA4 coactivator subunit Tra1 at 3.7 angstrom resolution. *Elife* **6**, doi:10.7554/eLife.28384 (2017).
26 Kurosaki, T. & Maquat, L. E. Nonsense-mediated mRNA decay in humans at a glance. *J Cell Sci* **129**, 461-467, doi:10.1242/jcs.181008 (2016).
27 Ohnishi, T. *et al.* Phosphorylation of hUPF1 induces formation of mRNA surveillance complexes containing hSMG-5 and hSMG-7. *Mol Cell* **12**, 1187-1200, doi:10.1016/s1097-2765(03)00443-x (2003).
28 Yamashita, A. Role of SMG-1-mediated Upf1 phosphorylation in mammalian nonsense-mediated mRNA decay. *Genes Cells* **18**, 161-175, doi:10.1111/gtc.12033 (2013).
29 Yamashita, A., Ohnishi, T., Kashima, I., Taya, Y. & Ohno, S. Human SMG-1, a novel phosphatidylinositol 3-kinase-related protein kinase, associates with components of the mRNA surveillance complex and is involved in the regulation of nonsense-mediated mRNA decay. *Genes Dev* **15**, 2215-2228, doi:10.1101/gad.913001 (2001).
30 Gat, Y. *et al.* InsP6 binding to PIKK kinases revealed by the cryo-EM structure of an SMG1-SMG8-SMG9 complex. *Nat Struct Mol Biol* **26**, 1089-1093, doi:10.1038/s41594-019-0342-7 (2019).
31 Zhu, L., Li, L., Qi, Y., Yu, Z. & Xu, Y. Cryo-EM structure of SMG1-SMG8-SMG9 complex. *Cell Res* **29**, 1027-1034, doi:10.1038/s41422-019-0255-3 (2019).
32 Kim, D. H. *et al.* GbetaL, a positive regulator of the rapamycin-sensitive pathway required for the nutrient-sensitive interaction between raptor and mTOR. *Mol Cell* **11**, 895-904, doi:10.1016/s1097-2765(03)00114-x (2003).
33 Guertin, D. A. *et al.* Ablation in mice of the mTORC components raptor, rictor, or mLST8 reveals that mTORC2 is required for signaling to Akt-FOXO and PKCalpha, but not S6K1. *Dev Cell* **11**, 859-871, doi:10.1016/j.devcel.2006.10.007 (2006).
34 Hwang, Y. *et al.* Disruption of the Scaffolding Function of mLST8 Selectively Inhibits mTORC2 Assembly and Function and Suppresses mTORC2-Dependent Tumor Growth In Vivo. *Cancer Res* **79**, 3178-3184, doi:10.1158/0008-5472.CAN-18-3658 (2019).

35 Wullschleger, S., Loewith, R., Oppliger, W. & Hall, M. N. Molecular organization of target of rapamycin complex 2. *J Biol Chem* **280**, 30697-30704, doi:10.1074/jbc.M505553200 (2005).
36 Hara, K. *et al.* Raptor, a binding partner of target of rapamycin (TOR), mediates TOR action. *Cell* **110**, 177-189, doi:10.1016/s0092-8674(02)00833-4 (2002).
37 Kim, D. H. *et al.* mTOR interacts with raptor to form a nutrient-sensitive complex that signals to the cell growth machinery. *Cell* **110**, 163-175, doi:10.1016/s0092-8674(02)00808-5 (2002).
38 Nojima, H. *et al.* The mammalian target of rapamycin (mTOR) partner, raptor, binds the mTOR substrates p70 S6 kinase and 4E-BP1 through their TOR signaling (TOS) motif. *J Biol Chem* **278**, 15461-15464, doi:10.1074/jbc.C200665200 (2003).
39 Schalm, S. S., Fingar, D. C., Sabatini, D. M. & Blenis, J. TOS motif-mediated raptor binding regulates 4E-BP1 multisite phosphorylation and function. *Curr Biol* **13**, 797-806, doi:10.1016/s0960-9822(03)00329-4 (2003).
40 Oshiro, N. *et al.* The proline-rich Akt substrate of 40 kDa (PRAS40) is a physiological substrate of mammalian target of rapamycin complex 1. *J Biol Chem* **282**, 20329-20339, doi:10.1074/jbc.M702636200 (2007).
41 Wang, L., Harris, T. E., Roth, R. A. & Lawrence, J. C., Jr. PRAS40 regulates mTORC1 kinase activity by functioning as a direct inhibitor of substrate binding. *J Biol Chem* **282**, 20036-20044, doi:10.1074/jbc.M702376200 (2007).
42 Yang, H. *et al.* Mechanisms of mTORC1 activation by RHEB and inhibition by PRAS40. *Nature* **552**, 368-373, doi:10.1038/nature25023 (2017).
43 Jacinto, E. *et al.* Mammalian TOR complex 2 controls the actin cytoskeleton and is rapamycin insensitive. *Nat Cell Biol* **6**, 1122-1128, doi:10.1038/ncb1183 (2004).
44 Sarbassov, D. D. *et al.* Rictor, a novel binding partner of mTOR, defines a rapamycin-insensitive and raptor-independent pathway that regulates the cytoskeleton. *Curr Biol* **14**, 1296-1302, doi:10.1016/j.cub.2004.06.054 (2004).
45 Frias, M. A. *et al.* mSin1 is necessary for Akt/PKB phosphorylation, and its isoforms define three distinct mTORC2s. *Curr Biol* **16**, 1865-1870, doi:10.1016/j.cub.2006.08.001 (2006).
46 Yang, Q., Inoki, K., Ikenoue, T. & Guan, K. L. Identification of Sin1 as an essential TORC2 component required for complex formation and kinase activity. *Genes Dev* **20**, 2820-2832, doi:10.1101/gad.1461206 (2006).
47 Pearce, L. R. *et al.* Identification of Protor as a novel Rictor-binding component of mTOR complex-2. *Biochem J* **405**, 513-522, doi:10.1042/BJ20070540 (2007).
48 Thedieck, K. *et al.* PRAS40 and PRR5-like protein are new mTOR interactors that regulate apoptosis. *PLoS One* **2**, e1217, doi:10.1371/journal.pone.0001217 (2007).
49 Peterson, T. R. *et al.* DEPTOR is an mTOR inhibitor frequently overexpressed in multiple myeloma cells and required for their survival. *Cell* **137**, 873-886, doi:10.1016/j.cell.2009.03.046 (2009).
50 Aylett, C. H. *et al.* Architecture of human mTOR complex 1. *Science* **351**, 48-52, doi:10.1126/science.aaa3870 (2016).
51 Baretic, D., Berndt, A., Ohashi, Y., Johnson, C. M. & Williams, R. L. Tor forms a dimer through an N-terminal helical solenoid with a complex topology. *Nat Commun* **7**, 11016, doi:10.1038/ncomms11016 (2016).
52 Yang, H. *et al.* mTOR kinase structure, mechanism and regulation. *Nature* **497**, 217-223, doi:10.1038/nature12122 (2013).
53 Sarbassov, D. D. *et al.* Prolonged rapamycin treatment inhibits mTORC2 assembly and Akt/PKB. *Mol Cell* **22**, 159-168, doi:10.1016/j.molcel.2006.03.029 (2006).

54 Liu, G. Y. & Sabatini, D. M. mTOR at the nexus of nutrition, growth, ageing and disease. *Nat Rev Mol Cell Biol* **21**, 183-203, doi:10.1038/s41580-019-0199-y (2020).
55 Mossmann, D., Park, S. & Hall, M. N. mTOR signalling and cellular metabolism are mutual determinants in cancer. *Nat Rev Cancer* **18**, 744-757, doi:10.1038/s41568-018-0074-8 (2018).
56 Zinzalla, V., Stracka, D., Oppliger, W. & Hall, M. N. Activation of mTORC2 by association with the ribosome. *Cell* **144**, 757-768, doi:10.1016/j.cell.2011.02.014 (2011).
57 Dazert, E. & Hall, M. N. mTOR signaling in disease. *Curr Opin Cell Biol* **23**, 744-755, doi:10.1016/j.ceb.2011.09.003 (2011).
58 Guri, Y. *et al.* mTORC2 Promotes Tumorigenesis via Lipid Synthesis. *Cancer Cell* **32**, 807-823 e812, doi:10.1016/j.ccell.2017.11.011 (2017).
59 Saxton, R. A. & Sabatini, D. M. mTOR Signaling in Growth, Metabolism, and Disease. *Cell* **169**, 361-371, doi:10.1016/j.cell.2017.03.035 (2017).
60 Gonzalez, A., Hall, M. N., Lin, S. C. & Hardie, D. G. AMPK and TOR: The Yin and Yang of Cellular Nutrient Sensing and Growth Control. *Cell Metab* **31**, 472-492, doi:10.1016/j.cmet.2020.01.015 (2020).
61 Dibble, C. C. *et al.* TBC1D7 is a third subunit of the TSC1-TSC2 complex upstream of mTORC1. *Mol Cell* **47**, 535-546, doi:10.1016/j.molcel.2012.06.009 (2012).
62 Inoki, K., Li, Y., Xu, T. & Guan, K. L. Rheb GTPase is a direct target of TSC2 GAP activity and regulates mTOR signaling. *Genes Dev* **17**, 1829-1834, doi:10.1101/gad.1110003 (2003).
63 Hara, K. *et al.* Amino acid sufficiency and mTOR regulate p70 S6 kinase and eIF-4E BP1 through a common effector mechanism. *J Biol Chem* **273**, 14484-14494, doi:10.1074/jbc.273.23.14484 (1998).
64 Sancak, Y. *et al.* The Rag GTPases bind raptor and mediate amino acid signaling to mTORC1. *Science* **320**, 1496-1501, doi:10.1126/science.1157535 (2008).
65 Bar-Peled, L., Schweitzer, L. D., Zoncu, R. & Sabatini, D. M. Ragulator is a GEF for the rag GTPases that signal amino acid levels to mTORC1. *Cell* **150**, 1196-1208, doi:10.1016/j.cell.2012.07.032 (2012).
66 de Araujo, M. E. G. *et al.* Crystal structure of the human lysosomal mTORC1 scaffold complex and its impact on signaling. *Science* **358**, 377-381, doi:10.1126/science.aao1583 (2017).
67 Sancak, Y. *et al.* Ragulator-Rag complex targets mTORC1 to the lysosomal surface and is necessary for its activation by amino acids. *Cell* **141**, 290-303, doi:10.1016/j.cell.2010.02.024 (2010).
68 Nada, S. *et al.* The novel lipid raft adaptor p18 controls endosome dynamics by anchoring the MEK-ERK pathway to late endosomes. *EMBO J* **28**, 477-489, doi:10.1038/emboj.2008.308 (2009).
69 Kim, E., Goraksha-Hicks, P., Li, L., Neufeld, T. P. & Guan, K. L. Regulation of TORC1 by Rag GTPases in nutrient response. *Nat Cell Biol* **10**, 935-945, doi:10.1038/ncb1753 (2008).
70 Anandapadamanaban, M. *et al.* Architecture of human Rag GTPase heterodimers and their complex with mTORC1. *Science* **366**, 203-210, doi:10.1126/science.aax3939 (2019).
71 Rogala, K. B. *et al.* Structural basis for the docking of mTORC1 on the lysosomal surface. *Science* **366**, 468-475, doi:10.1126/science.aay0166 (2019).
72 Bar-Peled, L. *et al.* A Tumor suppressor complex with GAP activity for the Rag GTPases that signal amino acid sufficiency to mTORC1. *Science* **340**, 1100-1106, doi:10.1126/science.1232044 (2013).

73 Shen, K. *et al.* Architecture of the human GATOR1 and GATOR1-Rag GTPases complexes. *Nature* **556**, 64-69, doi:10.1038/nature26158 (2018).
74 Shen, K., Valenstein, M. L., Gu, X. & Sabatini, D. M. Arg-78 of Nprl2 catalyzes GATOR1-stimulated GTP hydrolysis by the Rag GTPases. *J Biol Chem* **294**, 2970-2975, doi:10.1074/jbc.AC119.007382 (2019).
75 Peng, M., Yin, N. & Li, M. O. SZT2 dictates GATOR control of mTORC1 signalling. *Nature* **543**, 433-437, doi:10.1038/nature21378 (2017).
76 Wolfson, R. L. *et al.* KICSTOR recruits GATOR1 to the lysosome and is necessary for nutrients to regulate mTORC1. *Nature* **543**, 438-442, doi:10.1038/nature21423 (2017).
77 Saxton, R. A. *et al.* Structural basis for leucine sensing by the Sestrin2-mTORC1 pathway. *Science* **351**, 53-58, doi:10.1126/science.aad2087 (2016).
78 Wolfson, R. L. *et al.* Sestrin2 is a leucine sensor for the mTORC1 pathway. *Science* **351**, 43-48, doi:10.1126/science.aab2674 (2016).
79 Chantranupong, L. *et al.* The CASTOR Proteins Are Arginine Sensors for the mTORC1 Pathway. *Cell* **165**, 153-164, doi:10.1016/j.cell.2016.02.035 (2016).
80 Saxton, R. A., Chantranupong, L., Knockenhauer, K. E., Schwartz, T. U. & Sabatini, D. M. Mechanism of arginine sensing by CASTOR1 upstream of mTORC1. *Nature* **536**, 229-233, doi:10.1038/nature19079 (2016).
81 Shen, K. & Sabatini, D. M. Ragulator and SLC38A9 activate the Rag GTPases through noncanonical GEF mechanisms. *Proc Natl Acad Sci U S A* **115**, 9545-9550, doi:10.1073/pnas.1811727115 (2018).
82 Petit, C. S., Roczniak-Ferguson, A. & Ferguson, S. M. Recruitment of folliculin to lysosomes supports the amino acid-dependent activation of Rag GTPases. *J Cell Biol* **202**, 1107-1122, doi:10.1083/jcb.201307084 (2013).
83 Tsun, Z. Y. *et al.* The folliculin tumor suppressor is a GAP for the RagC/D GTPases that signal amino acid levels to mTORC1. *Mol Cell* **52**, 495-505, doi:10.1016/j.molcel.2013.09.016 (2013).
84 Duran, R. V. *et al.* Glutaminolysis activates Rag-mTORC1 signaling. *Mol Cell* **47**, 349-358, doi:10.1016/j.molcel.2012.05.043 (2012).
85 Inoki, K., Zhu, T. & Guan, K. L. TSC2 mediates cellular energy response to control cell growth and survival. *Cell* **115**, 577-590, doi:10.1016/s0092-8674(03)00929-2 (2003).
86 Gwinn, D. M. *et al.* AMPK phosphorylation of raptor mediates a metabolic checkpoint. *Mol Cell* **30**, 214-226, doi:10.1016/j.molcel.2008.03.003 (2008).
87 Jewell, J. L. *et al.* GPCR signaling inhibits mTORC1 via PKA phosphorylation of Raptor. *Elife* **8**, doi:10.7554/eLife.43038 (2019).
88 Liu, D. *et al.* Activation of mTORC1 is essential for beta-adrenergic stimulation of adipose browning. *J Clin Invest* **126**, 1704-1716, doi:10.1172/JCI83532 (2016).
89 Brugarolas, J. *et al.* Regulation of mTOR function in response to hypoxia by REDD1 and the TSC1/TSC2 tumor suppressor complex. *Genes Dev* **18**, 2893-2904, doi:10.1101/gad.1256804 (2004).
90 Katiyar, S. *et al.* REDD1, an inhibitor of mTOR signalling, is regulated by the CUL4A-DDB1 ubiquitin ligase. *EMBO Rep* **10**, 866-872, doi:10.1038/embor.2009.93 (2009).
91 Feng, Z. *et al.* The regulation of AMPK beta1, TSC2, and PTEN expression by p53: stress, cell and tissue specificity, and the role of these gene products in modulating the IGF-1-AKT-mTOR pathways. *Cancer Res* **67**, 3043-3053, doi:10.1158/0008-5472.CAN-06-4149 (2007).
92 Flamholz, A., Phillips, R. & Milo, R. The quantified cell. *Mol Biol Cell* **25**, 3497-3500, doi:10.1091/mbc.E14-09-1347 (2014).
93 Gingras, A. C. *et al.* Regulation of 4E-BP1 phosphorylation: a novel two-step mechanism. *Genes Dev* **13**, 1422-1437, doi:10.1101/gad.13.11.1422 (1999).

94 Hara, K. *et al.* Regulation of eIF-4E BP1 phosphorylation by mTOR. *J Biol Chem* **272**, 26457-26463, doi:10.1074/jbc.272.42.26457 (1997).
95 Pullen, N. *et al.* Phosphorylation and activation of p70s6k by PDK1. *Science* **279**, 707-710, doi:10.1126/science.279.5351.707 (1998).
96 Burnett, P. E., Barrow, R. K., Cohen, N. A., Snyder, S. H. & Sabatini, D. M. RAFT1 phosphorylation of the translational regulators p70 S6 kinase and 4E-BP1. *Proc Natl Acad Sci U S A* **95**, 1432-1437, doi:10.1073/pnas.95.4.1432 (1998).
97 Hannan, K. M. *et al.* mTOR-dependent regulation of ribosomal gene transcription requires S6K1 and is mediated by phosphorylation of the carboxy-terminal activation domain of the nucleolar transcription factor UBF. *Mol Cell Biol* **23**, 8862-8877, doi:10.1128/mcb.23.23.8862-8877.2003 (2003).
98 Mayer, C., Zhao, J., Yuan, X. & Grummt, I. mTOR-dependent activation of the transcription factor TIF-IA links rRNA synthesis to nutrient availability. *Genes Dev* **18**, 423-434, doi:10.1101/gad.285504 (2004).
99 Michels, A. A. *et al.* mTORC1 directly phosphorylates and regulates human MAF1. *Mol Cell Biol* **30**, 3749-3757, doi:10.1128/MCB.00319-10 (2010).
100 Shah, O. J., Wang, Z. & Hunter, T. Inappropriate activation of the TSC/Rheb/mTOR/S6K cassette induces IRS1/2 depletion, insulin resistance, and cell survival deficiencies. *Curr Biol* **14**, 1650-1656, doi:10.1016/j.cub.2004.08.026 (2004).
101 Duvel, K. *et al.* Activation of a metabolic gene regulatory network downstream of mTOR complex 1. *Mol Cell* **39**, 171-183, doi:10.1016/j.molcel.2010.06.022 (2010).
102 Peterson, T. R. *et al.* mTOR complex 1 regulates lipin 1 localization to control the SREBP pathway. *Cell* **146**, 408-420, doi:10.1016/j.cell.2011.06.034 (2011).
103 Kim, J. E. & Chen, J. regulation of peroxisome proliferator-activated receptor-gamma activity by mammalian target of rapamycin and amino acids in adipogenesis. *Diabetes* **53**, 2748-2756, doi:10.2337/diabetes.53.11.2748 (2004).
104 Ben-Sahra, I., Hoxhaj, G., Ricoult, S. J. H., Asara, J. M. & Manning, B. D. mTORC1 induces purine synthesis through control of the mitochondrial tetrahydrofolate cycle. *Science* **351**, 728-733, doi:10.1126/science.aad0489 (2016).
105 Ben-Sahra, I., Howell, J. J., Asara, J. M. & Manning, B. D. Stimulation of de novo pyrimidine synthesis by growth signaling through mTOR and S6K1. *Science* **339**, 1323-1328, doi:10.1126/science.1228792 (2013).
106 Robitaille, A. M. *et al.* Quantitative phosphoproteomics reveal mTORC1 activates de novo pyrimidine synthesis. *Science* **339**, 1320-1323, doi:10.1126/science.1228771 (2013).
107 Kim, J., Kundu, M., Viollet, B. & Guan, K. L. AMPK and mTOR regulate autophagy through direct phosphorylation of Ulk1. *Nat Cell Biol* **13**, 132-141, doi:10.1038/ncb2152 (2011).
108 Settembre, C. *et al.* A lysosome-to-nucleus signalling mechanism senses and regulates the lysosome via mTOR and TFEB. *EMBO J* **31**, 1095-1108, doi:10.1038/emboj.2012.32 (2012).
109 Martina, J. A., Chen, Y., Gucek, M. & Puertollano, R. MTORC1 functions as a transcriptional regulator of autophagy by preventing nuclear transport of TFEB. *Autophagy* **8**, 903-914, doi:10.4161/auto.19653 (2012).
110 Roczniak-Ferguson, A. *et al.* The transcription factor TFEB links mTORC1 signaling to transcriptional control of lysosome homeostasis. *Sci Signal* **5**, ra42, doi:10.1126/scisignal.2002790 (2012).
111 Gan, X., Wang, J., Su, B. & Wu, D. Evidence for direct activation of mTORC2 kinase activity by phosphatidylinositol 3,4,5-trisphosphate. *J Biol Chem* **286**, 10998-11002, doi:10.1074/jbc.M110.195016 (2011).

112 Alessi, D. R. & Cohen, P. Mechanism of activation and function of protein kinase B. *Curr Opin Genet Dev* **8**, 55-62, doi:10.1016/s0959-437x(98)80062-2 (1998).
113 Ebner, M., Sinkovics, B., Szczygiel, M., Ribeiro, D. W. & Yudushkin, I. Localization of mTORC2 activity inside cells. *J Cell Biol* **216**, 343-353, doi:10.1083/jcb.201610060 (2017).
114 Yue, F. *et al.* Pten is necessary for the quiescence and maintenance of adult muscle stem cells. *Nat Commun* **8**, 14328, doi:10.1038/ncomms14328 (2017).
115 Moore, S. F., Hunter, R. W. & Hers, I. mTORC2 protein complex-mediated Akt (Protein Kinase B) Serine 473 Phosphorylation is not required for Akt1 activity in human platelets [corrected]. *J Biol Chem* **286**, 24553-24560, doi:10.1074/jbc.M110.202341 (2011).
116 Manning, B. D. & Toker, A. AKT/PKB Signaling: Navigating the Network. *Cell* **169**, 381-405, doi:10.1016/j.cell.2017.04.001 (2017).
117 Oh, W. J. *et al.* mTORC2 can associate with ribosomes to promote cotranslational phosphorylation and stability of nascent Akt polypeptide. *EMBO J* **29**, 3939-3951, doi:10.1038/emboj.2010.271 (2010).
118 Partovian, C., Ju, R., Zhuang, Z. W., Martin, K. A. & Simons, M. Syndecan-4 regulates subcellular localization of mTOR Complex2 and Akt activation in a PKCalpha-dependent manner in endothelial cells. *Mol Cell* **32**, 140-149, doi:10.1016/j.molcel.2008.09.010 (2008).
119 Boulbes, D. R., Shaiken, T. & Sarbassov dos, D. Endoplasmic reticulum is a main localization site of mTORC2. *Biochem Biophys Res Commun* **413**, 46-52, doi:10.1016/j.bbrc.2011.08.034 (2011).
120 Gomez-Salinero, J. M. *et al.* The Calcineurin Variant CnAbeta1 Controls Mouse Embryonic Stem Cell Differentiation by Directing mTORC2 Membrane Localization and Activation. *Cell Chem Biol* **23**, 1372-1382, doi:10.1016/j.chembiol.2016.09.010 (2016).
121 Liu, X. & Zheng, X. F. Endoplasmic reticulum and Golgi localization sequences for mammalian target of rapamycin. *Mol Biol Cell* **18**, 1073-1082, doi:10.1091/mbc.e06-05-0406 (2007).
122 Khanna, A. *et al.* The small GTPases Ras and Rap1 bind to and control TORC2 activity. *Sci Rep* **6**, 25823, doi:10.1038/srep25823 (2016).
123 Saci, A., Cantley, L. C. & Carpenter, C. L. Rac1 regulates the activity of mTORC1 and mTORC2 and controls cellular size. *Mol Cell* **42**, 50-61, doi:10.1016/j.molcel.2011.03.017 (2011).
124 Senoo, H. *et al.* Phosphorylated Rho-GDP directly activates mTORC2 kinase towards AKT through dimerization with Ras-GTP to regulate cell migration. *Nat Cell Biol* **21**, 867-878, doi:10.1038/s41556-019-0348-8 (2019).
125 Kovalski, J. R. *et al.* The Functional Proximal Proteome of Oncogenic Ras Includes mTORC2. *Mol Cell* **73**, 830-844 e812, doi:10.1016/j.molcel.2018.12.001 (2019).
126 Menon, D. *et al.* Lipid sensing by mTOR complexes via de novo synthesis of phosphatidic acid. *J Biol Chem* **292**, 6303-6311, doi:10.1074/jbc.M116.772988 (2017).
127 Kooijman, E. E. & Burger, K. N. Biophysics and function of phosphatidic acid: a molecular perspective. *Biochim Biophys Acta* **1791**, 881-888, doi:10.1016/j.bbalip.2009.04.001 (2009).
128 Foster, D. A. Phosphatidic acid and lipid-sensing by mTOR. *Trends Endocrinol Metab* **24**, 272-278, doi:10.1016/j.tem.2013.02.003 (2013).
129 Veverka, V. *et al.* Structural characterization of the interaction of mTOR with phosphatidic acid and a novel class of inhibitor: compelling evidence for a central role

of the FRB domain in small molecule-mediated regulation of mTOR. *Oncogene* **27**, 585-595, doi:10.1038/sj.onc.1210693 (2008).
130 Frias, M. A. *et al.* Phosphatidic acid drives mTORC1 lysosomal translocation in the absence of amino acids. *J Biol Chem* **295**, 263-274, doi:10.1074/jbc.RA119.010892 (2020).
131 Zhang, C. *et al.* Glycerolipid signals alter mTOR complex 2 (mTORC2) to diminish insulin signaling. *Proc Natl Acad Sci U S A* **109**, 1667-1672, doi:10.1073/pnas.1110730109 (2012).
132 Moloughney, J. G. *et al.* mTORC2 Responds to Glutamine Catabolite Levels to Modulate the Hexosamine Biosynthesis Enzyme GFAT1. *Mol Cell* **63**, 811-826, doi:10.1016/j.molcel.2016.07.015 (2016).
133 Kazyken, D. *et al.* AMPK directly activates mTORC2 to promote cell survival during acute energetic stress. *Sci Signal* **12**, doi:10.1126/scisignal.aav3249 (2019).
134 Jacinto, E. & Lorberg, A. TOR regulation of AGC kinases in yeast and mammals. *Biochem J* **410**, 19-37, doi:10.1042/BJ20071518 (2008).
135 Su, B. & Jacinto, E. Mammalian TOR signaling to the AGC kinases. *Crit Rev Biochem Mol Biol* **46**, 527-547, doi:10.3109/10409238.2011.618113 (2011).
136 Cross, D. A., Alessi, D. R., Cohen, P., Andjelkovich, M. & Hemmings, B. A. Inhibition of glycogen synthase kinase-3 by insulin mediated by protein kinase B. *Nature* **378**, 785-789, doi:10.1038/378785a0 (1995).
137 Kaidanovich-Beilin, O. & Woodgett, J. R. GSK-3: Functional Insights from Cell Biology and Animal Models. *Front Mol Neurosci* **4**, 40, doi:10.3389/fnmol.2011.00040 (2011).
138 Brunet, A. *et al.* Akt promotes cell survival by phosphorylating and inhibiting a Forkhead transcription factor. *Cell* **96**, 857-868, doi:10.1016/s0092-8674(00)80595-4 (1999).
139 Kops, G. J. *et al.* Direct control of the Forkhead transcription factor AFX by protein kinase B. *Nature* **398**, 630-634, doi:10.1038/19328 (1999).
140 Gan, X. *et al.* PRR5L degradation promotes mTORC2-mediated PKC-delta phosphorylation and cell migration downstream of Galpha12. *Nat Cell Biol* **14**, 686-696, doi:10.1038/ncb2507 (2012).
141 Li, X. & Gao, T. mTORC2 phosphorylates protein kinase Czeta to regulate its stability and activity. *EMBO Rep* **15**, 191-198, doi:10.1002/embr.201338119 (2014).
142 Thomanetz, V. *et al.* Ablation of the mTORC2 component rictor in brain or Purkinje cells affects size and neuron morphology. *J Cell Biol* **201**, 293-308, doi:10.1083/jcb.201205030 (2013).
143 Leve, F., de Souza, W. & Morgado-Diaz, J. A. A cross-link between protein kinase A and Rho-family GTPases signaling mediates cell-cell adhesion and actin cytoskeleton organization in epithelial cancer cells. *J Pharmacol Exp Ther* **327**, 777-788, doi:10.1124/jpet.108.140798 (2008).
144 He, Y. *et al.* Mammalian target of rapamycin and Rictor control neutrophil chemotaxis by regulating Rac/Cdc42 activity and the actin cytoskeleton. *Mol Biol Cell* **24**, 3369-3380, doi:10.1091/mbc.E13-07-0405 (2013).
145 Morrison Joly, M. *et al.* Two distinct mTORC2-dependent pathways converge on Rac1 to drive breast cancer metastasis. *Breast Cancer Res* **19**, 74, doi:10.1186/s13058-017-0868-8 (2017).
146 Agarwal, N. K. *et al.* Rictor regulates cell migration by suppressing RhoGDI2. *Oncogene* **32**, 2521-2526, doi:10.1038/onc.2012.287 (2013).
147 Liu, L., Das, S., Losert, W. & Parent, C. A. mTORC2 regulates neutrophil chemotaxis in a cAMP- and RhoA-dependent fashion. *Dev Cell* **19**, 845-857, doi:10.1016/j.devcel.2010.11.004 (2010).

148 Sato, T. *et al.* Mammalian target of rapamycin (mTOR) complex 2 regulates filamin A-dependent focal adhesion dynamics and cell migration. *Genes Cells* **21**, 579-593, doi:10.1111/gtc.12366 (2016).
149 Zhou, A. X., Hartwig, J. H. & Akyurek, L. M. Filamins in cell signaling, transcription and organ development. *Trends Cell Biol* **20**, 113-123, doi:10.1016/j.tcb.2009.12.001 (2010).
150 Luo, Y., Xu, W., Li, G. & Cui, W. Weighing In on mTOR Complex 2 Signaling: The Expanding Role in Cell Metabolism. *Oxid Med Cell Longev* **2018**, 7838647, doi:10.1155/2018/7838647 (2018).
151 Albert, V. *et al.* mTORC2 sustains thermogenesis via Akt-induced glucose uptake and glycolysis in brown adipose tissue. *EMBO Mol Med* **8**, 232-246, doi:10.15252/emmm.201505610 (2016).
152 Kumar, A. *et al.* Muscle-specific deletion of rictor impairs insulin-stimulated glucose transport and enhances Basal glycogen synthase activity. *Mol Cell Biol* **28**, 61-70, doi:10.1128/MCB.01405-07 (2008).
153 Tang, Y. *et al.* Adipose tissue mTORC2 regulates ChREBP-driven de novo lipogenesis and hepatic glucose metabolism. *Nat Commun* **7**, 11365, doi:10.1038/ncomms11365 (2016).
154 Hagiwara, A. *et al.* Hepatic mTORC2 activates glycolysis and lipogenesis through Akt, glucokinase, and SREBP1c. *Cell Metab* **15**, 725-738, doi:10.1016/j.cmet.2012.03.015 (2012).
155 Betz, C. *et al.* Feature Article: mTOR complex 2-Akt signaling at mitochondria-associated endoplasmic reticulum membranes (MAM) regulates mitochondrial physiology. *Proc Natl Acad Sci U S A* **110**, 12526-12534, doi:10.1073/pnas.1302455110 (2013).
156 Masui, K. *et al.* mTOR complex 2 controls glycolytic metabolism in glioblastoma through FoxO acetylation and upregulation of c-Myc. *Cell Metab* **18**, 726-739, doi:10.1016/j.cmet.2013.09.013 (2013).
157 Caron, A., Richard, D. & Laplante, M. The Roles of mTOR Complexes in Lipid Metabolism. *Annu Rev Nutr* **35**, 321-348, doi:10.1146/annurev-nutr-071714-034355 (2015).
158 Li, S., Oh, Y. T., Yue, P., Khuri, F. R. & Sun, S. Y. Inhibition of mTOR complex 2 induces GSK3/FBXW7-dependent degradation of sterol regulatory element-binding protein 1 (SREBP1) and suppresses lipogenesis in cancer cells. *Oncogene* **35**, 642-650, doi:10.1038/onc.2015.123 (2016).
159 Chen, Y. *et al.* mTOR complex-2 stimulates acetyl-CoA and de novo lipogenesis through ATP citrate lyase in HER2/PIK3CA-hyperactive breast cancer. *Oncotarget* **7**, 25224-25240, doi:10.18632/oncotarget.8279 (2016).
160 Martinez Calejman, C. *et al.* mTORC2-AKT signaling to ATP-citrate lyase drives brown adipogenesis and de novo lipogenesis. *Nat Commun* **11**, 575, doi:10.1038/s41467-020-14430-w (2020).
161 Hanukoglu, I. & Hanukoglu, A. Epithelial sodium channel (ENaC) family: Phylogeny, structure-function, tissue distribution, and associated inherited diseases. *Gene* **579**, 95-132, doi:10.1016/j.gene.2015.12.061 (2016).
162 Valinsky, W. C., Touyz, R. M. & Shrier, A. Aldosterone, SGK1, and ion channels in the kidney. *Clin Sci (Lond)* **132**, 173-183, doi:10.1042/CS20171525 (2018).
163 Garcia-Martinez, J. M. & Alessi, D. R. mTOR complex 2 (mTORC2) controls hydrophobic motif phosphorylation and activation of serum- and glucocorticoid-induced protein kinase 1 (SGK1). *Biochem J* **416**, 375-385, doi:10.1042/BJ20081668 (2008).

164 Lu, M. *et al.* mTOR complex-2 activates ENaC by phosphorylating SGK1. *J Am Soc Nephrol* **21**, 811-818, doi:10.1681/ASN.2009111168 (2010).
165 Brown, A. L., Fluitt, M. B. & Ecelbarger, C. M. Mechanistic target of rapamycin: integrating growth factor and nutrient signaling in the collecting duct. *Am J Physiol Renal Physiol* **315**, F413-F416, doi:10.1152/ajprenal.00170.2018 (2018).
166 Lang, F. & Pearce, D. Regulation of the epithelial Na+ channel by the mTORC2/SGK1 pathway. *Nephrol Dial Transplant* **31**, 200-205, doi:10.1093/ndt/gfv270 (2016).
167 Palmada, M., Embark, H. M., Yun, C., Bohmer, C. & Lang, F. Molecular requirements for the regulation of the renal outer medullary K(+) channel ROMK1 by the serum- and glucocorticoid-inducible kinase SGK1. *Biochem Biophys Res Commun* **311**, 629-634, doi:10.1016/j.bbrc.2003.10.037 (2003).
168 Feehan, R. P. & Shantz, L. M. Negative regulation of the FOXO3a transcription factor by mTORC2 induces a pro-survival response following exposure to ultraviolet-B irradiation. *Cell Signal* **28**, 798-809, doi:10.1016/j.cellsig.2016.03.013 (2016).
169 Zou, Z. *et al.* mTORC2 promotes cell survival through c-Myc-dependent up-regulation of E2F1. *J Cell Biol* **211**, 105-122, doi:10.1083/jcb.201411128 (2015).
170 Manning, G., Whyte, D. B., Martinez, R., Hunter, T. & Sudarsanam, S. The protein kinase complement of the human genome. *Science* **298**, 1912-1934, doi:10.1126/science.1075762 (2002).
171 Leroux, A. E., Schulze, J. O. & Biondi, R. M. AGC kinases, mechanisms of regulation and innovative drug development. *Semin Cancer Biol* **48**, 1-17, doi:10.1016/j.semcancer.2017.05.011 (2018).
172 Knighton, D. R. *et al.* Crystal structure of the catalytic subunit of cyclic adenosine monophosphate-dependent protein kinase. *Science* **253**, 407-414, doi:10.1126/science.1862342 (1991).
173 Zheng, J. *et al.* 2.2 A refined crystal structure of the catalytic subunit of cAMP-dependent protein kinase complexed with MnATP and a peptide inhibitor. *Acta Crystallogr D Biol Crystallogr* **49**, 362-365, doi:10.1107/S0907444993000423 (1993).
174 Biondi, R. M. *et al.* Identification of a pocket in the PDK1 kinase domain that interacts with PIF and the C-terminal residues of PKA. *EMBO J* **19**, 979-988, doi:10.1093/emboj/19.5.979 (2000).
175 Biondi, R. M. *et al.* High resolution crystal structure of the human PDK1 catalytic domain defines the regulatory phosphopeptide docking site. *EMBO J* **21**, 4219-4228, doi:10.1093/emboj/cdf437 (2002).
176 Huse, M. & Kuriyan, J. The conformational plasticity of protein kinases. *Cell* **109**, 275-282, doi:10.1016/s0092-8674(02)00741-9 (2002).
177 Nolen, B., Taylor, S. & Ghosh, G. Regulation of protein kinases; controlling activity through activation segment conformation. *Mol Cell* **15**, 661-675, doi:10.1016/j.molcel.2004.08.024 (2004).
178 Kim, E. K. *et al.* Selective activation of Akt1 by mammalian target of rapamycin complex 2 regulates cancer cell migration, invasion, and metastasis. *Oncogene* **30**, 2954-2963, doi:10.1038/onc.2011.22 (2011).
179 Dillon, R. L. *et al.* Akt1 and akt2 play distinct roles in the initiation and metastatic phases of mammary tumor progression. *Cancer Res* **69**, 5057-5064, doi:10.1158/0008-5472.CAN-08-4287 (2009).
180 Irie, H. Y. *et al.* Distinct roles of Akt1 and Akt2 in regulating cell migration and epithelial-mesenchymal transition. *J Cell Biol* **171**, 1023-1034, doi:10.1083/jcb.200505087 (2005).
181 Frech, M. *et al.* High affinity binding of inositol phosphates and phosphoinositides to the pleckstrin homology domain of RAC/protein kinase B and their influence on kinase activity. *J Biol Chem* **272**, 8474-8481, doi:10.1074/jbc.272.13.8474 (1997).

182 Klippel, A., Kavanaugh, W. M., Pot, D. & Williams, L. T. A specific product of phosphatidylinositol 3-kinase directly activates the protein kinase Akt through its pleckstrin homology domain. *Mol Cell Biol* **17**, 338-344, doi:10.1128/mcb.17.1.338 (1997).
183 Lippa, B. *et al.* Synthesis and structure based optimization of novel Akt inhibitors. *Bioorg Med Chem Lett* **18**, 3359-3363, doi:10.1016/j.bmcl.2008.04.034 (2008).
184 Facchinetti, V. *et al.* The mammalian target of rapamycin complex 2 controls folding and stability of Akt and protein kinase C. *EMBO J* **27**, 1932-1943, doi:10.1038/emboj.2008.120 (2008).
185 Wu, W. I. *et al.* Crystal structure of human AKT1 with an allosteric inhibitor reveals a new mode of kinase inhibition. *PLoS One* **5**, e12913, doi:10.1371/journal.pone.0012913 (2010).
186 Parikh, C. *et al.* Disruption of PH-kinase domain interactions leads to oncogenic activation of AKT in human cancers. *Proc Natl Acad Sci U S A* **109**, 19368-19373, doi:10.1073/pnas.1204384109 (2012).
187 Siess, K. M. & Leonard, T. A. Lipid-dependent Akt-ivity: where, when, and how. *Biochem Soc Trans* **47**, 897-908, doi:10.1042/BST20190013 (2019).
188 Alessi, D. R. *et al.* Characterization of a 3-phosphoinositide-dependent protein kinase which phosphorylates and activates protein kinase Balpha. *Curr Biol* **7**, 261-269, doi:10.1016/s0960-9822(06)00122-9 (1997).
189 Sarbassov, D. D., Guertin, D. A., Ali, S. M. & Sabatini, D. M. Phosphorylation and regulation of Akt/PKB by the rictor-mTOR complex. *Science* **307**, 1098-1101, doi:10.1126/science.1106148 (2005).
190 Stokoe, D. *et al.* Dual role of phosphatidylinositol-3,4,5-trisphosphate in the activation of protein kinase B. *Science* **277**, 567-570, doi:10.1126/science.277.5325.567 (1997).
191 Balzano, D. *et al.* Alternative Activation Mechanisms of Protein Kinase B Trigger Distinct Downstream Signaling Responses. *J Biol Chem* **290**, 24975-24985, doi:10.1074/jbc.M115.651570 (2015).
192 Chu, N. *et al.* Akt Kinase Activation Mechanisms Revealed Using Protein Semisynthesis. *Cell* **174**, 897-907 e814, doi:10.1016/j.cell.2018.07.003 (2018).
193 Yang, J. *et al.* Crystal structure of an activated Akt/protein kinase B ternary complex with GSK3-peptide and AMP-PNP. *Nat Struct Biol* **9**, 940-944, doi:10.1038/nsb870 (2002).
194 Ebner, M., Lucic, I., Leonard, T. A. & Yudushkin, I. PI(3,4,5)P3 Engagement Restricts Akt Activity to Cellular Membranes. *Mol Cell* **65**, 416-431 e416, doi:10.1016/j.molcel.2016.12.028 (2017).
195 Lucic, I. *et al.* Conformational sampling of membranes by Akt controls its activation and inactivation. *Proc Natl Acad Sci U S A* **115**, E3940-E3949, doi:10.1073/pnas.1716109115 (2018).
196 Menon, S. *et al.* Spatial control of the TSC complex integrates insulin and nutrient regulation of mTORC1 at the lysosome. *Cell* **156**, 771-785, doi:10.1016/j.cell.2013.11.049 (2014).
197 Newton, A. C. Protein kinase C: perfectly balanced. *Crit Rev Biochem Mol Biol* **53**, 208-230, doi:10.1080/10409238.2018.1442408 (2018).
198 Leonard, T. A., Rozycki, B., Saidi, L. F., Hummer, G. & Hurley, J. H. Crystal structure and allosteric activation of protein kinase C betaII. *Cell* **144**, 55-66, doi:10.1016/j.cell.2010.12.013 (2011).
199 House, C. & Kemp, B. E. Protein kinase C pseudosubstrate prototope: structure-function relationships. *Cell Signal* **2**, 187-190, doi:10.1016/0898-6568(90)90022-3 (1990).

200 Colon-Gonzalez, F. & Kazanietz, M. G. C1 domains exposed: from diacylglycerol binding to protein-protein interactions. *Biochim Biophys Acta* **1761**, 827-837, doi:10.1016/j.bbalip.2006.05.001 (2006).
201 Sanchez-Bautista, S., Marin-Vicente, C., Gomez-Fernandez, J. C. & Corbalan-Garcia, S. The C2 domain of PKCalpha is a Ca2+ -dependent PtdIns(4,5)P2 sensing domain: a new insight into an old pathway. *J Mol Biol* **362**, 901-914, doi:10.1016/j.jmb.2006.07.093 (2006).
202 Sumimoto, H., Kamakura, S. & Ito, T. Structure and function of the PB1 domain, a protein interaction module conserved in animals, fungi, amoebas, and plants. *Sci STKE* **2007**, re6, doi:10.1126/stke.4012007re6 (2007).
203 Le Good, J. A. *et al.* Protein kinase C isotypes controlled by phosphoinositide 3-kinase through the protein kinase PDK1. *Science* **281**, 2042-2045, doi:10.1126/science.281.5385.2042 (1998).
204 Newton, A. C. Regulation of the ABC kinases by phosphorylation: protein kinase C as a paradigm. *Biochem J* **370**, 361-371, doi:10.1042/BJ20021626 (2003).
205 Matsuoka, H. *et al.* Tamoxifen inhibits tumor cell invasion and metastasis in mouse melanoma through suppression of PKC/MEK/ERK and PKC/PI3K/Akt pathways. *Exp Cell Res* **315**, 2022-2032, doi:10.1016/j.yexcr.2009.04.009 (2009).
206 Lang, F. *et al.* (Patho)physiological significance of the serum- and glucocorticoid-inducible kinase isoforms. *Physiol Rev* **86**, 1151-1178, doi:10.1152/physrev.00050.2005 (2006).
207 Tessier, M. & Woodgett, J. R. Role of the Phox homology domain and phosphorylation in activation of serum and glucocorticoid-regulated kinase-3. *J Biol Chem* **281**, 23978-23989, doi:10.1074/jbc.M604333200 (2006).
208 Virbasius, J. V. *et al.* Activation of the Akt-related cytokine-independent survival kinase requires interaction of its phox domain with endosomal phosphatidylinositol 3-phosphate. *Proc Natl Acad Sci U S A* **98**, 12908-12913, doi:10.1073/pnas.221352898 (2001).
209 Bogusz, A. M., Brickley, D. R., Pew, T. & Conzen, S. D. A novel N-terminal hydrophobic motif mediates constitutive degradation of serum- and glucocorticoid-induced kinase-1 by the ubiquitin-proteasome pathway. *FEBS J* **273**, 2913-2928, doi:10.1111/j.1742-4658.2006.05304.x (2006).
210 Biondi, R. M., Kieloch, A., Currie, R. A., Deak, M. & Alessi, D. R. The PIF-binding pocket in PDK1 is essential for activation of S6K and SGK, but not PKB. *EMBO J* **20**, 4380-4390, doi:10.1093/emboj/20.16.4380 (2001).
211 Kobayashi, T., Deak, M., Morrice, N. & Cohen, P. Characterization of the structure and regulation of two novel isoforms of serum- and glucocorticoid-induced protein kinase. *Biochem J* **344 Pt 1**, 189-197 (1999).
212 Sommer, E. M. *et al.* Elevated SGK1 predicts resistance of breast cancer cells to Akt inhibitors. *Biochem J* **452**, 499-508, doi:10.1042/BJ20130342 (2013).
213 Murray, J. T. *et al.* Exploitation of KESTREL to identify NDRG family members as physiological substrates for SGK1 and GSK3. *Biochem J* **384**, 477-488, doi:10.1042/BJ20041057 (2004).
214 Bhalla, V. *et al.* Serum- and glucocorticoid-regulated kinase 1 regulates ubiquitin ligase neural precursor cell-expressed, developmentally down-regulated protein 4-2 by inducing interaction with 14-3-3. *Mol Endocrinol* **19**, 3073-3084, doi:10.1210/me.2005-0193 (2005).
215 Brunet, A. *et al.* Protein kinase SGK mediates survival signals by phosphorylating the forkhead transcription factor FKHRL1 (FOXO3a). *Mol Cell Biol* **21**, 952-965, doi:10.1128/MCB.21.3.952-965.2001 (2001).

216 Zhao, B. *et al.* Crystal structure of the kinase domain of serum and glucocorticoid-regulated kinase 1 in complex with AMP PNP. *Protein Sci* **16**, 2761-2769, doi:10.1110/ps.073161707 (2007).
217 Chandra, M. *et al.* Classification of the human phox homology (PX) domains based on their phosphoinositide binding specificities. *Nat Commun* **10**, 1528, doi:10.1038/s41467-019-09355-y (2019).
218 Grabiner, B. C. *et al.* A diverse array of cancer-associated MTOR mutations are hyperactivating and can predict rapamycin sensitivity. *Cancer Discov* **4**, 554-563, doi:10.1158/2159-8290.CD-13-0929 (2014).
219 Wander, S. A., Hennessy, B. T. & Slingerland, J. M. Next-generation mTOR inhibitors in clinical oncology: how pathway complexity informs therapeutic strategy. *J Clin Invest* **121**, 1231-1241, doi:10.1172/JCI44145 (2011).
220 Benjamin, D., Colombi, M., Moroni, C. & Hall, M. N. Rapamycin passes the torch: a new generation of mTOR inhibitors. *Nat Rev Drug Discov* **10**, 868-880, doi:10.1038/nrd3531 (2011).
221 Hsieh, A. C. *et al.* The translational landscape of mTOR signalling steers cancer initiation and metastasis. *Nature* **485**, 55-61, doi:10.1038/nature10912 (2012).
222 Thoreen, C. C. *et al.* An ATP-competitive mammalian target of rapamycin inhibitor reveals rapamycin-resistant functions of mTORC1. *J Biol Chem* **284**, 8023-8032, doi:10.1074/jbc.M900301200 (2009).
223 Feldman, M. E. *et al.* Active-site inhibitors of mTOR target rapamycin-resistant outputs of mTORC1 and mTORC2. *PLoS Biol* **7**, e38, doi:10.1371/journal.pbio.1000038 (2009).
224 Rodrik-Outmezguine, V. S. *et al.* mTOR kinase inhibition causes feedback-dependent biphasic regulation of AKT signaling. *Cancer Discov* **1**, 248-259, doi:10.1158/2159-8290.CD-11-0085 (2011).
225 Bresin, A. *et al.* Preclinical Evidence for Targeting PI3K/mTOR Signaling with Dual-Inhibitors as a Therapeutic Strategy against Cutaneous T-Cell Lymphoma. *J Invest Dermatol* **140**, 1045-1053 e1046, doi:10.1016/j.jid.2019.08.454 (2020).
226 Choi, J., Chen, J., Schreiber, S. L. & Clardy, J. Structure of the FKBP12-rapamycin complex interacting with the binding domain of human FRAP. *Science* **273**, 239-242, doi:10.1126/science.273.5272.239 (1996).
227 Wang, L., Rhodes, C. J. & Lawrence, J. C., Jr. Activation of mammalian target of rapamycin (mTOR) by insulin is associated with stimulation of 4EBP1 binding to dimeric mTOR complex 1. *J Biol Chem* **281**, 24293-24303, doi:10.1074/jbc.M603566200 (2006).
228 Stuttfeld, E. *et al.* Architecture of the human mTORC2 core complex. *Elife* **7**, doi:10.7554/eLife.33101 (2018).
229 Chen, X. *et al.* Cryo-EM structure of human mTOR complex 2. *Cell Res* **28**, 518-528, doi:10.1038/s41422-018-0029-3 (2018).
230 Karuppasamy, M. *et al.* Cryo-EM structure of Saccharomyces cerevisiae target of rapamycin complex 2. *Nat Commun* **8**, 1729, doi:10.1038/s41467-017-01862-0 (2017).
231 Tatebe, H. *et al.* Substrate specificity of TOR complex 2 is determined by a ubiquitin-fold domain of the Sin1 subunit. *Elife* **6**, doi:10.7554/eLife.19594 (2017).
232 Furuita, K. *et al.* Utilization of paramagnetic relaxation enhancements for high-resolution NMR structure determination of a soluble loop-rich protein with sparse NOE distance restraints. *J Biomol NMR* **61**, 55-64, doi:10.1007/s10858-014-9882-7 (2015).
233 Pan, D. & Matsuura, Y. Structures of the pleckstrin homology domain of Saccharomyces cerevisiae Avo1 and its human orthologue Sin1, an essential subunit

of TOR complex 2. *Acta Crystallogr Sect F Struct Biol Cryst Commun* **68**, 386-392, doi:10.1107/S1744309112007178 (2012).
234 Ikenoue, T., Inoki, K., Yang, Q., Zhou, X. & Guan, K. L. Essential function of TORC2 in PKC and Akt turn motif phosphorylation, maturation and signalling. *EMBO J* **27**, 1919-1931, doi:10.1038/emboj.2008.119 (2008).
235 Xie, J., Wang, X. & Proud, C. G. mTOR inhibitors in cancer therapy. *F1000Res* **5**, doi:10.12688/f1000research.9207.1 (2016).
236 Benavides-Serrato, A. *et al.* Specific blockade of Rictor-mTOR association inhibits mTORC2 activity and is cytotoxic in glioblastoma. *PLoS One* **12**, e0176599, doi:10.1371/journal.pone.0176599 (2017).
237 Benavides-Serrato, A. *et al.* Correction: Specific blockade of Rictor-mTOR association inhibits mTORC2 activity and is cytotoxic in glioblastoma. *PLoS One* **14**, e0212160, doi:10.1371/journal.pone.0212160 (2019).
238 Gaubitz, C. *et al.* Molecular Basis of the Rapamycin Insensitivity of Target Of Rapamycin Complex 2. *Mol Cell* **58**, 977-988, doi:10.1016/j.molcel.2015.04.031 (2015).
239 Kelley, L. A., Mezulis, S., Yates, C. M., Wass, M. N. & Sternberg, M. J. The Phyre2 web portal for protein modeling, prediction and analysis. *Nat Protoc* **10**, 845-858, doi:10.1038/nprot.2015.053 (2015).
240 Dibble, C. C., Asara, J. M. & Manning, B. D. Characterization of Rictor phosphorylation sites reveals direct regulation of mTOR complex 2 by S6K1. *Mol Cell Biol* **29**, 5657-5670, doi:10.1128/MCB.00735-09 (2009).
241 Lee, S., Chanoit, G., McIntosh, R., Zvara, D. A. & Xu, Z. Molecular mechanism underlying Akt activation in zinc-induced cardioprotection. *Am J Physiol Heart Circ Physiol* **297**, H569-575, doi:10.1152/ajpheart.00293.2009 (2009).
242 Taniguchi, M. *et al.* Essential role of the zinc transporter ZIP9/SLC39A9 in regulating the activations of Akt and Erk in B-cell receptor signaling pathway in DT40 cells. *PLoS One* **8**, e58022, doi:10.1371/journal.pone.0058022 (2013).
243 Nimmanon, T., Ziliotto, S., Morris, S., Flanagan, L. & Taylor, K. M. Phosphorylation of zinc channel ZIP7 drives MAPK, PI3K and mTOR growth and proliferation signalling. *Metallomics* **9**, 471-481, doi:10.1039/c6mt00286b (2017).
244 Loewith, R. *et al.* Two TOR complexes, only one of which is rapamycin sensitive, have distinct roles in cell growth control. *Mol Cell* **10**, 457-468 (2002).
245 Liu, P. *et al.* Sin1 phosphorylation impairs mTORC2 complex integrity and inhibits downstream Akt signalling to suppress tumorigenesis. *Nat Cell Biol* **15**, 1340-1350, doi:10.1038/ncb2860 (2013).
246 Hwang, Y. *et al.* Disruption of scaffolding function of mLST8 selectively inhibits mTORC2 assembly and function and suppresses mTORC2-dependent tumor growth in vivo. *Cancer Res*, doi:10.1158/0008-5472.CAN-18-3658 (2019).
247 Wang, B. *et al.* TRAF2 and OTUD7B govern a ubiquitin-dependent switch that regulates mTORC2 signalling. *Nature* **545**, 365-369, doi:10.1038/nature22344 (2017).
248 Burke, J. E. Structural Basis for Regulation of Phosphoinositide Kinases and Their Involvement in Human Disease. *Mol Cell* **71**, 653-673, doi:10.1016/j.molcel.2018.08.005 (2018).
249 Hanakahi, L. A., Bartlet-Jones, M., Chappell, C., Pappin, D. & West, S. C. Binding of inositol phosphate to DNA-PK and stimulation of double-strand break repair. *Cell* **102**, 721-729 (2000).
250 Zhang, X. *et al.* Structures of the human spliceosomes before and after release of the ligated exon. *Cell Res* **29**, 274-285, doi:10.1038/s41422-019-0143-x (2019).

251 Toste Rego, A. & da Fonseca, P. C. A. Characterization of Fully Recombinant Human 20S and 20S-PA200 Proteasome Complexes. *Mol Cell* **76**, 138-147 e135, doi:10.1016/j.molcel.2019.07.014 (2019).
252 Ouyang, Z., Zheng, G., Tomchick, D. R., Luo, X. & Yu, H. Structural Basis and IP6 Requirement for Pds5-Dependent Cohesin Dynamics. *Mol Cell* **62**, 248-259, doi:10.1016/j.molcel.2016.02.033 (2016).
253 Fitzgerald, D. J. *et al.* Protein complex expression by using multigene baculoviral vectors. *Nat Methods* **3**, 1021-1032, doi:10.1038/nmeth983 (2006).
254 Andjelkovic, M. *et al.* Role of translocation in the activation and function of protein kinase B. *J Biol Chem* **272**, 31515-31524, doi:10.1074/jbc.272.50.31515 (1997).
255 Bossler, F. *et al.* Repression of Human Papillomavirus Oncogene Expression under Hypoxia Is Mediated by PI3K/mTORC2/AKT Signaling. *mBio* **10**, doi:10.1128/mBio.02323-18 (2019).
256 Sanjana, N. E., Shalem, O. & Zhang, F. Improved vectors and genome-wide libraries for CRISPR screening. *Nat Methods* **11**, 783-784, doi:10.1038/nmeth.3047 (2014).
257 Ahrne, E. *et al.* Evaluation and Improvement of Quantification Accuracy in Isobaric Mass Tag-Based Protein Quantification Experiments. *J Proteome Res* **15**, 2537-2547, doi:10.1021/acs.jproteome.6b00066 (2016).
258 Nesvizhskii, A. I., Keller, A., Kolker, E. & Aebersold, R. A statistical model for identifying proteins by tandem mass spectrometry. *Anal Chem* **75**, 4646-4658, doi:10.1021/ac0341261 (2003).
259 Kastner, B. Purification and Electron Microscopy of Spliceosomal snRNPs. *Schenkel J. (eds) RNP Particles, Splicing and Autoimmune Diseases. Springer Lab Manual.* (1998).
260 Tivol, W. F., Briegel, A. & Jensen, G. J. An improved cryogen for plunge freezing. *Microsc Microanal* **14**, 375-379, doi:10.1017/S1431927608080781 (2008).
261 Mastronarde, D. N. Automated electron microscope tomography using robust prediction of specimen movements. *J Struct Biol* **152**, 36-51, doi:10.1016/j.jsb.2005.07.007 (2005).
262 Zheng, S. Q. *et al.* MotionCor2: anisotropic correction of beam-induced motion for improved cryo-electron microscopy. *Nat Methods* **14**, 331-332, doi:10.1038/nmeth.4193 (2017).
263 Zhang, K. Gctf: Real-time CTF determination and correction. *J Struct Biol* **193**, 1-12, doi:10.1016/j.jsb.2015.11.003 (2016).
264 Ludtke, S. J., Baldwin, P. R. & Chiu, W. EMAN: semiautomated software for high-resolution single-particle reconstructions. *J Struct Biol* **128**, 82-97, doi:10.1006/jsbi.1999.4174 (1999).
265 Scheres, S. H. RELION: implementation of a Bayesian approach to cryo-EM structure determination. *J Struct Biol* **180**, 519-530, doi:10.1016/j.jsb.2012.09.006 (2012).
266 Punjani, A., Rubinstein, J. L., Fleet, D. J. & Brubaker, M. A. cryoSPARC: algorithms for rapid unsupervised cryo-EM structure determination. *Nat Methods* **14**, 290-296, doi:10.1038/nmeth.4169 (2017).
267 Pettersen, E. F. *et al.* UCSF Chimera--a visualization system for exploratory research and analysis. *J Comput Chem* **25**, 1605-1612, doi:10.1002/jcc.20084 (2004).
268 Zivanov, J., Nakane, T. & Scheres, S. H. W. A Bayesian approach to beam-induced motion correction in cryo-EM single-particle analysis. *IUCrJ* **6**, 5-17, doi:10.1107/S205225251801463X (2019).
269 Terwilliger, T. C., Sobolev, O. V., Afonine, P. V. & Adams, P. D. Automated map sharpening by maximization of detail and connectivity. *Acta Crystallogr D Struct Biol* **74**, 545-559, doi:10.1107/S2059798318004655 (2018).

270 Adams, P. D. *et al.* PHENIX: a comprehensive Python-based system for macromolecular structure solution. *Acta Crystallogr D Biol Crystallogr* **66**, 213-221, doi:10.1107/S0907444909052925 (2010).
271 Emsley, P., Lohkamp, B., Scott, W. G. & Cowtan, K. Features and development of Coot. *Acta Crystallogr D Biol Crystallogr* **66**, 486-501, doi:10.1107/S0907444910007493 (2010).
272 Goddard, T. D. *et al.* UCSF ChimeraX: Meeting modern challenges in visualization and analysis. *Protein Sci* **27**, 14-25, doi:10.1002/pro.3235 (2018).
273 Fernandez, I. S., Bai, X. C., Murshudov, G., Scheres, S. H. & Ramakrishnan, V. Initiation of translation by cricket paralysis virus IRES requires its translocation in the ribosome. *Cell* **157**, 823-831, doi:10.1016/j.cell.2014.04.015 (2014).
274 Baker, N. A., Sept, D., Joseph, S., Holst, M. J. & McCammon, J. A. Electrostatics of nanosystems: application to microtubules and the ribosome. *Proc Natl Acad Sci U S A* **98**, 10037-10041, doi:10.1073/pnas.181342398 (2001).
275 Sievers, F. *et al.* Fast, scalable generation of high-quality protein multiple sequence alignments using Clustal Omega. *Mol Syst Biol* **7**, 539, doi:10.1038/msb.2011.75 (2011).
276 Gouet, P., Courcelle, E., Stuart, D. I. & Metoz, F. ESPript: analysis of multiple sequence alignments in PostScript. *Bioinformatics* **15**, 305-308, doi:10.1093/bioinformatics/15.4.305 (1999).
277 Pei, J. & Grishin, N. V. AL2CO: calculation of positional conservation in a protein sequence alignment. *Bioinformatics* **17**, 700-712, doi:10.1093/bioinformatics/17.8.700 (2001).
278 Mallery, D. L. *et al.* IP6 is an HIV pocket factor that prevents capsid collapse and promotes DNA synthesis. *Elife* **7**, doi:10.7554/eLife.35335 (2018).
279 Blind, R. D. Structural analyses of inositol phosphate second messengers bound to signaling effector proteins. *Adv Biol Regul* **75**, 100667, doi:10.1016/j.jbior.2019.100667 (2020).
280 Daulat, A. M. & Borg, J. P. When mTORC2-AKT signaling meets cell polarity. *Cell Cycle* **15**, 3003-3004, doi:10.1080/15384101.2016.1214037 (2016).
281 Greber, B. J. *et al.* The cryo-electron microscopy structure of the human CDK-activating kinase. *bioRxiv*, 2020.2005.2013.094755, doi:10.1101/2020.05.13.094755 (2020).
282 Locke, M. N. & Thorner, J. Rab5 GTPases are required for optimal TORC2 function. *J Cell Biol* **218**, 961-976, doi:10.1083/jcb.201807154 (2019).
283 Tatebe, H., Morigasaki, S., Murayama, S., Zeng, C. T. & Shiozaki, K. Rab-family GTPase regulates TOR complex 2 signaling in fission yeast. *Curr Biol* **20**, 1975-1982, doi:10.1016/j.cub.2010.10.026 (2010).
284 Cheng, H. *et al.* RICTOR Amplification Defines a Novel Subset of Patients with Lung Cancer Who May Benefit from Treatment with mTORC1/2 Inhibitors. *Cancer Discov* **5**, 1262-1270, doi:10.1158/2159-8290.CD-14-0971 (2015).
285 Wang, L. *et al.* Overexpression of Rictor protein in colorectal cancer is correlated with tumor progression and prognosis. *Oncol Lett* **14**, 6198-6202, doi:10.3892/ol.2017.6936 (2017).
286 Collins, M. O., Yu, L., Campuzano, I., Grant, S. G. & Choudhary, J. S. Phosphoproteomic analysis of the mouse brain cytosol reveals a predominance of protein phosphorylation in regions of intrinsic sequence disorder. *Mol Cell Proteomics* **7**, 1331-1348, doi:10.1074/mcp.M700564-MCP200 (2008).
287 Davey, N. E. *et al.* Attributes of short linear motifs. *Mol Biosyst* **8**, 268-281, doi:10.1039/c1mb05231d (2012).

288 Fernandez-Leiro, R. & Scheres, S. H. Unravelling biological macromolecules with cryo-electron microscopy. *Nature* **537**, 339-346, doi:10.1038/nature19948 (2016).
289 Bhamidipati, P. K., Kantarjian, H., Cortes, J., Cornelison, A. M. & Jabbour, E. Management of imatinib-resistant patients with chronic myeloid leukemia. *Ther Adv Hematol* **4**, 103-117, doi:10.1177/2040620712468289 (2013).